INVESTIGATION OF FACTORS CONTRIBUTING TO THE DEPOSTION OF CONTAMINANTS ON DRYER CYLINDERS

A Thesis
Presented to
The Academic Faculty

by

Andrew Edward Clarke

In Partial Fulfillment
of the Requirements for the Degree
Master of Science in the
School of Mechanical Engineering

Georgia Institute of Technology
[May 2007]

INVESTIGATION OF FACTORS CONTRIBUTING TO THE

DEPOSITION OF CONTAMINANTS ON DRYER CYLINDERS

Approved by:

Dr. Tim Patterson, Advisor
School of Mechanical Engineering
Georgia Institute of Technology

Dr. Sujit Banerjee
School of Chemical Engineering
Georgia Institute of Technology

Dr. Fred Ahrens
School of Mechanical Engineering
Georgia Institute of Technology

Dr. David Orloff
School of Mechanical Engineering
Georgia Institute of Technology

Date Approved: November 28, 2006

TABLE OF CONTENTS

LIST OF TABLES

LIST OF FIGURES

LIST OF SYMBOLS

A_{rec}	Cross-sectional area recovered
A_{tot}	Total cross-sectional area
C_{layer}	Filler concentration in the layer
m_{fiber}	Mass of fiber
$m_{fiber\ L1}$	Mass of fiber in layer 1
$m_{fiber\ L2}$	Mass of fiber in layer 2
$m_{fiber\ L3}$	Mass of fiber in layer 3
$m_{fiber\ tot}$	Total mass of fiber
m_{filler}	Mass of filler
$m_{filler\ rec}$	Mass of filler recovered
$m_{filler\ add}$	Mass of filler added
$m_{filler\ cut}$	Mass of filler cut from sheet
$m_{filler\ tot}$	Total mass of filler
m_{water}	Mass of water
ρ_{water}	Density of water
R	Retention
R_{cut}	Retention of cut sheet
r_{rec}	radius of cross-sectional area recovered
r_{tot}	radius of total cross-sectional area
V_{water}	Volume of water
z_1	z-directional fiber mass at position 1
z_2	z-directional fiber mass at position 2
z_3	z-directional fiber mass at position 3

SUMMARY

Pulp from recycled paper products contains various waxes, glues, adhesives, filler, and inorganics that are collectively referred to as contaminants. Contaminants that are not drained out during the forming process are trapped in the sheet and carried down the paper machine. These contaminant particles and contaminants in solution can become deposited on the dryer cylinders. The contaminants which deposit on the dryer cylinders lead to reduced quality and production of paper on the machine. The process by which contaminants are deposited on a dryer cylinder has not been explored at a fundamental level. Rather, quick industrial fixes have been tested to try and eliminate the contaminant deposition and only reductions in deposition have been achieved. The literature reviewed does not relate the flow of particle suspensions through porous media to the heat transfer and fluid dynamics processes associated with drying paper. The experiments in the literature showed the general trends of particle and dye distributions across the thicknesses of different porous media during forming or filtration processes. Filler and fines distribution were not able to be changed by flows induced by pressing a sheet. The mechanisms for how particles move through porous media found in the literature were a basis for what kind of phenomena would be expected in the particle transport experiments.

A means of completely eliminating sticky deposits could be found by examining the parameters which contribute to the deposition process. The hypothesis proposed in this thesis is that contaminant particles and liquid containing contaminants are transported to the dryer can surface by liquid flows induced by the drying process. By performing particle flow experiments during drying, bounds for the particle size, initial drying surface temperature, drying time, and

initial solids content will be determined for which the hypothesis is true. The particle and dye transport studies performed showed an array of processes at work simultaneously. The results from the particle and dye transport studies show that a particle diameter of ~1.0 μm or less, handsheet solids content of less than 30%, open sheet structure and a high surface drying temperature (200°C) were needed to create a significant change in filler and dye distribution across the thickness of a handsheet.

CHAPTER 1

INTRODUCTION

Pulp from recycled paper products contains various waxes, glues, adhesives, filler, and inorganics that are collectively referred to as contaminants. Contaminants that are not drained out during the forming process are trapped in the sheet and carried down the paper machine. These contaminant particles can become deposited on the dryer cylinders. The contaminant deposits on the dryer cylinders lead to reduced quality and production of paper on the machine.

The process by which contaminants are deposited on a dryer cylinder has not been explored at a fundamental level. Rather, quick industrial fixes have been tested to try and eliminate the contaminant deposition and only reductions in deposition have been achieved. A means of completely eliminating sticky deposits could be found by examining the parameters which contribute to the deposition process. The hypothesis proposed in this thesis is that particles and liquid containing contaminants are transported to the dryer cylinder surface by liquid flows induced by the drying process.

The literature reviewed does not relate the flow of particles or fluid through porous media to the heat transfer and fluid dynamics processes associated with drying paper. The literature presented in Chapter 2 addresses phenomena related to the particle and solute movement through porous media. Section 1 is devoted to analytically and experimentally determined filler distributions in paper. The distribution of particles through the thickness of a sheet was modeled by Wei et al [1] and compared to actual filler distributions from handsheets manufactured by Tanaka et al [2]. The filler distribution through the z-direction of paper samples from different paper machines was also analyzed by Kilpelainen and Schlegel [4]. Section 2 contains

literature devoted to experiments using dye to study the liquid movement in a sheet during drying. Devlin [5] measured chlorine distributions through the thickness of handsheets to determine liquid movement during drying. Preston and co-workers [6-8] and Dreshfield [9] used nonsubstantive dye to characterize liquid movement through the thickness of a fibrous web during drying. Section 3 reviews an article by Szikla and Paulapuro [10]. They attempted to change the shape of the filler/fine distribution profile by pressing the sheet at different levels, which would generate different flow velocities through the thickness of the sheet. Experiments outside the realm of paper science have been performed to model flow of particles and solute through porous media. These studies are described in Section 4. Xiqing Li et al. [14] examined the transport of carboxylated latex microspheres (1.1 and 1.0 μm diameter) in columns of glass beads (417-600 μm diameter) under various flow and ionic strength conditions. Camesano et al. [15] also looked at the transport of microspheres (0.97 to 1.0 μm diameter), except southern Arizona soil, with an average equivalent diameter of 127 μm, was used. Finally, Section 5 describes a fluid mechanics model of a particle in a cylindrical tube proposed by Sugihara-Seki and Masako [28]. The models introduced by Sugihara-Seki and Masako [28] show how varying the particle diameter and vertical position in a tube effects the velocity of the particle relative to the fluid flow velocity in the tube. The mechanisms from the literature in flow in porous media and flow associated with drying paper are used as a platform to attempt to describe how particles move through a sheet during drying.

The experimental methods section in Chapter 3 describes the procedures used to perform particle transport and solute flow experiments through the thickness of a handsheet. Four types of experiments based on the four combinations of filler added to the sheet before drying were performed to characterize the transport of particles and dye through a sheet of paper during

drying. The steps that make up each of the four main experiments are described in separate sections of Chapter 3 because many of the steps are the same for each main type of experiment. The procedure begins with the preparation of the two major components used to make the sheet, the fiber and the filler. The pulp preparation procedure in Section 1 describes the steps used to make the pulp that is used in all experiments. Section 2 has the procedures for the preparation of the various types of filler used to model contaminants in the sheet. Section 3 describes how the handsheet was made when the filler was added to the handsheet mold. The solids content of the wet sheet before drying was determined following the procedure in Section 4. Laminate tape was used throughout the experiments to split the sheets after drying the sheets. Therefore, the mass and ash percentage of the tape was needed to perform later calculations. The procedure for determining the mass and ash percentage of laminate tape is located in Section 5. The experiments performed used various levels of drying, which are outlined in Section 6. To determine the distribution profile of filler or dye in the handsheets, the sheets had to be split into layers as described in Section 7 and then ashed in a muffle oven as described in Section 8. Digital images of the split handsheets were taken to quantify the dye concentration through the thickness of the sheet as shown in Section 9. A few basic calculations were performed to transform the raw data into quantities that would show the processes taking place during the experiments. The formulas for these calculations are presented in Section 10.

The results for the four basic experiments are reported in Chapter 4. The first three experiments were performed using three sizes of particles. The particles with diameters from 2-75 μm are called the large particles (G-800). The particles with diameters from 1-10 μm are called the medium particles (G-200). The particles with diameters 0.1-1 μm are called the small particles (PCC). The results presented in Sections 1-3 show the z-directional distribution and

retention for each size of particle in a handsheet dried on a surface with different initial surface temperatures. The fourth set of experiments involves adding the small particle and dye (PCC/Dye) to the handsheet during drying. The results from these experiments are the particle distributions of the small particles and the intensity plots from the digital images of the dyed handsheets shown in Sections 4 and 5. The experiments will be referred to using the abbreviations in parenthesis denoted above for the filler material used in the respective experiment.

The particle distribution and intensity distribution figures and retention values created from the results are analyzed in Chapter 5. The analysis and discussion of the results helps to quantify the bounds for which particles and solute could be induced to flow through a sheet of paper during drying. From the analysis of the results for the experiments involving adding the small particle and dye directly to the sheet, several mechanisms are proposed for the differences in filler distributions and dye intensity through the thickness of the sheet in Chapter 6. The mechanisms proposed help describe different scenarios involving contaminant behavior during drying. The conclusions drawn in Chapter 7 set constraints on the parameters necessary for inducing contaminant movement towards the surface of the dryer cylinders. By understanding the limiting factors for which particle flow through a sheet could occur, the processes by which contaminants could deposit on dryer cylinders is better understood. The parameters contributing to deposition can be isolated for further investigation proposed in Chapter 8 to attempt to completely understand these processes.

CHAPTER 2

LITERATURE REVIEW

2.1 Filler Particle Distribution in Paper

The distribution of particles through the thickness of paper has been investigated mainly for the forming section of the paper process. Wei et al. [1] demonstrated the application of a retention model to analyze particle retentions in the British hand sheet mold. They modeled pulp drainage as a gravity filtration process with Darcy's law describing the momentum balance for the flow. The retention problem is modeled as a depth filtration process and was restricted to low filler loadings so that particle capture efficiency was described by a constant. Analytical solutions for the drainage and retention of fine particles in a forming fibrous mat were obtained for constant average specific filtration resistance and constant capture efficiency. Figure 2.1 is one graph generated by their model that shows the filler concentration in the sheet versus non-dimensional thickness of the sheet as the mat forms on the wire. The filler concentration is the mass of filler per mass of fiber in a particular section of the sheet. The non-dimensional thickness is the location in the sheet from the wire side at 0.0 to the top side at 1.0. The five series plotted on this graph represent the concentration profile at different times from 0.4 to 7.0 seconds after the water was allowed to drain. Figure 2.1 shows that the retention is the highest at wire side and the lowest at the top, the same trends as have been observed in a number of handsheet experiments [2]. This phenomenon was said to occur because the lowest layers of the fibrous mat close to the screen have formed during the initial stages and thus captured particles for the longest time, while the top layers have formed in the final stages and are subjected to the shortest capture time.

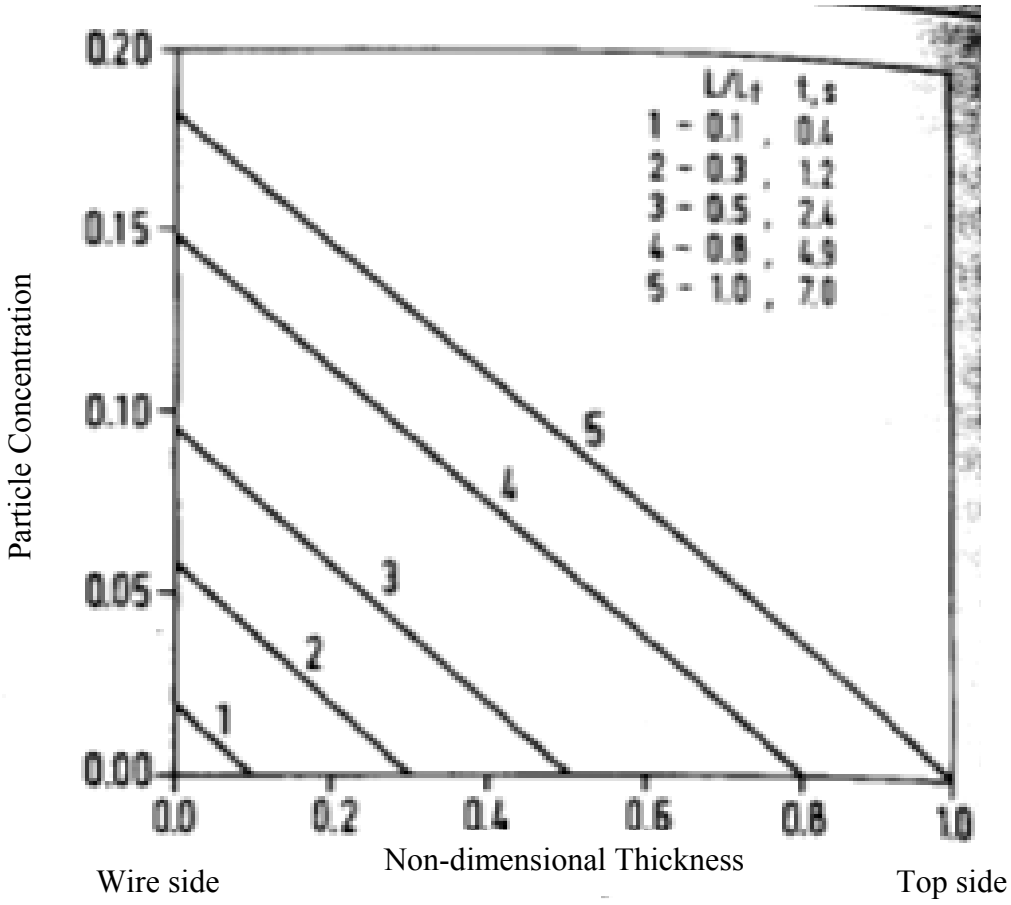

Figure 2.1. Fine Particle Concentration Distribution Inside the Fibrous Mat During Formation [1]

Results from the analytical solutions from Wei et al. [1] were also compared with the experimental data of Tanaka et al. [3]. Tanaka et al. [3] observed that the distributions of clay and TiO_2 in the z-direction become greater even when retention aids are added and the retention level increases. Figure 2.2 shows the comparison between the predicted (solid lines) and the observed distributions of TiO_2 (0.1-0.3 μm diameter) inside mats by Tanaka et al. [3] (column charts) for three levels of retention. Two series of filler profile data from Tanaka et al. [3] are shown as the solid and dashed column charts. Concentration of TiO_2 is shown versus non-dimensional thickness, Z/L_f, in Figure 2.2. It showed that the predictions agree well with the experiment when the retention level is low, as 19% show in Figure 2.2(A), or very high, as 95%

shown in Figure 2.2(C) while, at the middle level retention, there are deviations between the prediction and the experiment.

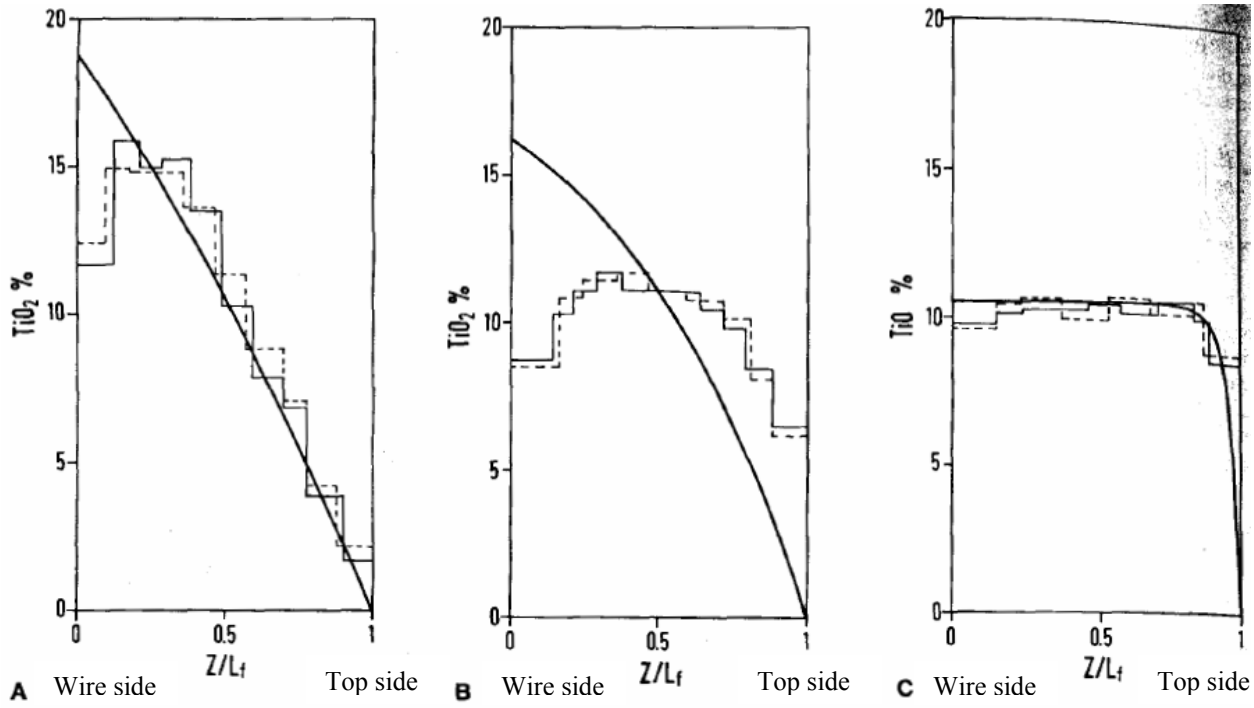

Figure 2.2. Distribution of TiO_2 Inside Fibrous Mats in British Handsheet Mold [1]
(A) retention rate: 19%; (B) retention rate: 48%; (C) retention rate: 95%

The observed particle distribution is more uniform than the theoretical prediction. The small decrease in the concentration very close to the wire was due to two processes. These layers represented the initial stage of mat formation where it was possible that some amount of fibers could pass through the screen before fiber retention reached 100%. Furthermore, the initially high velocity of the fluid as it filters through these layers could cause some re-entrainment of already deposited fines. These two causes could result in the maximum in the fine profile shifting to a region slightly away from the wire as was observed in the experimental data. The good agreement between theory and experiment suggested that, in very high levels of retention, particle retention may be treated as depth filtration with a high constant value of capture

coefficient. At the middle level of retention, both filtration and heteroflocculation were important. It appeared that particle deposition prior to mat formation may be necessary to account for the profiles in this region. They also found that the initial particle concentration had little effect on the retention rate.

Kilpelainen and Schlegel [4] analyzed the filler distributions from paper samples received from various mills to help with quality control. The typical z-direction filler distribution curves of wood-free fine and SC papers made on different formers are shown in Figure 2.3. The filler distributions were measured using the ash method. The paper was divided into 12-16 sections in the z-direction. Each section was approximately 2" x 8" in size. The z-direction ash distributions were measured as an average of three samples.

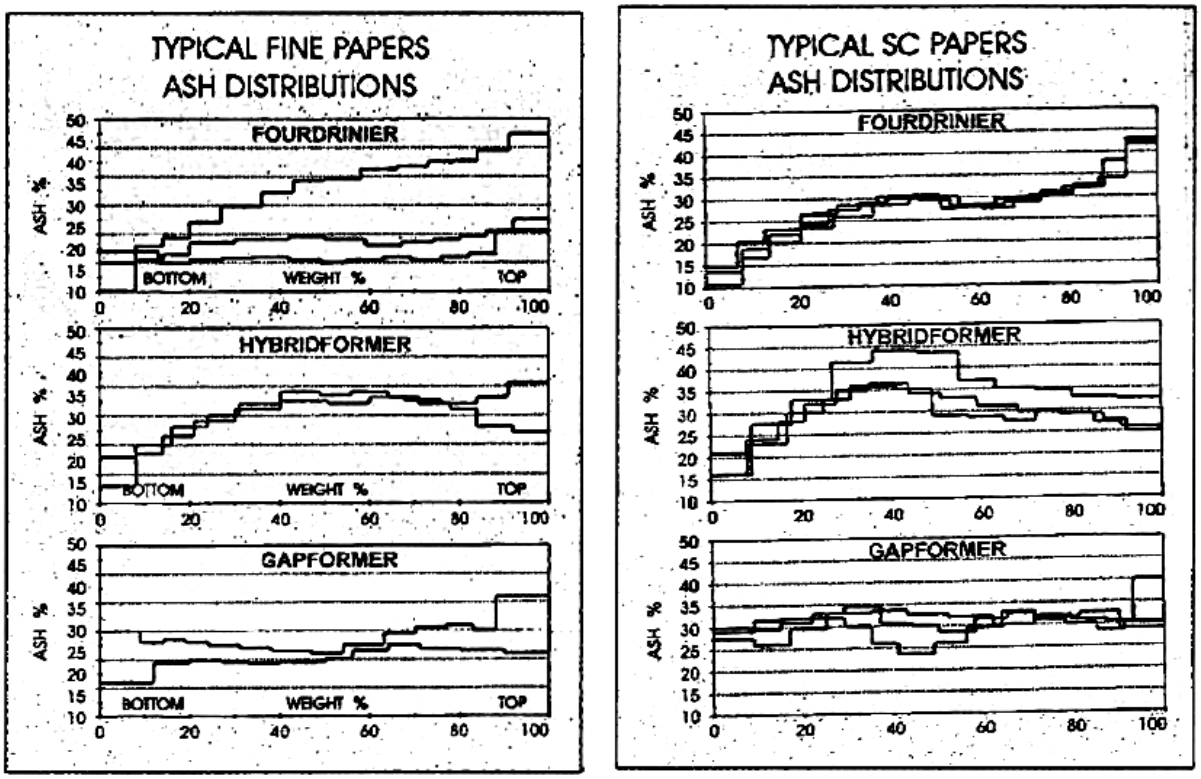

Figure 2.3. Filler Distributions Made on Different Formers for Typical Fine and SC Papers [4]

2.2 Dye Migration

Distributions of various dyes through the thickness of the sheet have been used to try and quantify fluid movements in the z-direction of the sheet during high-intensity drying. Devlin [5] performed a liquid movement study by measuring the chlorine distributions through the thickness of handsheets. The chlorine distribution through the thickness of the sheet was indicative of the local cumulative evaporation in the sheet, and hence, net liquid movement since the chlorine only moved with the liquid and not with the vapor. The handsheets were made of unbleached kraft pulp with basis weights and initial moisture contents of approximately 42 lb/1000 ft^2 and 57%, respectively. Lithium chloride was added to the handsheet stock slurry. The handsheets were dried under applied pressures of 400 psi and 700 psi, and hot surface temperatures of 300˚F and 525˚F. Figure 2.4 shows the final chlorine distributions for sheets dried at the four drying conditions. Also given was a distribution for a freeze-dried sheet intended to show the initial moisture distribution in the sheet before high-intensity drying. The freeze-dried distribution is the top middle intensity versus thickness plot in Figure 2.4 with no temperature or pressure labels above it. The hot surface was that part of the sheet which was in contact with the heater block. The cold surface is that part of the sheet which contacts the screens, as shown by their experimental arrangement depicted in Figure 2.5. The data was only semiquantitative in that the absolute amount of chlorine in the sheet was not measured. Only the relative occurrence of chlorine in a section of the sheet is measured. All of the drying conditions induced significant amounts of liquid movement. To varying degrees, each condition had a U-shaped chlorine distribution. However, Devlin [5] could not explain why the distributions took on this shape.

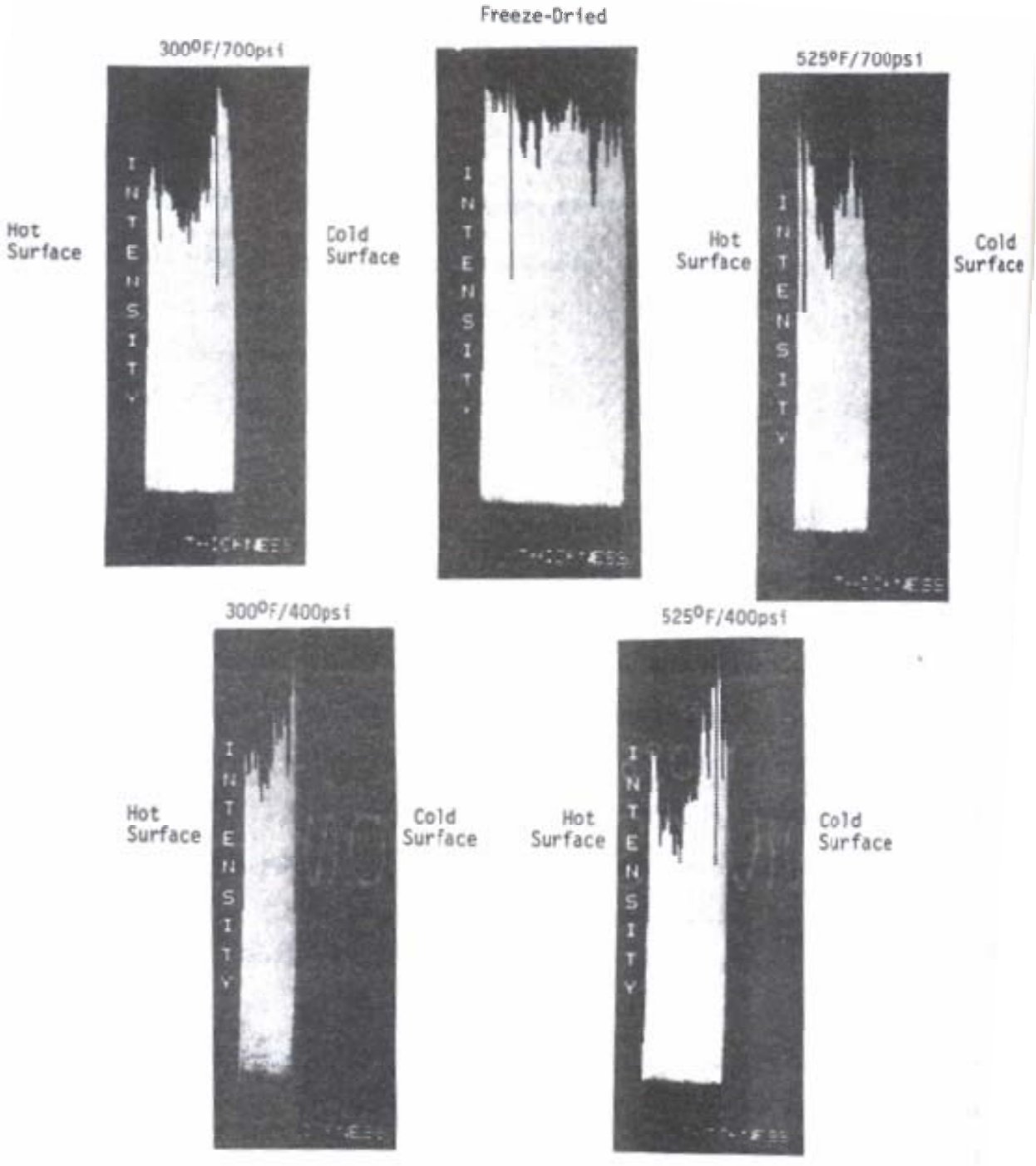

Figure 2.4. Chlorine Distribution Data [5]

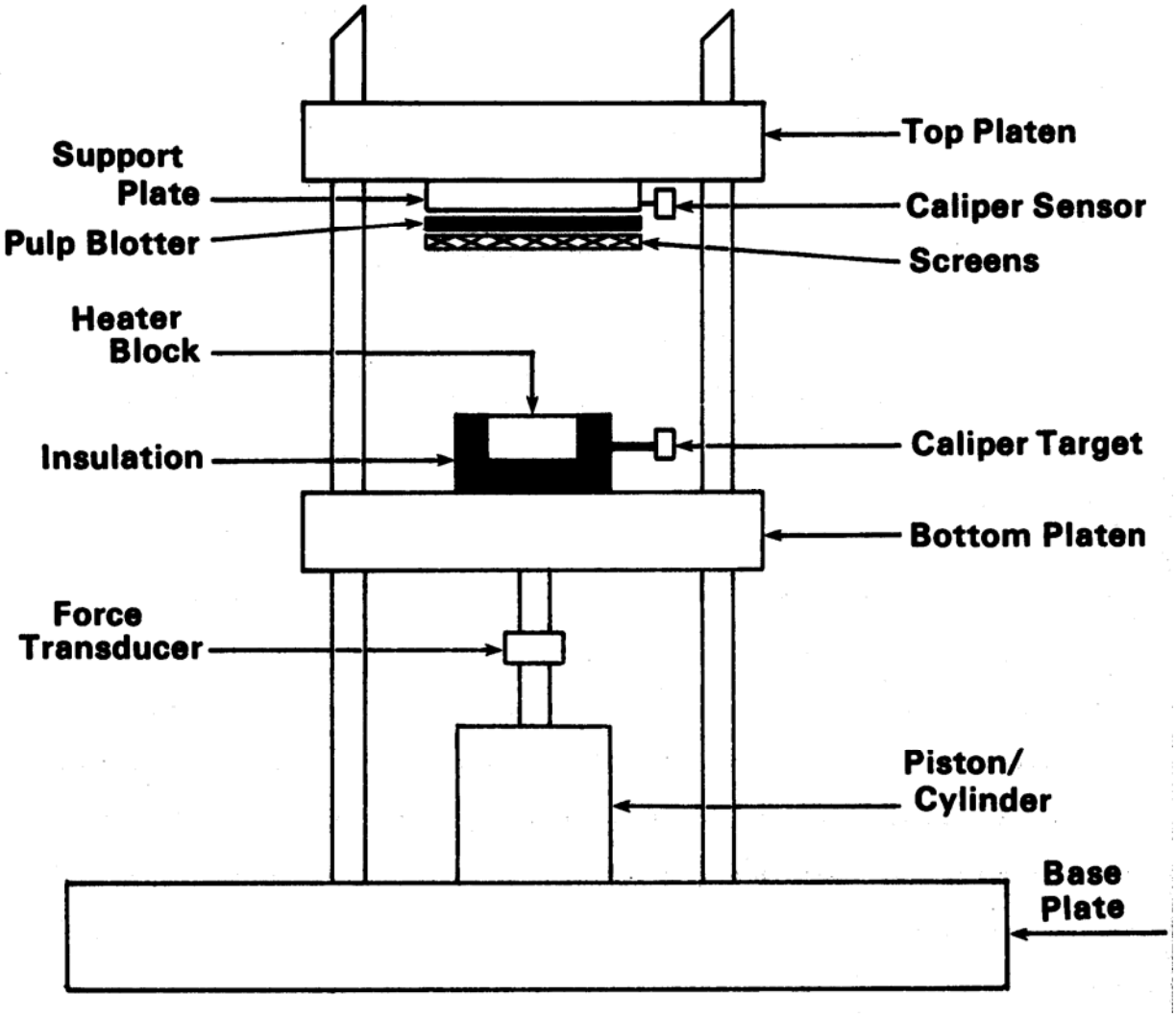

Figure 2.5. Experimental Drying Setup for Chlorine Distribution Determination [5]

Preston and co-workers [6-7] have studied dye migration from drying a uniformly dyed fibrous web. They found that a nonsubstantive dye migrates to a hot surface during drying. The migration is more rapid and pronounced given a higher initial moisture content of the web. The rate of migration decreased greatly when the critical moisture content was reached. These experiments were qualitative in nature. Some of the experiments were performed with a textile web, which was initially dyed uniformly across the web. Other experiments used a stack of filter

paper in which the center sheet was dyed. These results are interpreted by Preston as verification of a vaporization-recondensation cycle occurring within the material during drying. Since a temperature gradient existed, vapor formed at the hot side had a higher partial pressure than the saturation pressure of the remainder of the sheet. Therefore, some vapor condensed in the cooler portions of the sheet. Thus, a cycle was set up with liquid water moving toward the hot surface, vaporizing there, and part of the vapor condensing within the sheet.

Dreshfield [8] performed solute migration studies during drying. These studies were used to show the effects of basis weight, initial moisture content and hot-surface temperature on the final dye distribution in similar sheets. The sheets used for this work were made from Weyerhaeuser bleached sulfite pulp. The sheets for drying were made to the desired basis weight in a British sheet mold and wet pressed together for a desired thickness for later delamination. The basis weights for the sheets ranged from 71-282 g/m^2. Each sheet was air dried to 0.25 g. less than the desired final weight, and then sprayed with 0.25 g. of a solution of 10% dextrinized starch and 6% tartrazine (the selected solute). Each sheet was sealed in a polyethylene bag and allowed to stand overnight at 73˚F before being dried. The initial moisture content of the sheets was 200%. The sheet was dried for the desired length of time to give moisture contents from 200% to 0% moisture content. The hot surface temperature was varied from 189-221°F. The dye from each section was extracted with distilled water. The total extract from each laminate was diluted to a measured volume. The General Electric Recording Spectrophotometer was used to measure the transmittance of the dye solution. The measured transmittance value could then be converted to dye concentration.

In all sheets with constant basis weight, the dye was concentrated at both surfaces, and the zone of minimum dye concentration was at 15-50% basis weight of the sheet, which is

measured from 0% at the air interface (top surface) and 100% at the hot-surface interface (bottom surface). A greater percentage of dye migrated to the surfaces in the sheets of higher initial moisture content. Increasing the hot-surface temperature did not cause a measurable change in the total migration to the surfaces of the sheet, but a greater amount of dye moved to the hot surface and a correspondingly smaller amount to the air surface. The net migration across the midplane of the sheet was greater in the sheet dried at the higher hot-surface temperature. For the sheets with different basis weights but constant initial moisture contents and hot surface temperatures, there was no significant difference in the final dye distribution in sheets of different basis weight.

In all dye migration studies, it was visually obvious that there was a very marked concentration of dye at both surfaces of the sheet. Most of the dye in the upper and lower 15% fractional thickness was concentrated at the air interface and the hot-surface interface, respectively. The dye moved from the interior of the sheet to both the hot and cold surfaces of the sheet. This migration started very early during drying and continued at least part way into the falling-rate period. An interesting finding was the fact that a zone of minimum dye concentration existed within the sheets. The 35% of the sheet just above the midplane contained less dye at all times during drying than did the 35% of the sheet just below the midplane of the sheet.

The general conditions existing within sheets during the constant-rate period and the first part of the falling-rate period are summarized by Figure 2.6. In all sheets studied, the maximum moisture content was found in a zone from 20 to 30% of the distance from the cold to the hot surface. In this same region, a zone of minimum dye content existed. There appeared to be no movement of dye and therefore no movement of liquid water across this zone. Liquid water,

which was initially between this zone and the hot surface, moved toward the hot surface. Liquid water, which was between this zone and the cold surface, moved toward the cold surface. Liquid water movement was in the direction of decreasing moisture content and was predominantly toward the hot surface of the sheet.

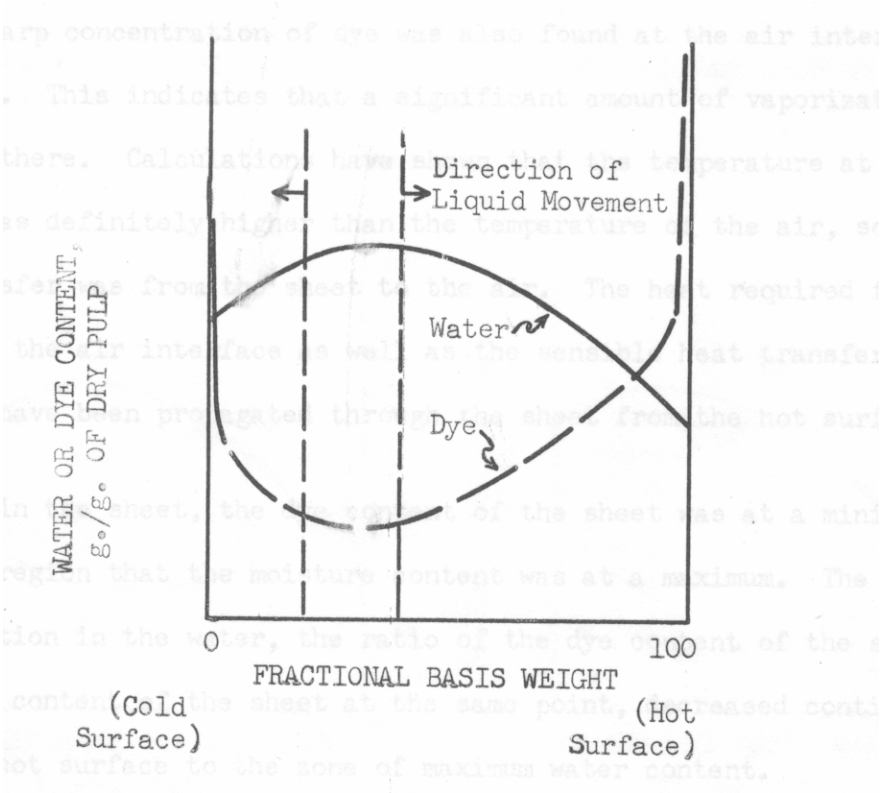

Figure 2.6. Typical Distribution and Movement of Water and Dye Within Sheets During Drying [8]

Water vapor could leave the sheet only at the air interface. Therefore, the liquid water moving to the hot surface must have been vaporized there, and this vapor must have moved back through the sheet in order to escape from the open surface. The sharp concentration of dye right at the hot-surface interface indicates that most of the vaporization occurred right at the interface. A sharp concentration of dye was also found at the air interface of the sheet. This indicates that a significant amount of vaporization occurred there. Within the sheet, the dye content of the sheet

was at a minimum in the same region that the moisture content was at a minimum. The dye concentration in the water, the ratio of the dye content of the sheet to the water content at the same point, decreased continuously from the hot surface to the zone of maximum water content.

The mechanism for explaining the solute transport during drying is vaporization at both surfaces with internal recondensation. Dye was concentrated at the surfaces of the sheet, indicating that liquid water had moved to and evaporated from these regions. Within the sheet, the dye concentration in liquid water decreased continuously from just below each surface to the region of maximum water content, which was also the region of minimum dye content. This indicates that the liquid water originally within the sheet (the water containing dye) must have been diluted with water that did not contain dye. Such water could only be condensate from vapor, which had been formed elsewhere.

2.3 Filler and Fines Movement Induced by Pressing

Szikla and Paulapuro [9] studied the effect of wet pressing on the z-directional distribution of the fines and filler materials. Szikla and Paulapuro [9] extended previous studies done by MacGregor [10] and Busker [11]. While investigating the marking tendency of the suction press roll, MacGregor [10] succeeded in creating conditions where significant amounts of material moved from one place to another in the web. However, this result cannot be considered proof that the fines or filler particles would move significantly under normal pressing conditions. Busker [11] made attempts to determine the fines content in different layers of the sheet before and after wet pressing. No conclusions were drawn from the results due to large scatter inherent in the method.

The sequence of phenomena proposed by Szikla and Paulapuro [9] was that viscous drag of the flowing water tends to create movement in the network material. Consequently, the water

flow compresses the fiber network. The more rapid the flow the higher the compression force is and vice versa. This can cause a permanent z-direction density gradient in the web. The bonds between the network elements are not yet well developed under wet pressing conditions. The flowing water can separate particles from each other. The separated particles can be transported to new positions or out of the web. Thus, it is conceivable that the material composition can change in the z-direction of the web.

For studying the movement of fines, sheets were made by mixing the fibrous fractions obtained by the Bauer McNett classification. The fines material was either fraction –200 or –325 of the Bauer McNett classifier. The pressure was increased step-wise until the sheet was crushed in the final test. The flow velocity created by the pressure reached a maximum of 3.5 m/s on the web surface not in contact with the press. This flow velocity only maintained for a short time, the average velocity being 0.1 to 0.3 m/s, during the water removal pulse. In these tests about one third of the water initially contained by the samples was removed. The water always flowed through the layers containing most of the fines, i.e. through the wire side of the sheet. The solids content before and after pressing was 18.5-20.8% and 32.2-40.0%, respectively. After pressing, the sheets were split into 9 layers by a Beloit Sheet Splitter.

The data for the fines distribution tests are shown in Figure 2.7 for paper made from chemical and mechanical pulps. There are no statistically significant differences between the distributions. In the confirmative tests, the water removed from the sheets was filtered through a membrane filter with openings of 0.45 μm. Only a few fines particles were collected in the filter, which showed that the water removed from the sheet contained little fines material. There were no big differences in the amounts of fines material collected in the different tests. Only a slight

fractionalization could be seen, even when the web was crushed by excessively rapid water removal.

Test sheets were also made with different filler particles with 0.6-6.0 μm diameter in a sheet mold. After pressing, the sheets were split into 6 layers with a Beloit Sheet Splitter and the filler content of each layer was determined from the ash content. The first observation from the filler distribution tests was that the water removed from the sheets was milky and that filler particles were gradually collected in the felts used, which turned white. Measurement of the filler distributions showed that this observation was misleading. In most cases, no significant changes were discernible in the z-distribution of the filler material. Small filler particles are already able to change the color of the water in very small concentrations. In the study by Szikla and Paulapuro [9], movement of filler or fines was only detectable when the following conditions were met simultaneously:

- The flow velocity in the z-direction was at a maximum in layers which contained high amounts, 30-50%, of filler material, i.e. on the wire side of the sheet.
- The fiber network was very loose.
- The size of the particles was 2.7 μm or less in diameter.
- The state of the fibers of which the network is composed was smooth and unfibrillated.

Simultaneous fulfillment of all the above conditions is very unlikely in practice. The consistent findings of the study by Szikla and Paulapuro [9] is that the flows normally prevailing in a sheet under wet pressing can only move small particles in the fiber network, and even those only in special circumstances. These special circumstances can occur possibly in the initial phases of the wet pressing. When filler movement could be detected, it always occurred so that

the filler content was lower compared with the original distribution and the difference increased in the direction of the flow.

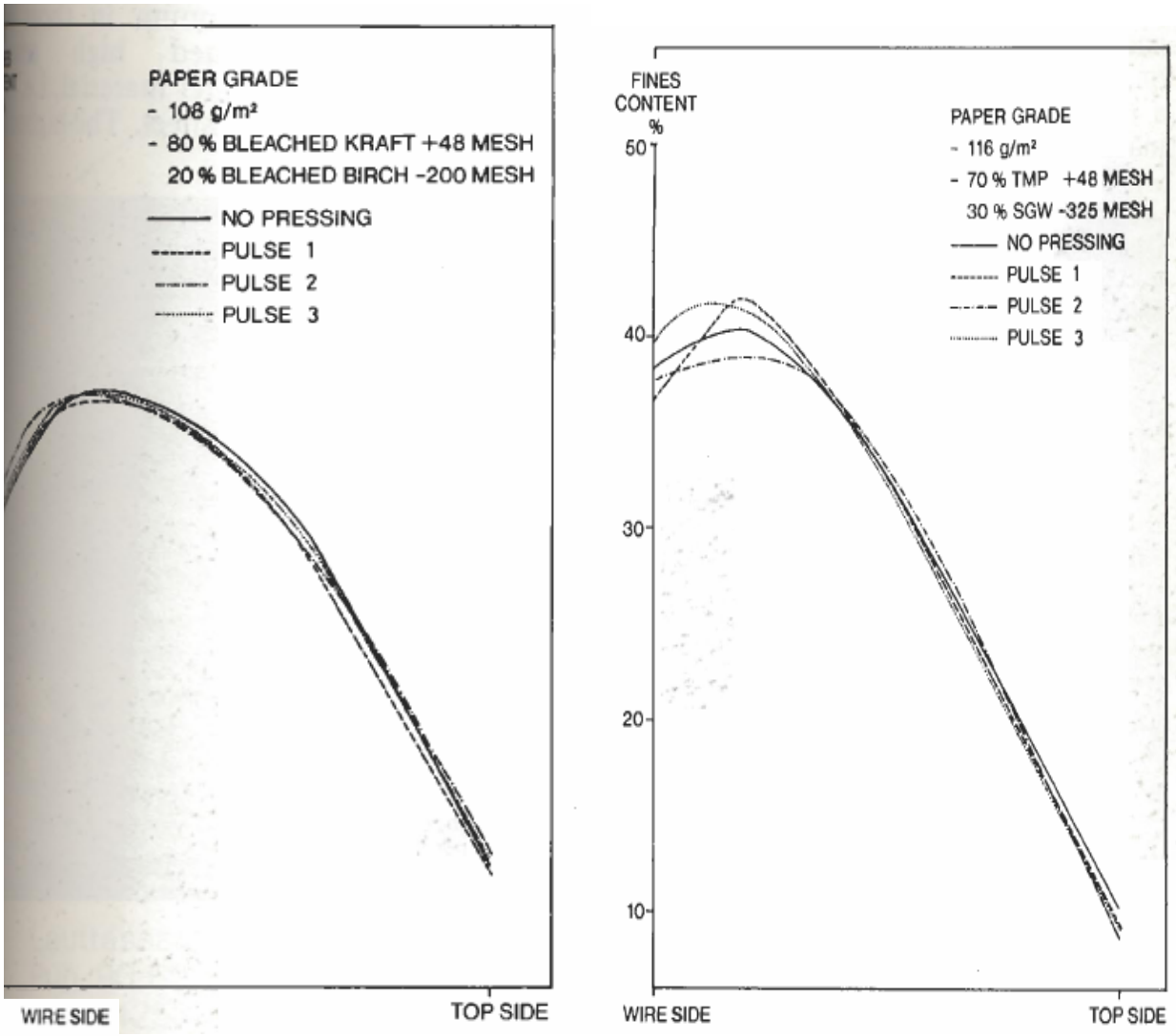

Figure 2.7. Effect of Different Press Pulses on the z-directional Fines Distribution of Paper Made from Chemical (left) and Mechanical (right) Pulps [10]

2.4 Microsphere Transport through Packed Granular Columns

Studies have also been done outside the paper field on the flow of particles and fluid in porous media. In these experiments the porous media has been a packed soil or bed of glass beads. Li et al. [13] hypothesized that physical straining caused enhanced deposition at the

influent end of the column on the basis that deposition was favored by larger particle diameters and smaller collector diameters. The objective of their paper is to describe a series of experiments examining the transport of carboxylated latex microspheres in glass beads under various flow and ionic strength conditions. The intent of the experiments was to examine trends in the simulated deposition and re-entrainment parameters and their relationship to interaction forces and hydrodynamic drag. The microspheres used in column experiments were spherical fluorescent carboxlate-modified polystyrene latex microspheres of two similar sizes but different surface charge densities (1.1 and 1.0 μm diameter). The influent concentration was 3.5×10^6 ±15% particles-mL^{-1}. Spherical soda lime glass beads were used as the porous media. The beads were in sizes ranging from 417 to 600 μm. The cylindrical plexiglass columns were 20 cm in length and 3.81 cm in inner diameter. Column effluent samples were collected. Following the experiment, the sediment was dissected into 10 2 cm-long segments, as the sediment was released from the column under gravity. These samples were analyzed using flow cytometry. A one-dimensional discrete random-walk particle-tracking model was used to simulate colloid transport in the column experiments.

Mass recoveries (total from effluent and sediment) were virtually all between 89% and 107%, with the vast majority showing between 95% and 105% recovery. Although the effluent and retained concentrations were adjusted to yield 100% mass balance for the simulations, these adjustments were small as a result of the good mass balance and would not affect the analysis presented by Li et al [13]. Figure 2.8 shows the retention profiles for different ionic strengths at a constant flow rate and using the 1.1-μm microspheres. The error bars represent standard deviations in results from replicate experiments (n = 2). Simulations using the particle transport

model with a single deposition rate coefficient (single k_f, linear profile) are contrasted against those using a deposition rate coefficient distribution (distributed k_f, nonlinear profile).

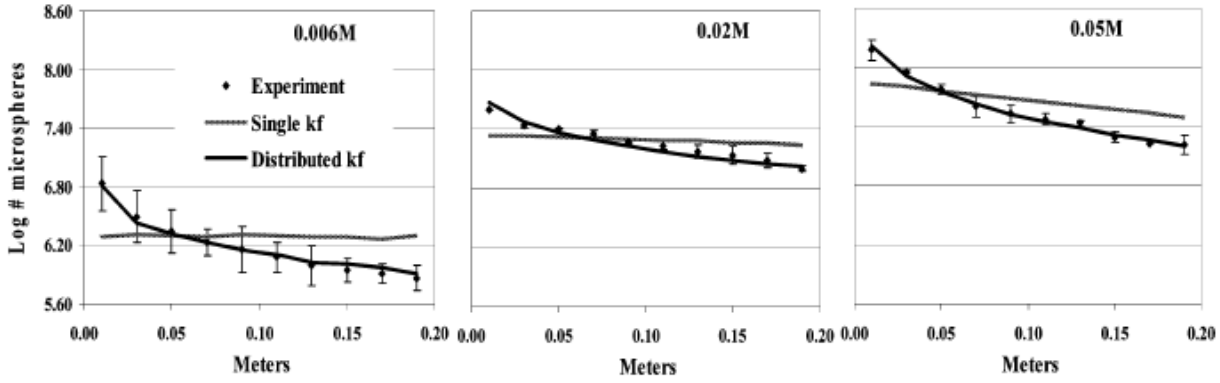

Figure 2.8. Ionic Strength Series for 1.1 μm Microspheres at Flow Rate = 4 m-day^{-1} Showing Retained Profiles [13]

Figure 2.9 shows the retained profiles for different flow rates at a constant ionic strength using the 1.1 μm microspheres. Simulations are shown using the particle transport model with and without k_f distribution (nonlinear and linear profiles, respectively).

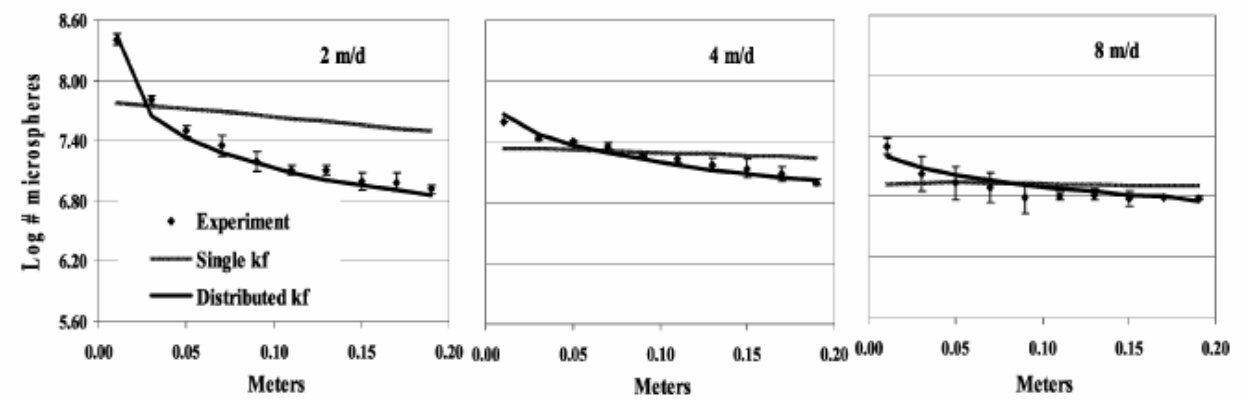

Figure 2.9. Flow Rate Series at Ionic Strength = 0.02M for 1.1 μm Microspheres Showing Retained Profiles [13]

Figure 2.10 shows the retained profiles for the 2 particle sizes at a constant ionic strength and flow rate. Simulations are shown using the particle transport model with and without k_f distribution (nonlinear and linear profiles, respectively).

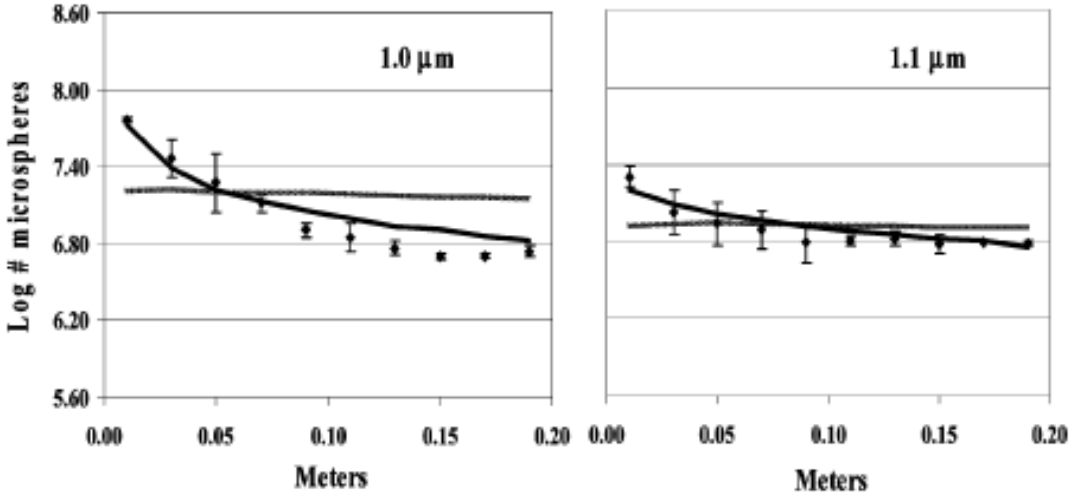

Figure 2.10. Comparison of the Retained Profiles for the 1.0-µm and 1.1-µm Microspheres at Ionic Strength = 0.02M and Flow Rate = 8 m-day^{-1} [13]

The total number of microspheres retained increased with increasing ionic strength shown by the upward shift of the profiles in Figure 2.8. The total number of microspheres retained increased with decreasing flow rates as shown by the downward shift of the profiles in Figure 2.9. The particle transport model was able to simulate the number of particles that passed completely through the column and ended up in the effluent regardless of whether the deposition rate coefficient used was constant or a distribution. However, the retained profiles of microspheres could not be simulated using a constant rate coefficient of deposition. Simulations using a distribution of deposition rate coefficients were capable of fitting the retained profiles well (Figures 2.8-2.10).

Figure 2.11 shows the retained profiles of amine-modified microspheres (0.93 µm) at 2 different flow rates and a constant ionic strength. The total injected number was normalized to

the average total injected number of carboxylated microspheres (3.5 x 10^6 particles-mL^{-1}). In contrast to those of the carboxylated microspheres, retained profiles of the amine-modified microspheres could be simulated using a single deposition rate coefficient.

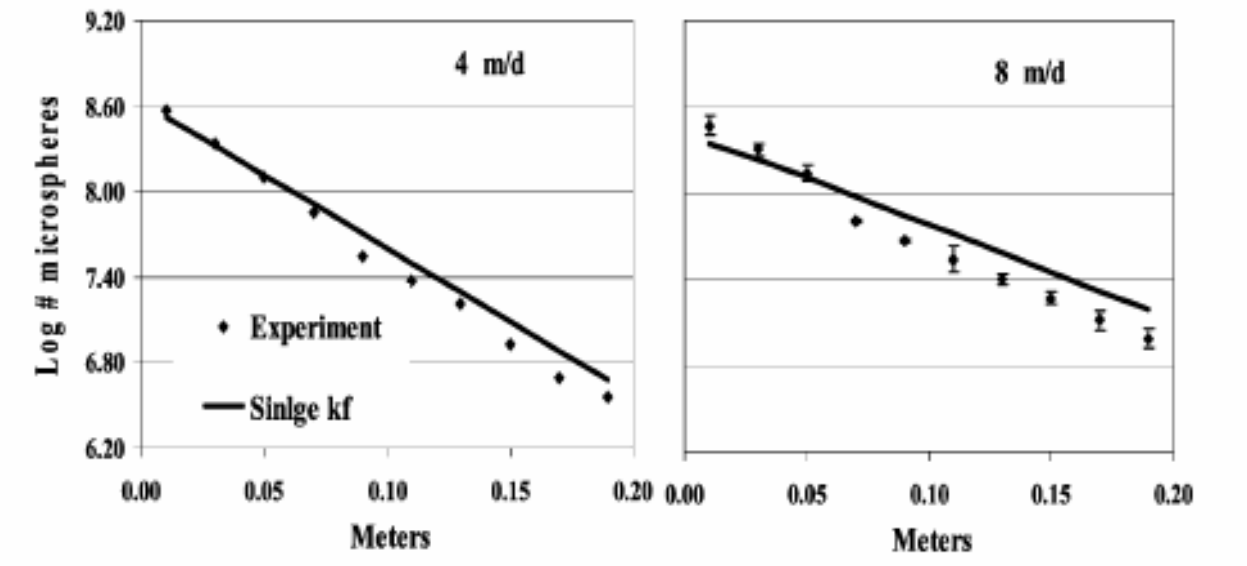

Figure 2.11. Retained Profiles of Amine-modified Microspheres at Flow Rate = 4 m-day^{-1} and 8 m-day^{-1} at Ionic Strength = 0.001 M [14]

The generality of apparent decreases in deposition rate coefficient with increased transport distance among nonbiological and biological colloids indicates control by processes that are fundamental to filtration under unfavorable conditions (no induced electrostatic charge on particles to make them more attracted to the porous medium). Although straining may be a significant contributor to decreases in deposition rate coefficient with increasing transport distance at low ionic strength, it is a minor contributor at high ionic strength where much greater overall retention is observed. Interaction between charged particles and the porous media remain a viable contributor to decreased particle deposition with increasing transport distance.

Camesano et al. [14] developed a filtration-based model explicitly accounting for blocking that could be used to predict the effect of influent colloid concentration on the

deposition of colloids in porous media. Using the model and column experimental data, it was demonstrated that blocking occurred to differing extents for several different colloids. The model was used to demonstrate that blocking could result in enhanced transport of bacteria in porous media.

Solutions to an advection-dispersion equation for colloid transport and/or colloid filtration models are typically used to quantify the deposition of colloids in porous media [15-19]. Model calculations are performed by assuming that the rate of colloid deposition is independent of previously attached colloids. However, this assumption is only valid for initial deposition rates, when the particles are deposited onto clean collectors. The deposition rate may decrease rapidly as particles start to accumulate on the collectors [20]. One explanation for this drop in deposition rate is that as the fraction of the surface covered by colloids increases, deposited colloids may prevent the further attachment of colloids due to a process termed blocking [21]. When blocking is occurring, an attached particle reduces the area available for deposition by an amount that is greater than the projected area of the particle [20]. In some systems, an alternate process (filter ripening) occurs when attached particles can act as additional collectors for attachment by forming multi-layer films [20,22-23].

In a prior bacterial transport study, injecting higher concentrations of *Burkholderia cepacia* G4 into porous media columns led to an enhancement in transport, which was attributed to blocking [24]. This occurred even when the fractional surface coverage in portions of the column was much lower than that previously reported to demonstrate blocking. Ripening accounted for the deposition of *Pseudomonas fluorescens* P17 in porous media columns [24], as multi-layer deposition appeared to occur at a surface coverage that was <1% (assuming homogeneous spherical collectors). It is well known that injection concentration affects bacterial

retention in soils [25-26], but these previous studies have not considered blocking as an explanation.

For Camesano et al. [14], two types of microspheres differing in charge densities were used. Fluorescent carboxylated latex microspheres (CL) with a 0.97 μm diameter and fluorescent carboxylated (modified) latex microspheres with diameters from 0.97 to 1.0 μm were used for this study. Microspheres with negative charges but differing degrees of surface charge were chosen to mimic bacterial cells, which overall are negatively charged, but to different extents. The microspheres were washed twice in low ionic strength water and suspended in a sterile KCL solution.

The soil used in these studies was a southern Arizona soil, with an average equivalent particle diameter of 127 μm. Soils were packed dry and without pretreatment into glass columns that were 7 cm long and 1.5 cm in diameter. The column media was extruded from the column at the conclusion of each experiment and sliced into 1 cm increments to determine deposition as a function of column length. The increments were put in solution and the concentration of spheres was determined using 0.2 μm polycarbonate filters or spectrophotometrically.

The low cell injection used in the simulation (N = 6.38 x 10^8 or 4.4 x 10^7 cells per dry g soil) was not high enough to produce blocking, while the higher injection (N = 4.55 x 10^{10} or 3.09 x 10^9 cells per dry g soil) was sufficient to cause blocking. A blocking model for colloidal deposition under unfavorable conditions was developed and applied to latex microspheres and bacteria at low surface coverages. The bacteria and microspheres studied exhibited blocking, due to their negative charge, the relatively low ionic strength of the suspending phases, and the heterogeneity of the soil. The model was used to illustrate the effect of blocking on bacteria

transport. Using a concentration of cells that is great enough to produce blocking can be advantageous in enhancing the transport of bacteria in bioaugmentation experiments.

2.5 Motion of Sphere through Cylindrical Tube

On the most basic level, the movement of small particles through a sheet of paper could be modeled as the motion of a single sphere, representing the particle, moving through a cylindrical tube, representing a pore in the sheet. The motion of a sphere in a cylindrical tube filled with a Brinkman medium has been modeled based on the geometry of the system by Sugihara-Seki and Masako [27]. A Brinkman medium is a material characterized by a Newtonian viscosity μ and a hydraulic resistivity K, which is kinematic viscosity divided by the product of the permeability and the gravitational acceleration, and was originally derived for evaluating the force exerted by a flowing fluid on a swarm of particles (Brinkman [28]). The geometry of the system is shown in Figure 2.12.

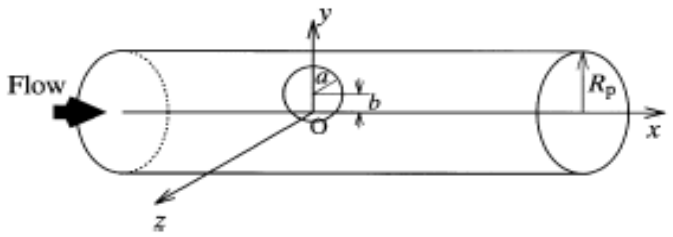

Figure 2.12. Geometry of a Sphere in a Circular Cylindrical Tube [29]

A no-slip and no-penetration boundary condition was used on the wall of the tube and the particle surface. In the absence of the particle, flow is driven by a pressure drop along the x-axis. This is shown in Figure 2.13 where u_0/V is the velocity relative to the mean velocity, V, and r/R_p

is the radial position relative to the radius of the tube. The parameter $\alpha = R_p\sqrt{(K/\mu)}$ represents the ratio of the tube radius to the representative thickness of the velocity-varying layer in the Brinkman medium.

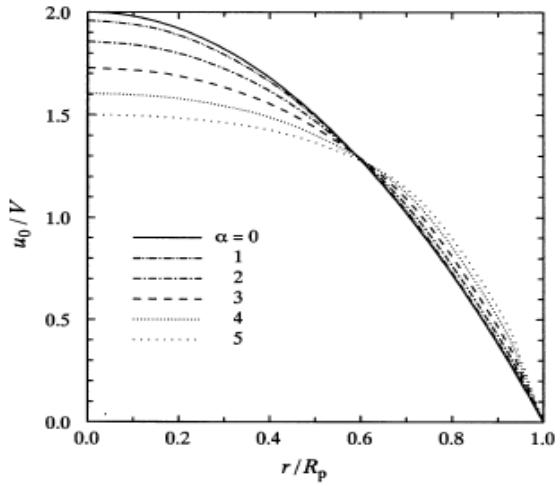

Figure 2.13. Velocity Profile of a Brinkman Medium Driven by a Pressure Gradient Along the Centerline Through a Circular Cylindrical Tube [29]

It is shown that for a larger α, the velocity profile gradually approaches plug flow and the effect of the tube wall is confined to a limited region closer to the wall. Figure 2.14(a) shows that, as α increases from 0 for constant a/R_p and b/R_p, a small particle (a/R_p = 0.3) has a smaller translational velocity when it is placed near the centerline of the tube, while it has a larger velocity close to the tube wall. This tendency is in accordance with that of the medium velocity of the undisturbed flow shown in Figure 2.13. On the other hand, particles with a size ratio a/R_p larger than approximately 0.5 translate faster for larger α over the range of b/R_p examined. In addition, the translational velocity of a large particle (a/R_p = 0.7) decreases only slightly with increasing radial position, b/R_p, until they approach the tube wall very closely. This behavior is

also reported for a large particle floating in a tube flow of a Newtonian medium (Sugihara-Seki and Skalak [29]).

A comparison of the translational velocity of the force-free and torque-free particle in Figure 2.14(a) with the velocity profile of the medium far from the particle in Figure 2.13 indicates that the particle translates even faster than the undisturbed medium velocity at the center of the particle when α is larger than a certain critical value. The critical value of α depends on the size ratio a/R_p and the radial position b/R_p, and it decreases for smaller a/R_p and/or smaller b/R_p.

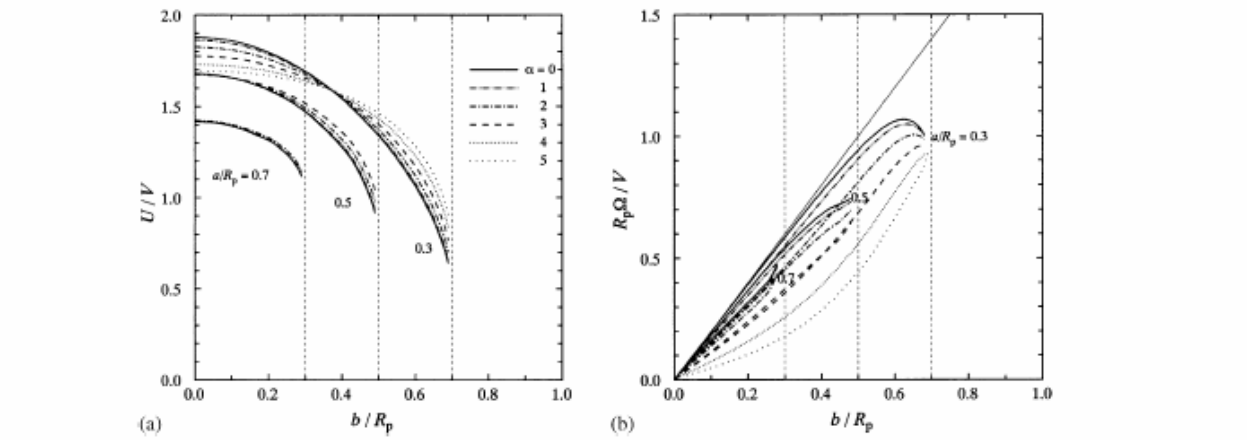

Figure 2.14. (a) The Translational Velocity of a Freely Floating Sphere in a Tube Filled With a Brinkman Medium, Normalized by a Mean Flow Velocity Over a Cross-section of the Tube. (b) The Normalized Angular Velocity of a Freely Floating Sphere [29]

Figure 2.14(b) shows that the angular velocity of the force-free and torque-free particle normalized by a representative shear rate V/R_p. For comparison, one-half of the velocity gradient of a Poiseuille flow, which corresponds to the angular velocity of a spherical particle freely suspended in a Newtonian fluid in the limit of $a/R_p \rightarrow 0$, is plotted in Figure 2.14(b) as thin straight line. It is seen that for smaller values of α, particles as large as $a/R_p = 0.7$ have a normalized angular velocity only slightly smaller than that of very small particles, when it is not placed very close to the tube wall. As α increases for constant a/R_p and b/R_p, the angular

velocity of the particle decreases, which may be easily understood from the velocity profile of the undisturbed medium flow shown in Figure 2.13.

Sugihara-Seki and Masako [27] noticed that a free-floating particle travels faster than the undisturbed medium velocity at the center of the particle when α is larger than a critical value because an increase in α increases negative pressure exerted on the downstream half of the particle surface and positive pressure on the upstream half. A marked enlargement of pressure variation with increasing α propels the particle forward, which makes the particle velocity faster than the medium velocity of the undisturbed flow.

2.6 Conclusions from Literature Review

The literature reviewed gave a preview of the results expected in the particle transport experiments that were performed. The experiments in the literature showed the general trends of particle and dye distributions across the thicknesses of different porous media. The concentration of particles at the wire side of a handsheet is larger than the concentration of particles on the top side. However, the different paper machines from the study by Kilpelainen and Schlegel [4] show that the concentration of particles at the top is greater than the concentration at the bottom, or wire side. These results match with the experiments of particles through soil columns where more particles are found at the top of the column than at the bottom. The dye distribution experiments show that water tends to travel to either the top or bottom surface of the sheet to evaporate. The higher concentration of dye at the bottom of the sheet showed that the majority of the evaporation took place at the heated surface.

A pressing experiment was done by Szikla and Paulapuro [9] to try and change the filler distribution in a sheet. They found that fines or filler particles do not move across the thickness of a sheet if the sheet was subject to conditions normally found on a paper machine. The

particles had to be 2.7 μm or less in diameter and the sheet needed to have an open structure. The sheet would have to be subjected to a large pressing force. The experiment by Szikla and Paulapuro [9] showed that it would be difficult to produce any change in particle distribution without specific initial conditions.

The mechanisms for how particles move through porous media found in the literature were a basis for what kind of phenomena would be expected in the particle flow experiments. Size exclusion and blocking mechanisms contributed to how effectively microspheres moved through packed soil columns. The fluids model of a particle in a cylindrical tube proposed by Sugihara-Seki and Masako [27] demonstrated that particle velocity in a tube is dependent on the particle diameter in relation to the tube diameter and the particle position relative to the center of the tube. The main conclusion from this study was that a particle could move faster than the bulk flow velocity when the particle diameter is 50% of the tube diameter. For the particle flow experiments, it is possible that filler particles could move even though the fluid velocities due to evaporating water are small.

CHAPTER 3

EXPERIMENTAL METHODS

3.1 Introduction

The experiments performed can be separated into four categories: G-800, G-200, PCC and PCC/Dye experiments. These main categories are subdivided into tests performed using the four main filler materials. The G-800 and PCC experiments consisted of two different types of tests and the G-200 and PCC/Dye experiment consisted of a single type of test. The goals of each test were to determine whether there was a change in filler or dye distribution through the thickness of a sheet between a sheet that was air-dried and a sheet dried on a heated surface. The procedures were designed to show a large change in filler or dye distribution between the two drying conditions thus producing outer bounds for the parameters that would induce particle and dye flow through a sheet. By analyzing a change in filler or dye distribution, methods for contaminant transport through a sheet during drying could be proposed.

The sections of Chapter 3 are divided by the major steps taken to produce a sheet, dry the sheet, and split the sheet into sections to determine the filler and dye distribution through the thickness of the sheet. The sections include pulp preparation, filler preparation, handsheet making, drying the sheets, splitting the sheets, and ashing the sheets. Procedures for aquiring data necessary for mass balances are described in the section about ashing of laminate tape. Details of how the raw data are converted into meaningful experiments results is described in the calculations section. The test for which a certain procedure is used is denoted in that section describing the procedure.

3.2 Pulp Preparation

The following procedure was used to prepare the pulp and determine the consistency of the pulp before the various types of handsheets were made. The handsheets for all tests were made using the pulping procedure described in this section. A southern softwood (albawood) once dried market pulp was used. The dried board was wetted and torn into ~1 in^2 pieces in a standard disintegrator (Noram L-3200) shown in Tappi T205 sp02. The pulp was disintegrated at 3000 rpm for 10,000 revolutions in tap water. The pulp was disintegrated at a consistency between 0.5-0.7%.

Three handsheets from this stock pulp were made to determine the actual consistency of the pulp. 250 mL of stock pulp was measured with a 250-mL graduated cylinder with 2-mL resolution to make the handsheets. These handsheets were made on a standard cylindrical handsheet mold according to the procedure in TAPPI T205 sp02. The only modifications to this procedure were that the sheets were not pressed and they were dried on a steam cylinder to save time in determining the dry weight of the sheets. The dried handsheet was weighed on a digital mass balance with 0.001-gram resolution. The weights were recorded for three handsheets. Consistency is defined using Equation (3.1), where m_{fiber} is the mass of the fiber and m_{water} is the mass of the water.

$$\%\,\text{consistency} = \frac{m_{\text{fiber}}\,[\text{g}]}{m_{\text{fiber}}\,[\text{g}] + m_{\text{water}}\,[\text{g}]} \times 100\% \tag{3.1}$$

For low consistencies used in these experiments, the assumption in Equation (3.2) is made.

$$m_{\text{fiber}} << m_{\text{water}} \tag{3.2}$$

The consistency is approximated as shown in Equation (3.3)

$$\%\,\text{consistency} = \frac{m_{\text{fiber}}}{m_{\text{water}}} \times 100\% \tag{3.3}$$

The denominator of Equation (3.3) can be rewritten as shown in Equation (3.4), where ρ_{water} is the density of water and V_{water} is the volume of water.

$$m_{water} = \rho_{water} V_{water} = \left(1\,\mathrm{g}/\mathrm{cm}^3\right) V_{water} \tag{3.4}$$

Therefore, using the average dry weight of the three handsheets and the volume of pulp used to make the handsheets, an average consistency of the stock pulp can be computed using Equation (3.5).

$$\%\,\mathrm{consistency} = \frac{m_{fiber}\,[\mathrm{g}]}{V_{water}\,[\mathrm{mL}]} \times 100\% \tag{3.5}$$

3.3 Filler Preparation

3.3.1 Microsphere Slurry

Two different types of microspheres were used for the particle movement study experiments. Both tests for the G-800 experiment and the one test for the G-200 experiment used the microsphere slurry procedure to prepare the respective filler particles for addition to the handsheets. The specifications for each type of microsphere are given in Table 3.1.

Table 3.1. Microsphere Specifications

Manufacturer	Type	Density [g/cm^2]	Material	10%	50%	90%
3M	Zeeospheres G-200	2.5	Ceramic	1 μm	4 μm	10 μm
3M	Zeeospheres G-800	2.2	Ceramic	2 μm	18 μm	75 μm

To make the slurry for addition into the handsheet mold, 1 gram of solid filler particles was weighed on a 0.001-gram resolution mass balance. This mass of filler particle was then added to

a pitcher containing 30-40 mL of tap water. This mixture was made to make the addition of filler particle to the handsheet mold quick and efficient.

3.3.2 PCC Solution

The procedure for the PCC solution was used to prepare the PCC for both tests in the PCC experiment. An unknown concentration of PCC solution (Albagloss S) was diluted with tap water into a large container. The specifications for PCC are given in Table 3.2.

Table 3.2. PCC Specifications

Name	Density [g/cm^2]	Material	Aspect Ratio	20%	50%	90%
Albagloss S	2.71	Calcite	~1.5 to 2.0	0.4 μm	0.6 μm	1.0 μm

Figure 3.1 shows these PCC particles.

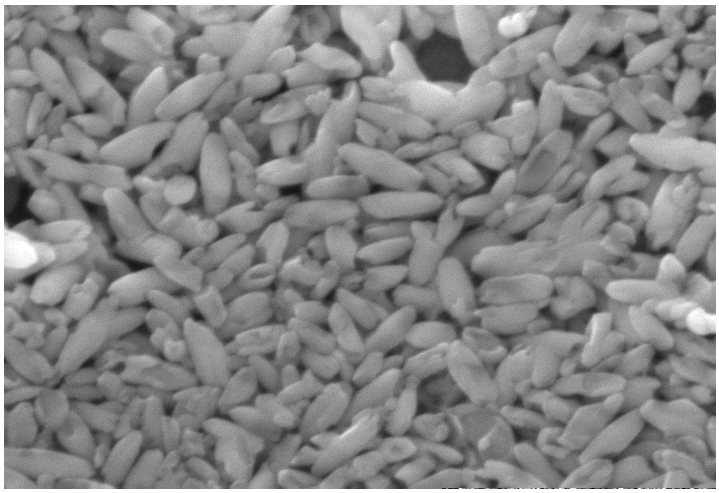

Figure 3.1. Albagloss S (PCC)

A mechanical stirrer was used to keep the mixture uniform. Three clean pyrex dishes were weighed on a 0.001-gram resolution mass balance and the mass was recorded. A volume of 5

mL was measured with a 10 mL graduated cylinder with 0.2 mL resolution. The 5 mL of PCC solution was poured into the pyrex dish and this combined mass was weighed on the 0.001 gram resolution mass balance. The sample dishes were placed in an oven and dried until only the solid PCC remained in the dishes. The dishes were removed from the oven and weighed again on the 0.001-gram resolution mass balance. The three masses were used to calculate the volume of liquid needed to give 1 gram of solid PCC. The data for determining the concentration of the PCC solution is given in Table 3.3.

Table 3.3. PCC Solution Masses

Pyrex dish	Dish mass [g]	Solution mass [g]	Solid mass [g]	PCC mass [g]	Average PCC mass [g]
Green	33.602	39.151	34.602	1.000	0.994
Blue	44.325	49.955	45.332	1.007	
Yellow	32.763	38.192	33.738	0.975	

By taking the average solid PCC mass in 5 mL of solution, the amount of solution needed to give 1 gram solid PCC is found using Equation (3.2).

$$1\,\text{g PCC} \times \frac{5\,\text{mL PCC solution}}{0.994\,\text{g PCC}} = 5.03\,\text{mL PCC solution} \tag{3.2}$$

5 mL of PCC solution was measured in a 10 mL graduated cylinder with 0.2 mL resolution for the PCC Test 1. Since the retention for this experiment was poor, 10 mL of solution was measured for the PCC Test 2 to give 2 grams solid PCC.

3.3.3 PCC and Dye Mixture

The PCC/Dye solution procedure was used in the one test for the PCC/Dye experiment. To create the PCC/Dye solution, 10 mL of the PCC solution was measured to give 2 g of solid

PCC. The stock dye solution was made by measuring 10 mL of red food coloring dye (non-substantive) with a 10 mL graduated cylinder with 0.2 mL resolution. This volume of dye was added to 90 mL of water that was measured in a 100 mL graduated cylinder with 1 mL resolution to yield a 100 mL stock dye solution. From this stock dye solution, 30 mL is measured with a 50 mL graduated cylinder with 1 mL resolution. To make the PCC/Dye solution, the 10 mL of PCC solution is mixed with the 30 mL of the dye solution. This slurry is mixed and put in a syringe to be added to the handsheet during the drying part of the PCC/Dye test.

3.4 Handsheet Making with Filler Added to Handsheet Mold

The appropriate volume of pulp was measured in a 1000-mL graduated cylinder with 10-mL resolution to give 4 grams dry weight of fiber (200 g/m^2) using the consistency found in Section 3.2 (pulp preparation procedure). Water was added to the handsheet mold until the level was ~1 in. above the wire. The pulp was added to the handsheet mold and then the handsheet mold was filled to a specific level. Originally the handsheet mold was filled all the way to the top line. The level was lowered so that there would be less force pulling the particles through the sheet with the intent of improving retention. Another method to slow drainage and possibly improve retention was using a wire with a smaller mesh size. A 70-μm teflon mesh screen was placed on top of the 100 μm wire mesh screen for some of the experiments to slow drainage and improve filler retention. Table 3.4 gives the water level and wire mesh size for each test for the four main experiments. After the appropriate level of water was added, the pulp mixture was stirred with a standard stirrer as in TAPPI T205 sp02 to mix the pulp solution in order to get a uniform random sheet to form on the wire. Immediately after the mixture in the handsheet mold was stirred, the filler particle slurry or the PCC solution was quickly poured into the top of the

handsheet mold with effort made to transfer the entire particle mass to the mold and to uniformly distribute the mixture over the surface.

Table 3.4. Water Level and Mesh Size for Particle Movement Tests

Filler Particle	Test Number	Water Level [in. above wire]	Wire mesh size [μm]
G-800	1	Standard line	100
G-800	2	5	100
G-200		7.5	70
PCC	1	7.5	100
PCC	2	7.5	70
PCC/Dye		7.5	70

The PCC/Dye solution was not added to the handsheet mold as with the other tests. The addition of the PCC/Dye solution for the PCC/Dye test is described in the Section 3.7.4 (Drying sheets for PCC/Dye mixture). The mold was drained after the slurry was added so that the filler particles would not settle out of the handsheet mold. Rather, they would be retained in the forming sheet as the water drained. The wet sheet was allowed to sit on the wire for ~5 minutes so that adequate bonding would occur to allow the wet sheet to be removed from the wire by hand. The wet sheet was carefully peeled off the wire by hand and placed in a plastic bag with the wire side clearly labeled. The wet sheets were stored in a refrigerator until the drying portion of the experiment was performed.

3.5 Solids Content of the Wet Sheet

Five handsheets were made to determine the solids content of the wet sheet. These sheets were made following the procedure for PCC Test 2 without the addition of PCC. The entire

uncut wet sheet was weighed in the crucible so that the solids content could be measured. The sheet was then dried to 100% solids and weighed. The data for the solids content of each wet sheet is shown in Table 3.5.

Table 3.5. Percent Solids in Handsheets

Sheet Number	Fiber mass [g]	Water mass [g]	% Solids
2	4.2143	41.0240	9.32
3	4.1143	40.6646	9.19
4	3.7551	36.8605	9.25
5	4.0637	39.3971	9.35
6	3.8471	36.6483	9.50

3.6 Mass and Ash Percent of 5 in. Diameter Laminate Tape

The mass of the laminate tape and its ash percentage needed to be determined so that a complete mass balance could be performed on samples where the laminate tape attached to the split was ashed. All tests except for G-800 Test 1 had laminate tape ashed along with the split. Two handsheets were made on a standard cylindrical handsheet mold according to TAPPI 205 sp02 except that the handsheets were dried on a steam cylinder to save time. The two handsheets were cut into 5 in. diameter circles using the precision die cutting machine. The dry handsheets were weighed on a 0.001-gram resolution mass balance and the masses were recorded. The handsheets were laminated with the 3M dual laminating system, which laminates a sheet on both sides. The excess laminate tape was trimmed off with scissors so that only a 5 in. diameter piece of tape remained on both sides of the sheet. Trimming with scissors was used for the preparation of the split for ashing in Section 3.9 so there is consistency in the procedures used. The 5 in. diameter laminated sheet was weighed on a 0.001-gram resolution mass balance and the mass

was recorded. From these masses, the average mass of a 5 in. diameter piece of laminate tape can be determined. Table 3.6 shows the recorded masses and the computed mass of the laminate tape.

Table 3.6. Mass of Laminate Tape

Sheet number	Dry sheet [g]	Sheet and double laminate [g]	5 in. diameter laminate tape [g]	Average mass of 5 in. diameter laminate tape [g]
1	0.785	2.543	0.879	0.882
2	0.764	2.533	0.885	

Since it cannot be assumed that there are no inorganic materials in the laminate tape, 5 samples of laminate tape were ashed. Dry clean crucibles were weighed on a 0.0001-gram resolution mass balance and the masses were recorded. A piece of laminate tape was placed in each crucible and the combined mass was measured and recorded using a 0.0001-gram resolution mass balance. The crucibles are placed in the muffle oven and ashed according to the following program:

1. Ramp oven to 105°C
2. Hold at 105°C for 5 minutes
3. Ramp oven to 225°C at 10°C/min
4. Hold at 225°C for 15 minutes
5. Ramp oven to 325°C at 2°C/min
6. Ramp oven to 525°C at 5°C/min
7. Hold at 525°C for 2 hours.
8. Ramp oven to 105°C (~1.5-2 hours for this step).

The crucibles are removed from the oven and placed in a dessicator for 15 minutes to allow them to cool. The crucibles are weighed on a 0.0001-gram resolution mass balance and the mass is recorded. If the ash has black specks in it, the sample is put in the muffle oven again until all organic material is removed from the sample. From the various masses recorded, the mass of the tape and ash in the tape can be determined. Table 3.7 shows the mass of tape, the mass of ash in the tape and the ash percentage in each sample.

Table 3.7. Ash Percentage in Laminate Tape Data

Sample number	Tape mass [g]	Ash mass [g]	Ash percentage [%]	Average ash percentage [%]
1	0.1711	0.0004	0.23	0.79
2	0.1577	0.0013	0.82	
3	0.1961	0.0044	2.19	
4	0.1614	0.0005	0.31	
5	0.2239	0.0009	0.40	

3.7 Drying

3.7.1 Air Drying on Plastic Sheet

For each test except for the PCC/Dye experiment, five handsheets were placed wire side up on a plastic sheet and allowed to completely dry. The fluid flow during air drying was likely to be small so the air dry sheets served as the control case for the sheets dried on a hot surface. The sheets dried on a hot surface were placed wire side up because literature [1-3] shows that during forming, the majority of the filler is concentrated on the wire side of the sheet. If the hypothesis that particles are transported through the thickness of the sheet by the fluid flow, then the higher concentration of filler at the wire side, due to forming, should move towards the center of the sheet. To keep the orientation of the sheets during drying consistent between air and hot

surface drying, the air dry sheets were also placed wire side up. In all the tests, the time for drying was ~24 hours. After the sheet reached 95% solids, it was peeled off the plastic sheet.

For the PCC/Dye test, the 40 mL of PCC/Dye solution was added to the top surface of the wet sheet (6 handsheet samples used) with a syringe. The sheet reached an average of 4.8% solids after the addition of the PCC/Dye solution. Care was taken to uniformly distribute the solution over the top surface and to insure that none spilled over the edges of the handsheet. Also, the solution was dripped on gently so that the structure of the fiber network was not damaged. The handsheet was left on the plastic sheet until the handsheet reached 95% solids. PCC and fiber from the bottom of the sheet stuck to the plastic sheet after the bulk of the sheet was peeled off the plastic sheet. This residue was washed off into a beaker so that it could be dried and ashed as if it were another split of the handsheet.

3.7.2 Drying on a Hot Plate

The sheets for G-800 Test 1 were dried on a 1118-watt Fisher Scientific hot plate. The wet sheet was placed wire side up on the hot plate. The wire mesh from the handsheet mold was placed on top of the wet sheet to restrain it. The placement of the sheet, wire mesh and hot plate are shown in the Figure 3.2. The temperature was monitored with a K-type thermocouple attached to an Omega HH12 meter with 0.6°C resolution. The thermocouple contacted the surface of the hot plate next to the drying handsheet. Table 3.8 shows the maximum and minimum temperatures of the hot plate surface along with the time for the sheet to dry to 95% solids. Sheets 12-15 were dried at 205°C because when Sheet 16 was dried at 260°C, it was burned on the bottom surface. Burning a sheet would consume the fiber mass at the bottom of the sheet. The goal was to keep the fiber mass constant during the drying process. The

temperature of the hot plate could not be kept constant without the use of controls so the drying setup was changed for the subsequent tests.

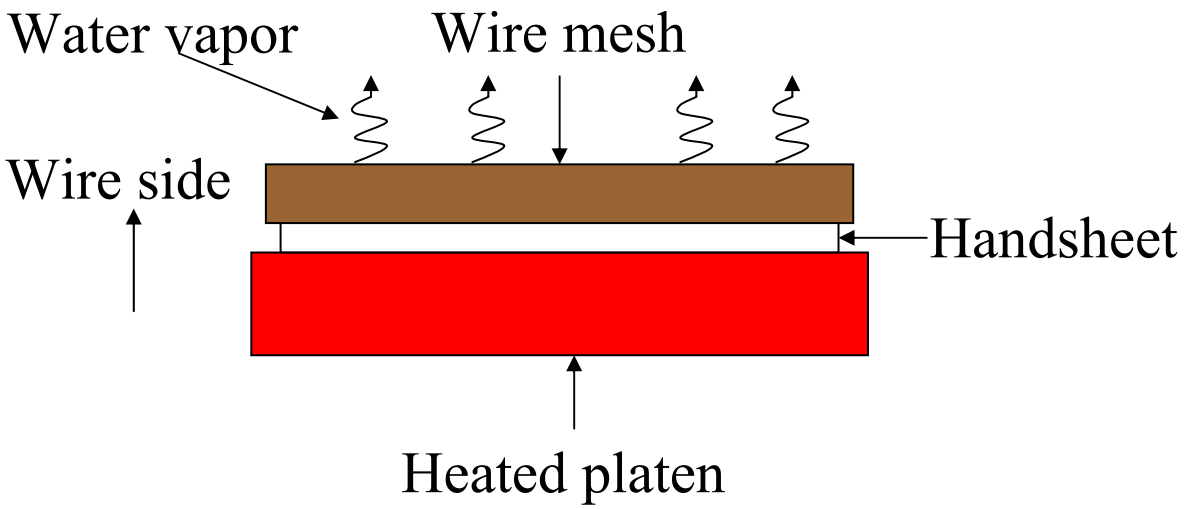

Figure 3.2. Drying Diagram for the Hot Platen with Wire Mesh

The drying setup described in Section 3.7.3 was employed to reduce or eliminate the 50-140°C temperature drop experienced by the hot plate during the drying time because of the energy required to evaporate the water from the sheet.

Table 3.8. G-800 Test 1 Drying Data

Sheet Number	T_{max} [°C]	T_{min} [°C]	Drying Time [min]
7	120	63	15
8	120	60	15
9	120	66	15
10	120	71	15
11	120	71	15
12	205	93	6
13	205	93	6
14	205	93	6
15	205	104	5
16	260	121	5

3.7.3 Drying on the MTS Setup

The sheets for all tests except for G-800 Test 1 were dried on the same MTS apparatus. Figure 3.3 is a diagram of this setup.

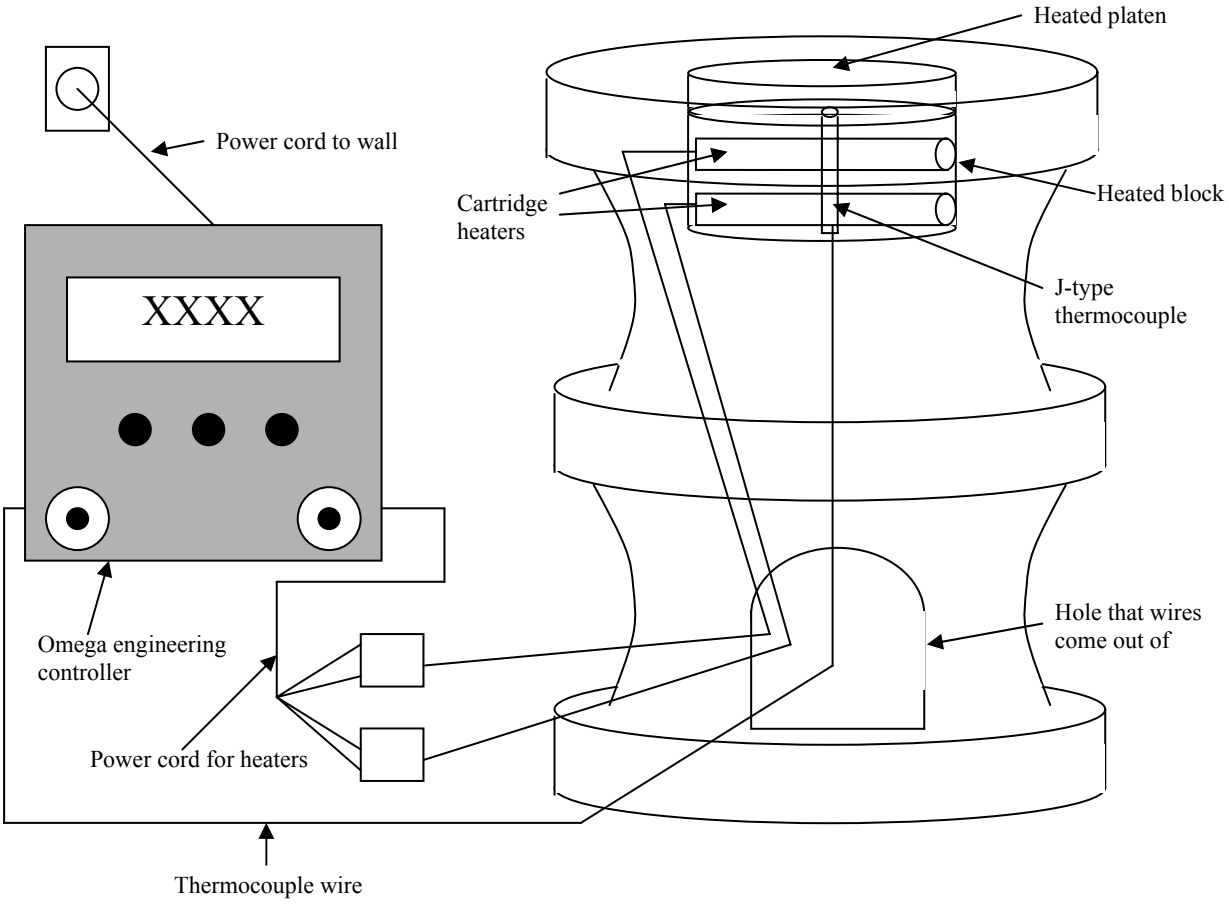

Figure 3.3. MTS Drying Apparatus

The sheets was cut into 5 in. diameter circles to be dried on this setup. The wet sheet was placed on a plastic block with a 5 in. diameter cutting die on top of the sheet. This was then placed between the plates of an Alfa Hydraulic precision sample cutter with 1000 psi of force applied to cut the sheet. Figure 3.4 shows the diagram for cutting the handsheet into a 5 in. diameter circle.

The hot platen was heated until the temperature became stable. The temperature was measured with a J-type thermocouple attached to an Omega Engineering Controller with 1°C resolution.

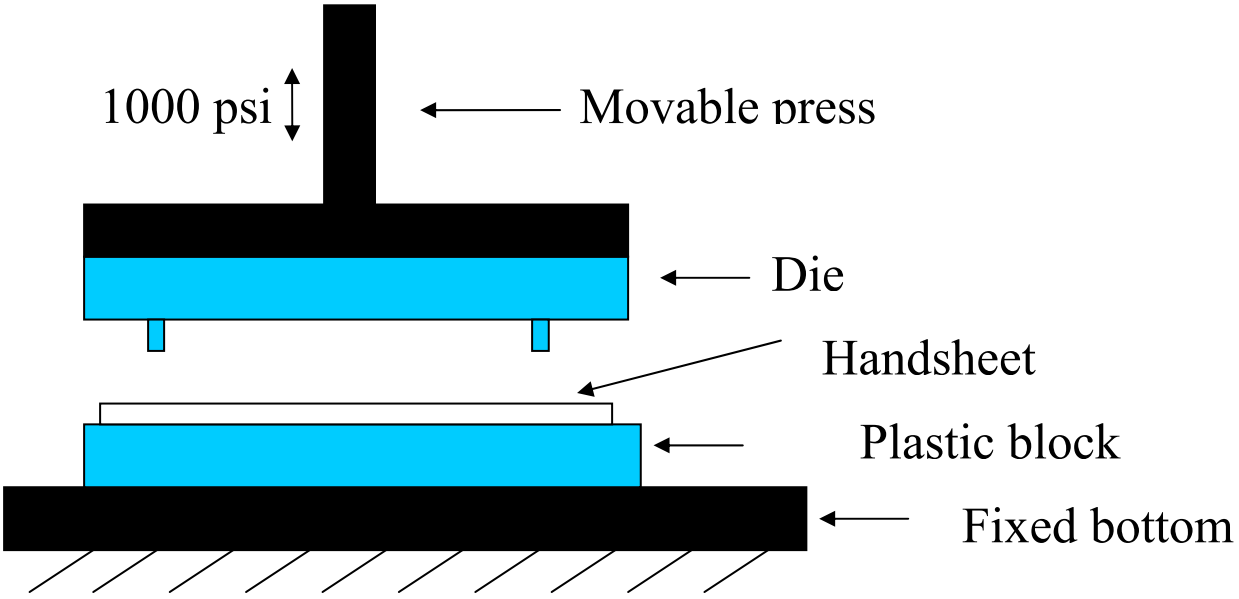

Figure 3.4. Hydraulic Sample Cutter Diagram

The controller maintained the platen temperature at 200°C. The sheet was placed wire side up on the hot platen and either the wire screen mesh, as shown in Figure 3.2, or the couch plate and wire screen mesh, as shown in Figure 3.5, were placed on top of the drying sheet to restrain it.

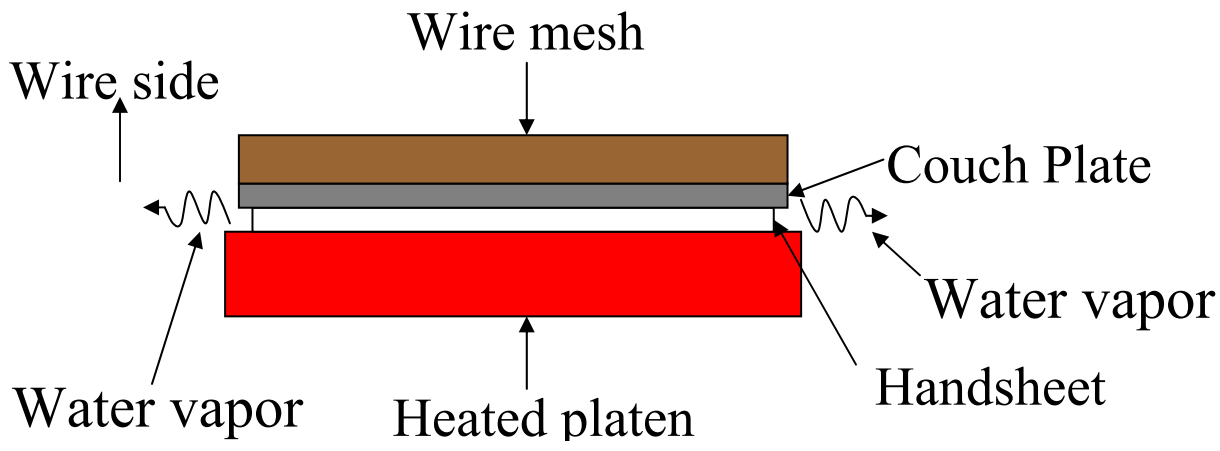

Figure 3.5. Drying Diagram for the Hot Platen with Wire Mesh and Couch Plate

The couch plate was added on top to minimize any effect that z-directional vapor flows might have on the filler distribution in the z-direction of the sheet. The initial, minimum and maximum temperatures and drying time were recorded for each sheet that was dried. The drying time was the time necessary to reach 95% solids for the sheet. The drying conditions for the remaining tests are recorded in Tables 3.9-3.12.

Table 3.9. G-800 Test 2 Drying Data

Sheet Number	$T_{initial}$ [°C]	T_{max} [°C]	T_{min} [°C]	Drying Time to 95% solids [min]	Wire mesh	Couch plate
6	200	206	176	5	X	
7	201	206	180	5	X	
8	201	206	177	5	X	
9	201	206	175	6	X	
10	201	220	169	7	X	

Table 3.10. G-200 Test Drying Data

Sheet Number	$T_{initial}$ [°C]	T_{max} [°C]	T_{min} [°C]	Drying Time to 95% solids [min]	Wire mesh	Couch plate
7	201	209	172	7	X	
8	201	209	174	7	X	
9	201	208	173	7	X	
10	201	208	175	7	X	
11	201	207	171	7	X	
12	200	212	175	10	X	X
13	201	212	176	10	X	X
14	201	212	172	10	X	X
15	201	212	171	10	X	X
16	201	212	170	10	X	X

Table 3.11. PCC Test 1 Drying Data

Sheet Number	$T_{initial}$ [°C]	T_{max} [°C]	T_{min} [°C]	Drying Time to 95% solids [min]	Wire mesh	Couch plate
12	200	203	193	5	X	
13	200	thermocouple fell out		5	X	
14	200	203	192	5	X	
15	200	204	191	5	X	
16	200	204	192	5	X	

Table 3.12. PCC Test 2 Drying Data

Sheet Number	$T_{initial}$ [°C]	T_{max} [°C]	T_{min} [°C]	Drying Time to 95% solids [min]	Wire mesh	Couch plate
7	201	204	191	5	X	
8	200	204	190	5	X	
9	200	204	191	5	X	
10	201	204	192	5	X	
11	201	204	193	5	X	
12	201	204	191	7	X	X
13	201	204	191	7	X	X
14	201	204	192	7	X	X
15	201	204	192	7	X	X
16	201	204	192	7	X	X

3.7.4 Drying for PCC/Dye Experiment

The hot platen on the MTS setup was heated until it stabilized at 200°C. The wet handsheet was placed wire side up on the hot platen. Immediately, the 40 mL of PCC/Dye solution is syringed onto the top of the handsheet. Care was taken to evenly distribute the PCC/Dye solution over the top surface of the handsheet. The solution is also dripped on gently so that the structure of the fiber network is not altered. After the 40 mL of PCC/Dye solution was added to the top of the handsheet, the wire mesh screen was placed on top of the handsheet to restrain it as shown in Figure 3.4. The sheet was removed from the platen after there was no

more vapor visibly escaping from the sheet and the appearance of the sheet was similar to the appearance of the handsheets that were air dried to 95% solids. The initial, maximum and minimum temperatures along with the dry time to reach 95% solids were recorded for each sheet dried in this manner. Since a layer of fiber, ~10% of the sheet's dry fiber mass, remained stuck to the platen when the dried sheet was peeled off, this layer was washed off into a beaker so it could be dried and ashed as if it were another split of the handsheet. A second platen was added to the MTS setup so that the next sheet could be dried while the stuck layer was being removed from the previous platen. The platen material used to dry the particular sample is noted in Table 3.13. Platen temperatures, drying time to 95% solids and wire mesh or couch plate for each sample is also shown in Table 3.13. The drying time for the PCC/Dye Test is longer than the other experiments because the initial solids content was 4.8% compared to 9% for the other experiments.

Table 3.13. PCC/Dye Test Drying Data

Sheet Number	$T_{initial}$ [°C]	T_{max} [°C]	T_{min} [°C]	Drying Time to 95% solids [min]	Wire mesh	Couch plate	Platen Material
8	200	215	173	18	X		Chrome
9	200	215	176	18	X		Ceramic
10	201	218	176	18	X		Iron
11	201	220	166	16	X		Ceramic
12	200	215	170	?	X		Iron
13	201	220	159	16	X		Ceramic

3.8 Splitting the Handsheets

All tests used the handsheet splitting method described in this section. Each handsheet was laminated using the 3M laminating system LS950. This system applies laminate tape to each side of the handsheet. The handsheets were placed between blotter paper and pressed at

120 psi so that the tape would adhere to the handsheet completely. The sheet was then pulled apart carefully into two splits as shown in Figure 3.6.

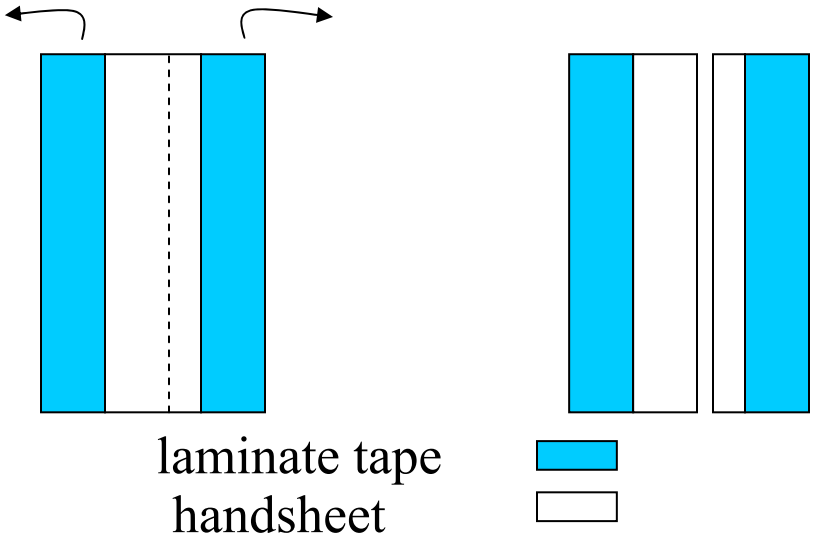

Figure 3.6. Splitting Handsheet into 2 Layers

If 3 layers were used, the thicker of the 2 splits for this test was laminated, pressed and split. The steps for splitting a sheet into 3 layers is shown in Figure 3.7.

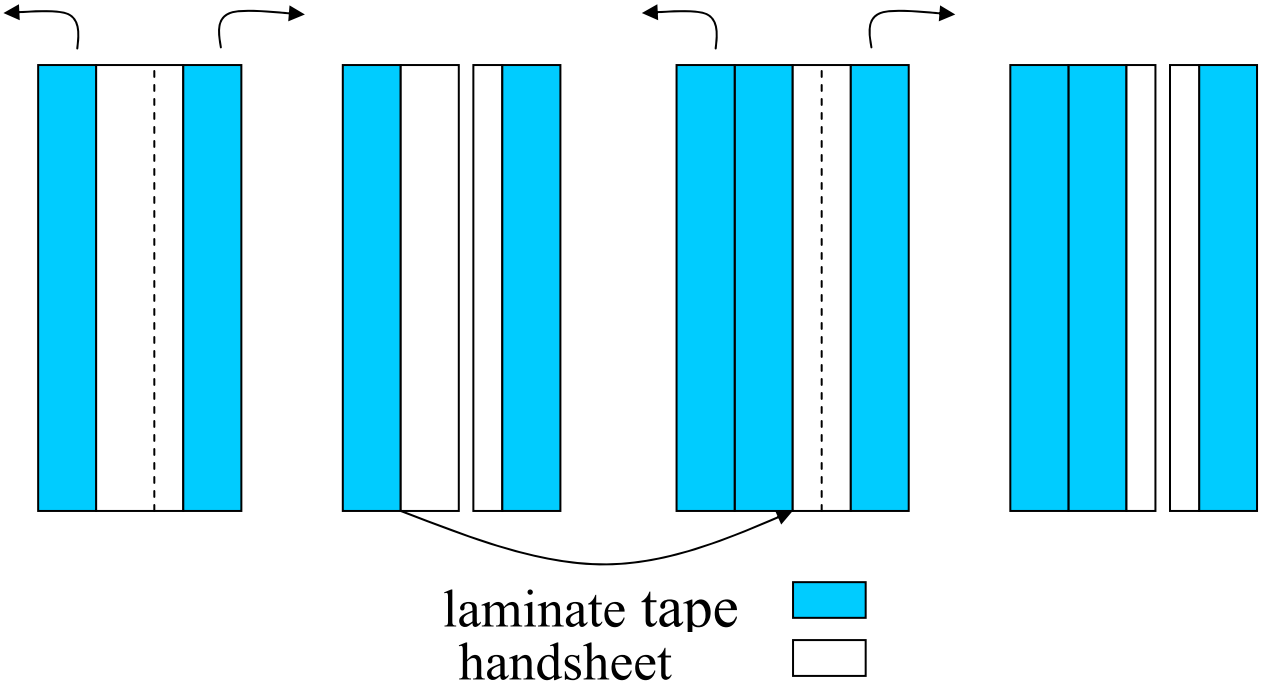

Figure 3.7. Splitting Handsheet into 3 Layers

The excess laminate tape was trimmed off the edges so that the split was a 5 in. diameter circle before the splits were ashed. For the G-800 Test 1, the laminate tape was dissolved off the paper by submerging the split in ethyl acetate before the layers were ashed.

3.9 Ashing Handsheet Splits

The ash procedure was performed to determine the amount of filler in each split of the handsheet. This procedure was used to ash the splits for each test. Dry, clean crucibles were weighed on a 0.0001-gram resolution mass balance and the mass of the crucible was recorded. The splits were cut into small pieces and placed into their respective crucibles. The splits were cut to insure complete ashing of the sample. The crucibles with the cut splits were placed in an oven at 105°C for 15 minutes to completely dry the splits. The crucibles were removed from the oven and placed in a dessicator for 15 minutes to further dry the splits. The crucibles with the dry splits were weighed on the 0.0001-gram resolution mass balance and the mass was recorded. The crucibles were placed in the muffle oven and ashed according to the following program:

1. Ramp oven to 105°C
2. Hold at 105°C for 5 minutes
3. Ramp oven to 225°C at 10°C/min
4. Hold at 225°C for 15 minutes
5. Ramp oven to 325°C at 2°C/min
6. Ramp oven to 525°C at 5°C/min
7. Hold at 525°C for 2 hours.
8. Ramp oven to 105°C (~1.5-2 hours for this step).

The crucibles were removed from the oven and placed in a dessicator for 15 minutes to allow them to cool. The crucibles were weighed on a 0.0001-gram resolution mass balance and the mass was recorded. If the ash had black specks in it, the sample was put in the muffle oven again and the above program was run followed by placing the samples in the dessicator for 15 minutes until all organic material was removed from the sample. From the various masses recorded, the mass of the fiber, ash in the fiber, tape, ash in the tape and filler can be determined.

3.10 Digital Images of Handsheets

Digital pictures were taken of each side of the splits for the PCC/Dye handsheets. A Nikon D1H camera was attached to a tripod at a fixed distance from the handsheet. The handsheet was placed on a stack of 5 standard sheets of blotter paper to give a consistent background for all the pictures. The illumination for all the pictures was also the same. 12 images were produced for each handsheet as shown in Figure 3.8, where the number on each face of the handsheet represents the face of the handsheet that was imaged. Some faces, for example 1, 3 and 7, represent the same surface of the handsheet that was imaged. The faces 3 and 7 were imaged after the handsheet was split to determine whether the intensity values for the surface changed with the thickness of the split being imaged. The dotted line represents where the handsheet was split after the images for the faces of that layer were taken.

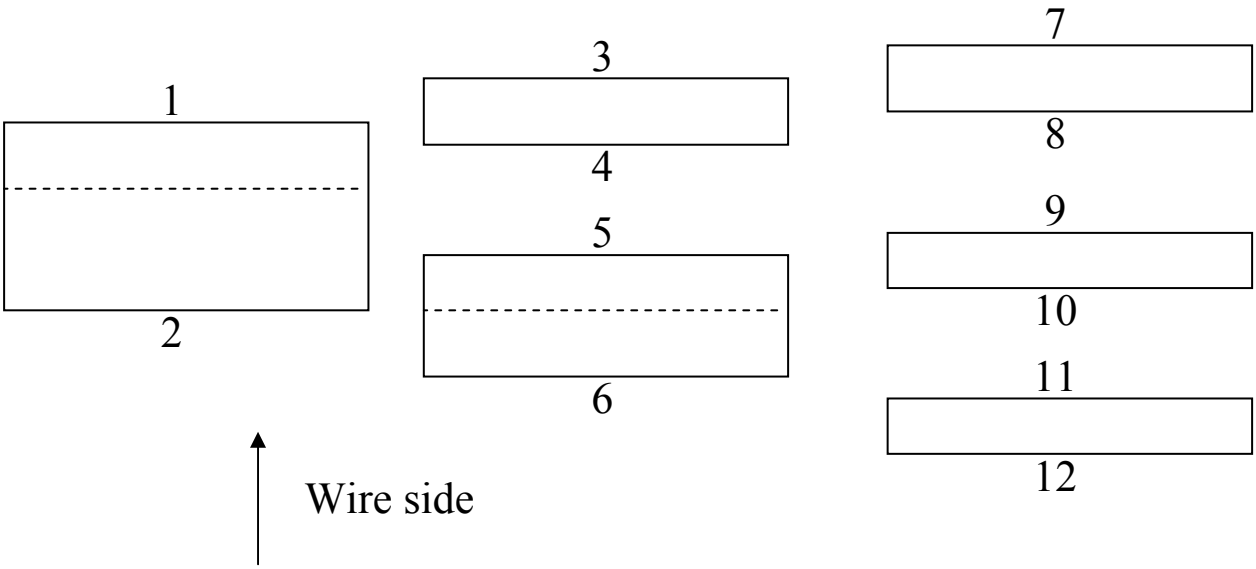

Figure 3.8. Imaging Progression of the Faces of the PCC/Dye Handsheets

After the picture of a certain face was taken, it was cropped so that only the face of the handsheet remained in the picture. Then the digital images were analyzed using a Matlab program written by the author to be used specifically to return color and intensity values for each of the pictures. The Matlab program is located in Appendix A.

3.11 Calculations for each test

3.11.1 Concentration

The concentration of filler in the sheet is the mass of filler particles divided by the mass of fiber in which those filler particles are contained. Since the sheets were split into layers, the concentration per layer is defined as below in Equation (3.3), where C_{layer} is the concentration of

filler in the particular layer, m_{filler} is the mass of filler particles in grams that was contained in the particular layer and m_{fiber} is the mass of fiber in the particular layer.

$$C_{\text{layer}} = \frac{m_{\text{filler}}}{m_{\text{fiber}}} \tag{3.3}$$

3.11.2 z-direction fiber mass

Now, the concentration has to be associated with a relative position in the sheet. A mass based metric was used for this purpose. Since the concentration is the average filler mass per fiber mass of the entire split, the associated position should be the midpoint of the layer. For a sheet split into 2 layers, the positions are z_1 and z_2. For a sheet split into 3 layers, the positions are z_1, z_2, and z_3. $m_{\text{fiber LX}}$ is the mass of the fiber in layer X. Equation (3.4) shows how to compute this z-directional fiber mass.

$$\begin{aligned} z_1 &= \frac{m_{\text{fiber L1}}}{2} \\ z_2 &= m_{\text{fiber L1}} + \frac{m_{\text{fiber L2}}}{2} \\ z_3 &= m_{\text{fiber L1}} + m_{\text{fiber L2}} + \frac{m_{\text{fiber L3}}}{2} \end{aligned} \tag{3.4}$$

3.11.3 Retention

The retention of particles in the sheet is a parameter for determining the significance of the changes in the concentration profiles. For example, a shift between the air dry and forced dried cases cannot be entirely attributed to the drying process if only a small fraction of the particles are retained in the sheet. To ensure that drying causes the movement of particles, a larger mass of particles must be retained. Then, a shift in the profiles shows that the drying processes moved a significant mass of particles. The retention, R, is the mass of particles in

grams recovered from ashing the splits, $m_{\text{filler rec}}$, divided by the mass of particles in grams added to the sheet, $m_{\text{filler add}}$, as shown in Equation (3.5).

$$R = \frac{m_{\text{filler rec}}}{m_{\text{filler add}}} \tag{3.5}$$

For the G-800 Test 1, the handsheet was not modified after the sheets were formed so the values for $m_{\text{filler rec}}$ and $m_{\text{filler add}}$ were recorded exactly. The handsheets for the PCC/Dye test were cut after forming but the particles were not added until after the sheet had been cut. $m_{\text{filler rec}}$ and $m_{\text{filler add}}$ were recorded for the PCC/Dye test. For the remainder of the tests, the sheets were cut after the particles were added because the diameter of the handsheet needed to be equal to the diameter of the platen so the sheet would fit on the MTS setup. The entire sheet was not ashed as a result so particles near the edge of the handsheet were not recovered in the ashing process. Figure 3.9 shows the three different processes and the tests associated with each process.

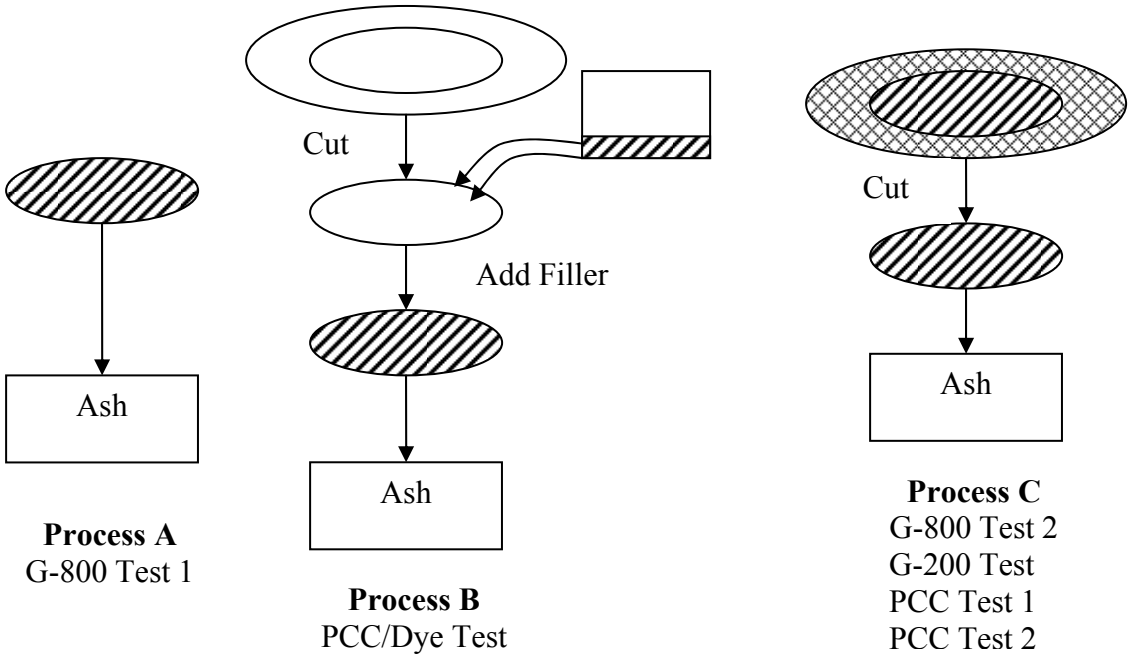

Figure 3.9. Filler Addition and Sheet Cutting Order for Particle Movement Tests

A modified retention value for the tests using Process C needed to be calculated to account for the filler retained in the edges of the sheet as shown in the cross-hatched area. To determine the original mass of filler that was present in the sheet before it was cut, an average concentration was determined for the entire sheet as shown in Equation (3.6). $m_{\text{filler rec}}$ is the mass of filler recovered after ashing the diagonal filled portion of the sheet shown in Process C of Figure 3.9. $m_{\text{fiber rec}}$ is the amount of fiber in the diagonal filled portion of the sheet shown in Process C of Figure 3.9.

$$C_{sheet} = \frac{m_{\text{filler rec}}}{m_{\text{fiber rec}}} \tag{3.6}$$

The total mass of fiber in the uncut sheet, $m_{\text{fiber tot}}$, is shown in Equation (3.7), where $m_{\text{fiber cut}}$ is the mass of fiber removed from the sheet by cutting. From Figure 3.9, this is the sum of the fiber in the diagonal filled part plus the cross-hatched part.

$$m_{\text{fiber tot}} = m_{\text{fiber rec}} + m_{\text{fiber cut}} \tag{3.7}$$

Since $m_{\text{fiber cut}}$ is unknown, $m_{\text{fiber tot}}$ has to be determined by a ratio of areas for the total sheet and the cut sheet as in Equation (3.8), where A_{rec} is the area of the cut sheet and A_{tot} is the area of the uncut sheet. The thickness and density of the sheet are assumed to be uniform to give the equality in Equation (3.8).

$$m_{\text{fiber tot}} = \left(\frac{A_{\text{tot}}}{A_{\text{rec}}} \right) m_{\text{fiber rec}} \tag{3.8}$$

Reducing Equation (3.8) gives Equation (3.9), whereby the area ratio is reduced to a ratio of radii squared.

$$m_{\text{fiber tot}} = \left(\frac{\pi r_{\text{tot}}^2}{\pi r_{\text{rec}}^2} \right) m_{\text{fiber rec}} = \left(\frac{(8\,\text{cm})^2}{(2.5\text{ in})^2} \right) m_{\text{fiber rec}} \tag{3.9}$$

Finally, the concentration of the sheet can be multiplied by this total fiber mass to give the total filler mass in the uncut sheet, $m_{\text{filler tot}}$, as shown in Equation (3.10). $m_{\text{filler tot}}$ would be the mass of filler in the diagonal and cross hatched portion of the sheet of Process C in Figure 3.9. C_{sheet} is assumed to be constant across the area of the handsheet.

$$m_{\text{filler tot}} = C_{\text{sheet}} m_{\text{fiber tot}} \tag{3.10}$$

The retention for sheets dried on the MTS set up can now be determined using Equation (3.11).

$$R_{\text{cut}} = \frac{m_{\text{filler tot}}}{m_{\text{filler add}}} \tag{3.11}$$

CHAPTER 4

EXPERIMENTAL RESULTS

4.1 Introduction

The experimental results are divided into four sections that follow the four types of experiments, G-800, G-200, PCC, and PCC/Dye, performed in this study. The sections for the G-800, G-200, PCC and PCC/Dye experiments contain filler concentration versus z-directional fiber mass plots along with a table of retention values for the particular filler particle. The section for the PCC/Dye experiments also contains digital images of different faces of the sheet and intensity versus z-directional fiber mass plots. The addition of trendlines and discussion of the figures and tables will be covered in Chapter 5, Discussion and Analysis.

4.2 G-800 (2-75 μm diameter)

G-800 Test 1 had two initial hot plate surface temperatures, which are labeled as the low dry and high dry series. The low drying series corresponds to the sheets that were placed on the hot plate with an initial temperature of 120°C while the high dry series corresponds to the sheets that were placed on the hot plate with an initial temperature of 205°C or 260°C. These two forced drying cases were compared to the samples dried at room temperature to see if there was any re-distribution of filler particles caused by less uniform evaporation and fluid flow through the thickness of the handsheet. Five handsheets were made for each case (air dry, low dry, high dry) and these were split into 3 layers. Figure 4.1 shows the filler concentration versus the z-directional fiber mass for G-800 Test 1.

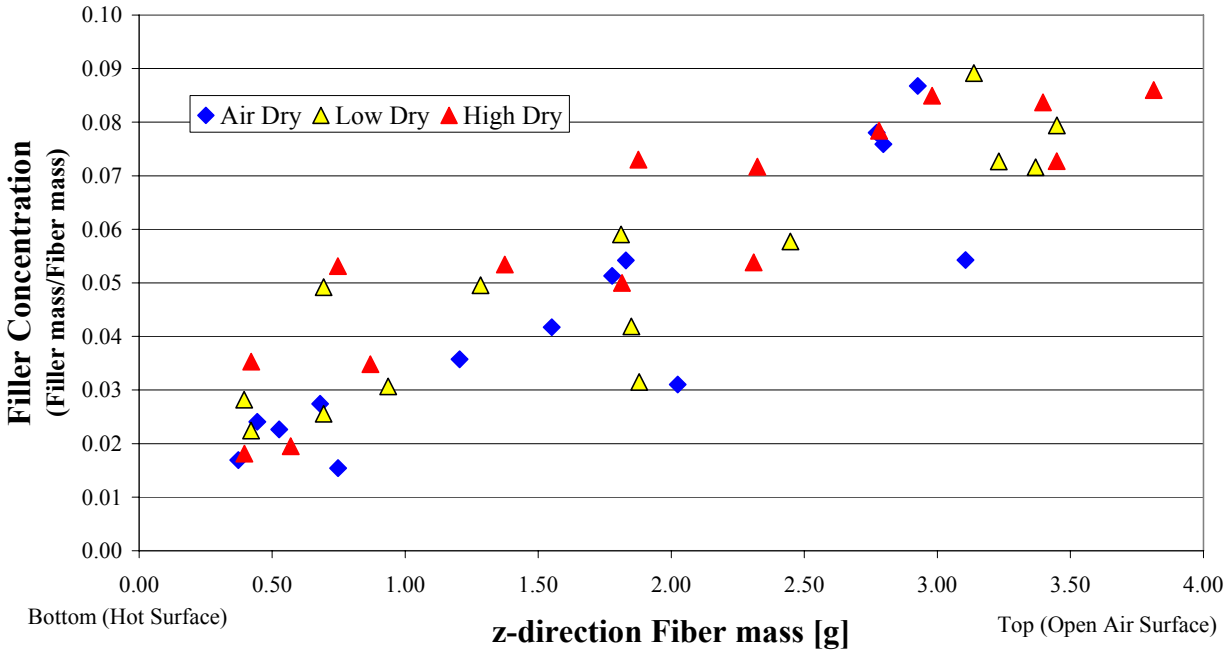

Figure 4.1. Filler Concentration Versus z-direction Fiber Mass for G-800 Test 1

Retention calculations were performed to determine how much of the 1 gram solid G-800 measured actually remained in the sheet. The retention data for G-800 Test 1 is shown in Table 4.1.

Table 4.1. G-800 Test 1 Retention Data

	Average Retention (%)	Standard Deviation	Max	Min
Air Dry	35.3	13.8	56.6	19.1
Low Dry	38.3	6.3	49.0	32.2
High Dry	37.2	3.4	42.5	34.2

Brown [30] reported retention values as a function of particle size for bleached softwood sulphite pulp beaten to 300 CSF and used to form 60 g/m^2 handsheets with no retention aid used, which is shown in Figure 4.2. This figure is a reproduction of a graph in the paper by Brown. The pulp

was 30% filler by weight. These sheets retained ~60% of 20 μm diameter clay particles, which is the size of 50% of the particles in G-800, originally added to the pulp compared to 35.3-38.3% retention for Test 1 with 2-75 μm filler particles. The test here was for 200 g/m^2 handsheets with 20% weight percent of filler in the pulp. The discrepancy in retention can be attributed to the fact that the pulp used for this experiment was not beaten so the fibrillation of the fibers was minimal yielding a more open structure for particles to flow through, hence a smaller probability of the filler particles being retained.

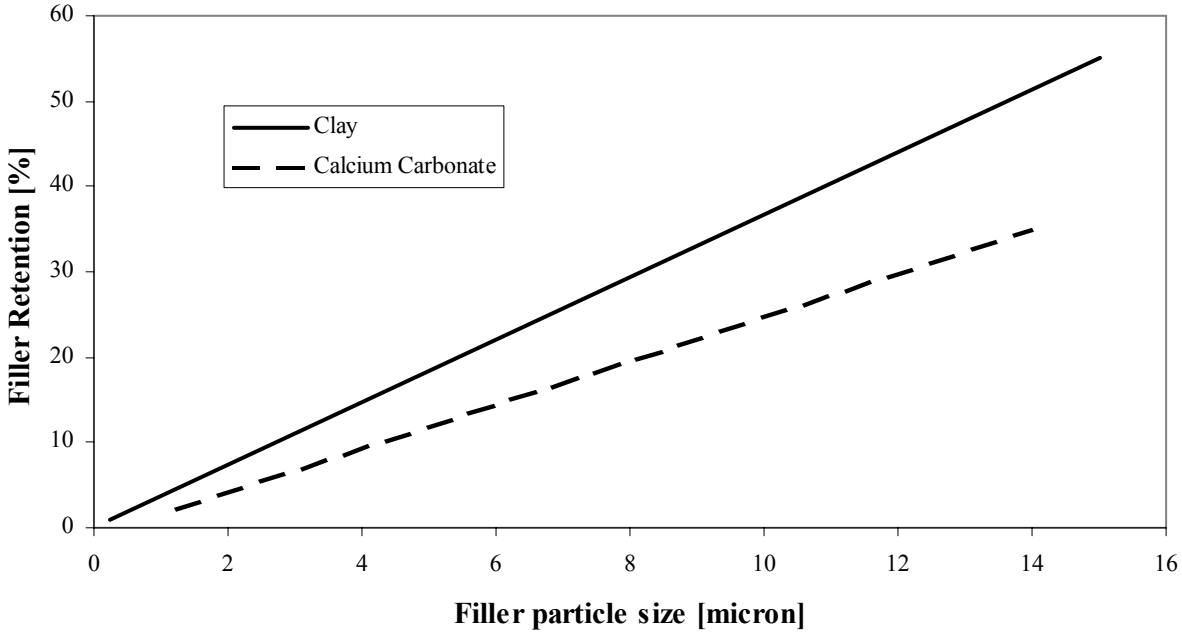

Figure 4.2. Relationship Between Retention and Particle Size for Bleached Sulphite Pulp

G-800 Test 2 was performed on the MTS drying setup for the high dry case, which allowed for temperature control of the hot platen surface. The mass of particles added and the water level was reduced in the handsheet mold to attempt to retain a larger mass of particles in

the sheet. The handsheets were only split into two layers for the air dry and high dry cases. The laminating tape attached to the split was ashed along with the split to eliminate particles becoming dislodged when the sheet was placed in an ethyl acetate bath to dissolve the adhesive and remove the tape from the sheet. The mass of the tape and the mass of ash in the tape was already pre-determined so that these could be subtracted to yield the mass of fiber and filler. Figure 4.3 shows the concentration versus the z-direction fiber mass for these sheets. The high drying series corresponds to the sheets that were placed on the platen with an initial temperature of 200°C.

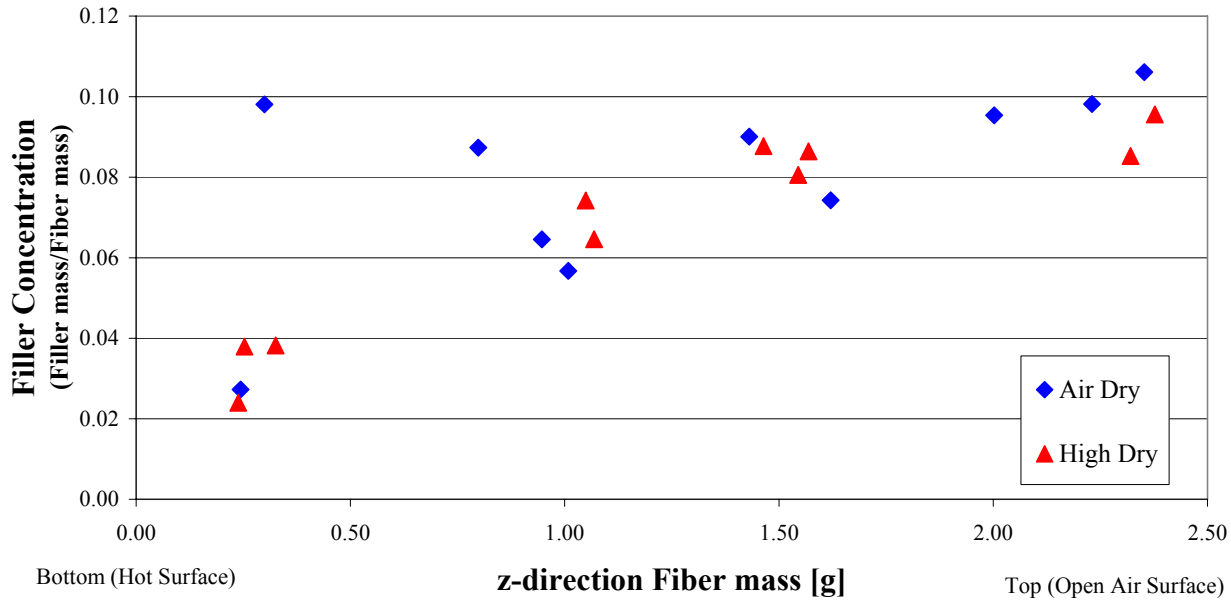

Figure 4.3. Filler Concentration Versus z-direction Fiber Mass for G-800 Test 2

Retention values were determined for this experiment to compare with Brown [30] and G-800 Test 1. The retention data for G-800 Test 2 is shown in Table 4.2.

Table 4.2. G-800 Test 2 Retention Data

	Average Retention (%)	Standard Deviation	Max	Min
Air Dry	31.0	2.4	34.2	29.0
High Dry	29.4	1.0	30.5	28.9

The retention values for G-800 Test 2 are lower than for G-800 Test 1 and the data presented by Brown [30]. By lowering the water level, the particles could have settled to the bottom before the water was drained out and there would have been less time for interaction before forming with the fibers due to the shorter draining time. However, the standard deviation for G-800 Test 2 is 1.0-2.4% retention compared to 3.4-14.8% retention for G-800 Test 1. The smaller standard deviation for G-800 Test 2 confirms the consistency of the procedure for manufacturing these handsheets.

4.3 G-200 (1-10 μm diameter)

One test was performed using the medium particles, G-200 (1-10 μm diameter). A 70-μm wire and a lower fill height of the handsheet mold were used to help improve retention of the microspheres in the handsheet. Handsheets were dried using the MTS drying setup to be compared to sheets dried on a plastic sheet. The handsheets on the MTS setup had either the wire mesh screen on the top surface or a couch plate and wire mesh screen on top. The couch plate was added to eliminate z-directional vapor flows that might be affect the particle transport through the thickness of the sheet. The air dry sheets were split into 2 layers while the high dry cases were split into 3 layers. Figure 4.4 shows the concentration comparison between the 3 different drying conditions.

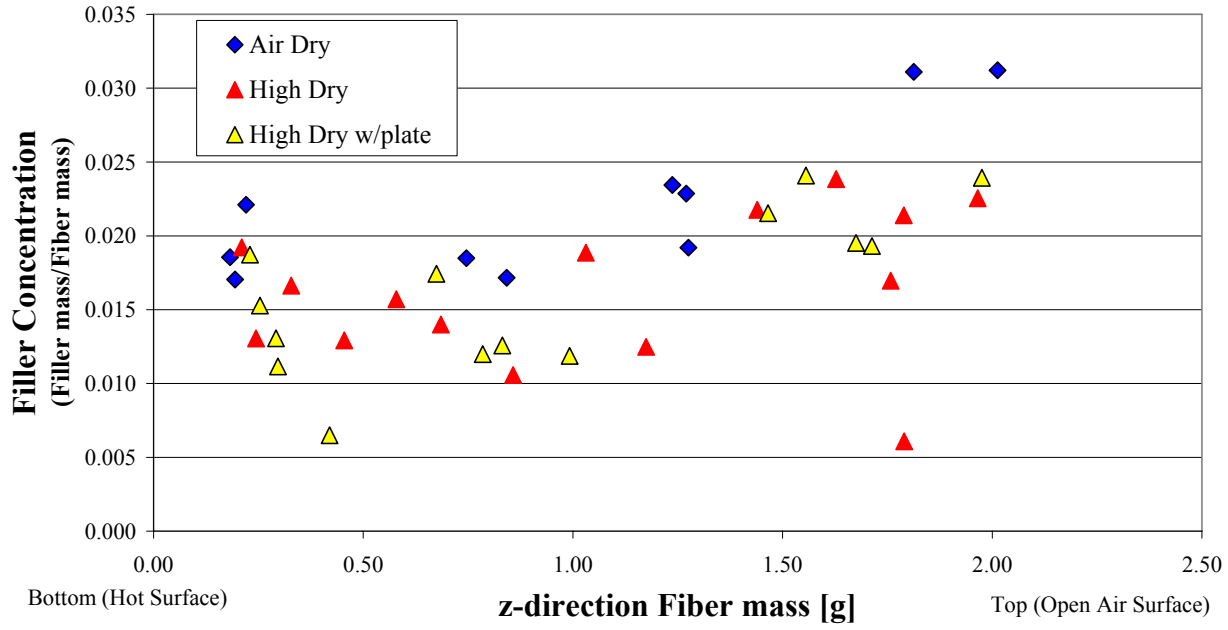

Figure 4.4. Filler Concentration Versus z-direction Fiber Mass for G-200 Experiment

Retention calculations were performed for the G-200 particles. The retention data for the G-200 particles is shown in Table 4.3.

Table 4.3. G-200 Retention Data

	Average Retention (%)	Standard Deviation	Max	Min
Air Dry	7.3	0.5	7.8	6.4
High Dry	5.9	1.6	7.6	3.6
High Dry w/plate	6.4	1.0	7.6	5.1

The retention values for 1-10 μm diameter clay particles from Brown [30] were 5-30% as compared to 5.9-7.3% for this experiment. These values are consistent with the literature even though the fibers, filler percentage in the pulp, and water level in the handsheet mold were

different. The standard deviation for the medium particle test is 0.5-1.6% retention confirming the consistency of the procedure for manufacturing these handsheets.

4.4 PCC (0.1-1 μm diameter)

The first experiment run with PCC as the filler material produced very low retention. The retention data for the small particles is shown in Table 4.4.

Table 4.4. PCC Test 1 Retention Data

	Average Retention (%)	Standard Deviation	Max	Min
Air Dry	1.2	0.1	1.4	1.1
High Dry	2.9	2.6	6.6	0.7

For particles with a 0.1-1.0 μm diameter, Brown [30] generated 0.2-5% retention compared to 1.2-2.9% retention for PCC Test 1. The spread of the retention values for the handsheets in PCC Test 1 shows that for particles this small, producing multiple handsheets with consistent masses of filler in them is not possible. A second run of the PCC experiment was performed to try and increase the retention. Two grams of solid PCC for PCC Test 2 were added to the handsheet mold instead of 1 gram of solid PCC for PCC Test 1 and a 70-μm wire was used to attempt to improve retention. The changes to increase retention failed. The retention data for the PCC Test 2 are shown in Table 4.5.

Table 4.5. PCC Test 2 Retention Data

	Average Retention	Standard Deviation	Max	Min
Air Dry	1.8	0.6	2.8	1.2
High Dry	0.8	0.5	1.6	0.3
High Dry w/plate	1.3	0.3	1.7	1.1

In both tests, the effluent water from the handsheet mold was milky in color suggesting that particles were flowing directly through the fiber matrix as it was forming on the wire.

The retention of PCC in the handsheets was ~1%. The random scatter of the points due to the low retention values would not yield a meaningful concentration profile. Particles less than 1 μm are too small to be filtered by the fiber network as the fiber mat forms on the wire in a standard cylindrical handsheet mold. Therefore, another method for retaining this size particle in the sheet before drying was tried by pouring the particles directly on an already formed handsheet.

4.5 PCC (0.1-1 μm diameter) and Dye

The final test was pouring a PCC and dye mixture on the top surface of a saturated sheet. By pouring the particles onto the already formed network of fibers, any movement of particles through the sheet would be due to fluid flow induced by drying and/or settling of the particles. The high moisture content in the sheets caused the sheets dried on the MTS setup to swell to an approximate thickness of 2 inches before all of the PCC/Dye mixture could be added to the sheet. The mixture was added so that none of the liquid drained off the edges of the handsheet even when the blister formed. Figure 4.5 shows roughly how the handsheet looked on the platen before and during the addition of the PCC and dye mixture. The sheet appeared to form a "blister." To form a blister, a bubble of steam would have formed under the bottom of the sheet and caused the middle of sheet to lift off the platen while remained attached to the platen at the edges of the sheet.

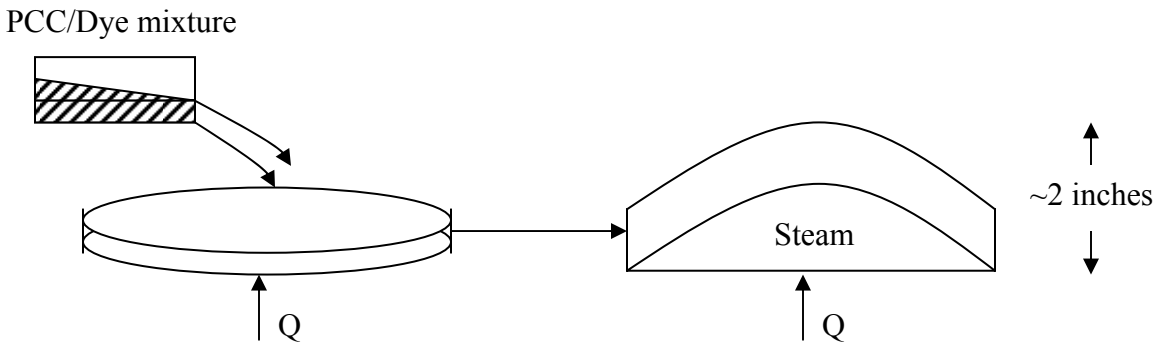

Figure 4.5. Handsheet Swelling during PCC/Dye Mixture Addition

The high dried sheets were promptly compressed when the wire mesh screen was added to the top of the sheet after adding the PCC/Dye mixture. The addition of PCC/Dye solution to the handsheet took 30 seconds.

After the air-dried sheets were completely dry, they were peeled off the plastic sheets. A small amount of PCC and fiber remained stuck to the plastic sheet where the sheet had been. This residue was washed off, dried, and ashed as if it were the very bottom layer of the sheet. The same result happened when the high dried sheets were peeled off the hot platen. In this case, a significant mass of the sheet stuck to the hot platen. The material stuck on the platen was washed off, dried and ashed as if it were the very bottom layer of the sheet. The difference between the air dry residue and the high dry residue was that the air dry case had a small mass of filler (~0.003 g) and almost no fiber while the high dry case had 20% of the sheet's total fiber at a concentration of ~3 g filler/g of fiber.

The concentration profile for the PCC/Dye sheets is shown in Figure 4.6. The residue from the air-dry case was not plotted because the concentration was high since there was almost no fiber left on the plastic sheet. If it were plotted, it would not be an accurate representation of

the average concentration at the bottom of the sheet. The retention data for the PCC/Dye test is shown in Table 4.6.

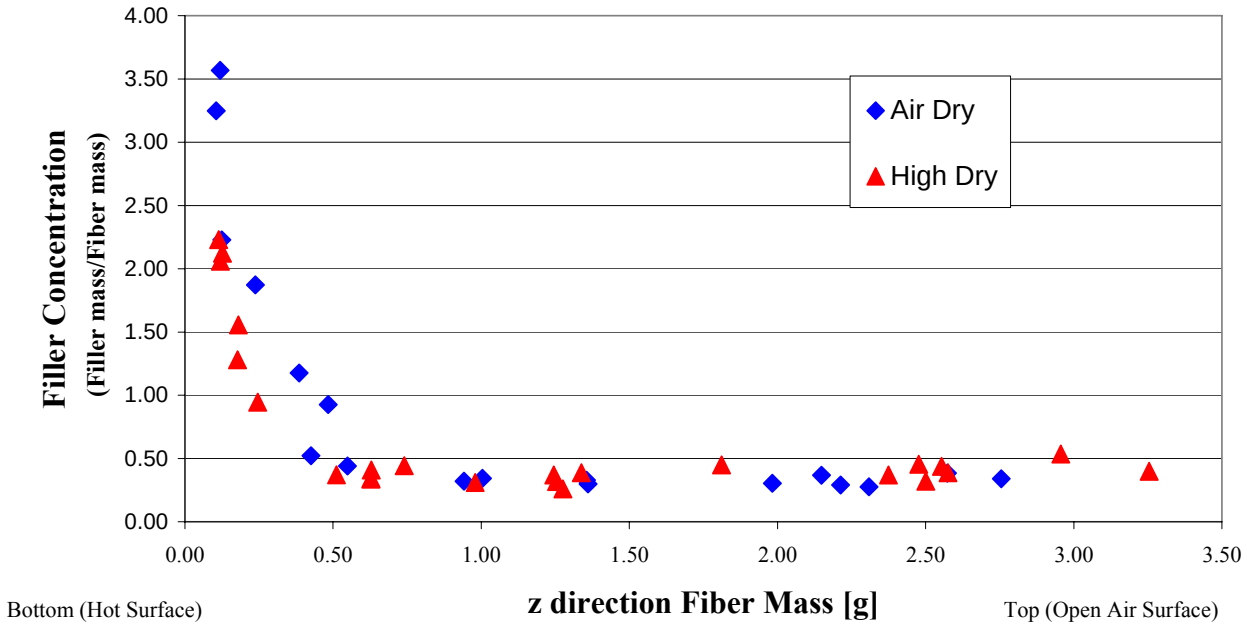

Figure 4.6. Filler Concentration Versus z-direction Fiber Mass for PCC/Dye Experiment

Table 4.6. PCC/Dye Retention Data

	Average Retention (%)	Standard Deviation	Max	Min
Air Dry	88.0	3.3	91.2	83.6
High Dry	84.3	5.5	92.6	76.7

The retention values of 84.3-88.0% are expected to be high because a solid surface was underneath the sheet to act as a barrier to catch the particles that might have normally flowed out

of the sheet if the particles had been added directly to the handsheet mold. The spread of the retention values was small, 3.3-5.5% retention, so the methods used were consistent for each sample.

4.6 Digital images of Dyed Handsheets

The digital images on one sample from the air dry case and one sample from the high dry case are shown below in Figures 4.7-4.10.

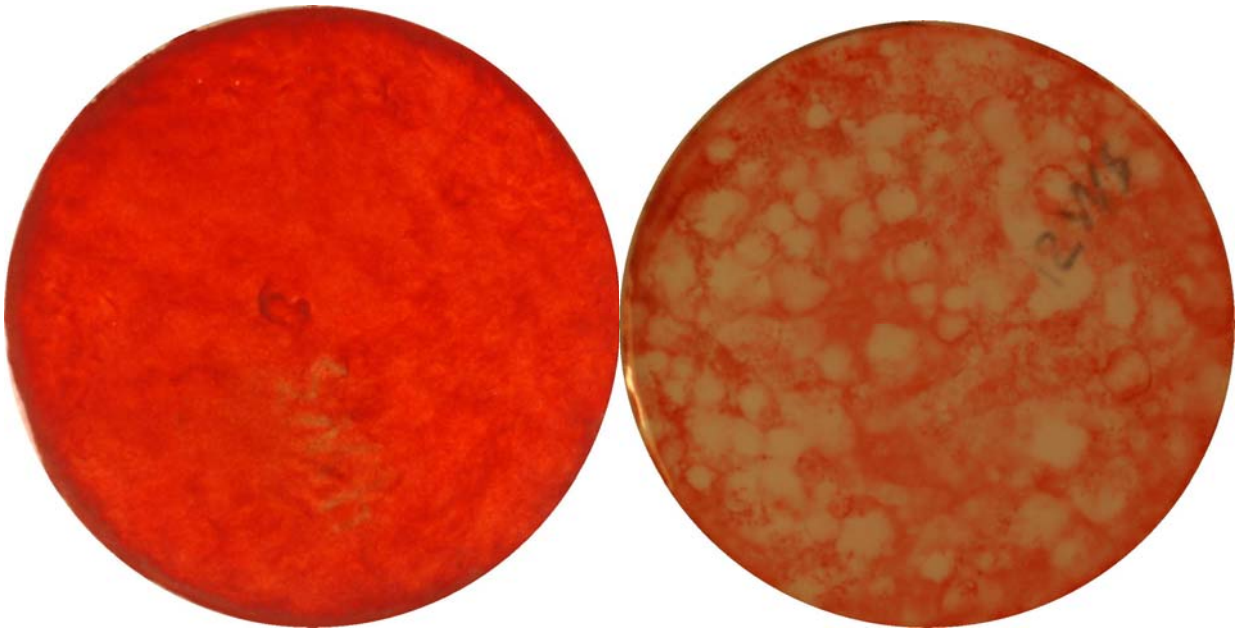

Figure 4.7. Air Dry (left) and High Dry (right) Top Open Air Surface (Face 1)

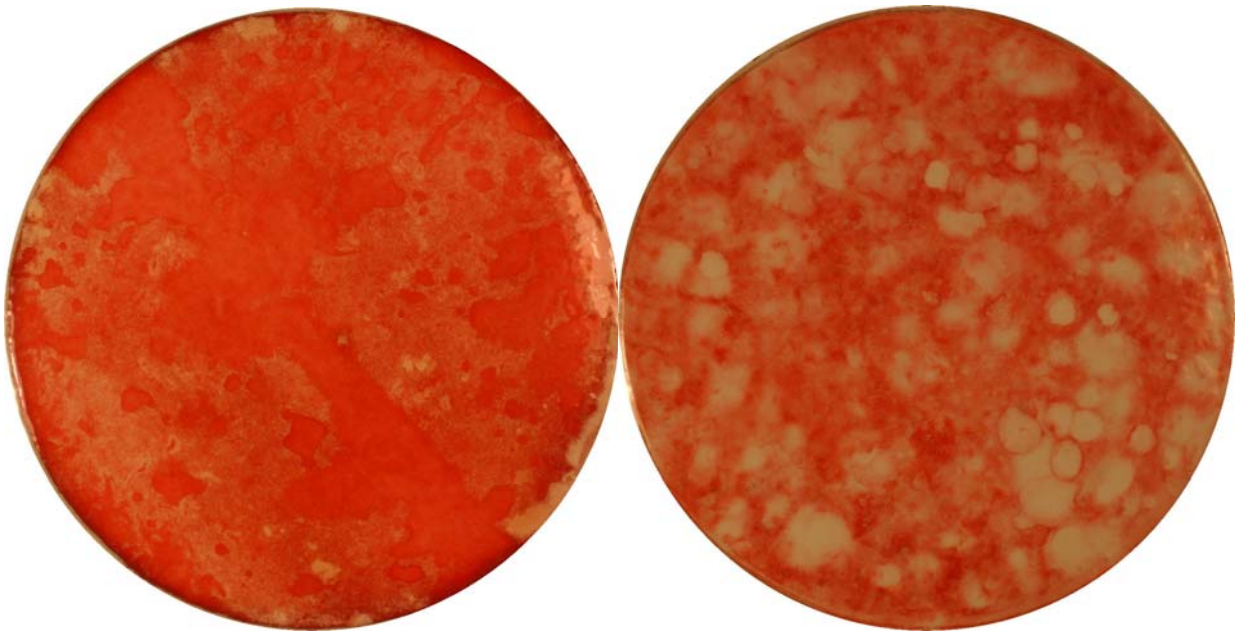

Figure 4.8. Air Dry (left) and High Dry (right) Backside of Top Open Air Surface (Face 4)

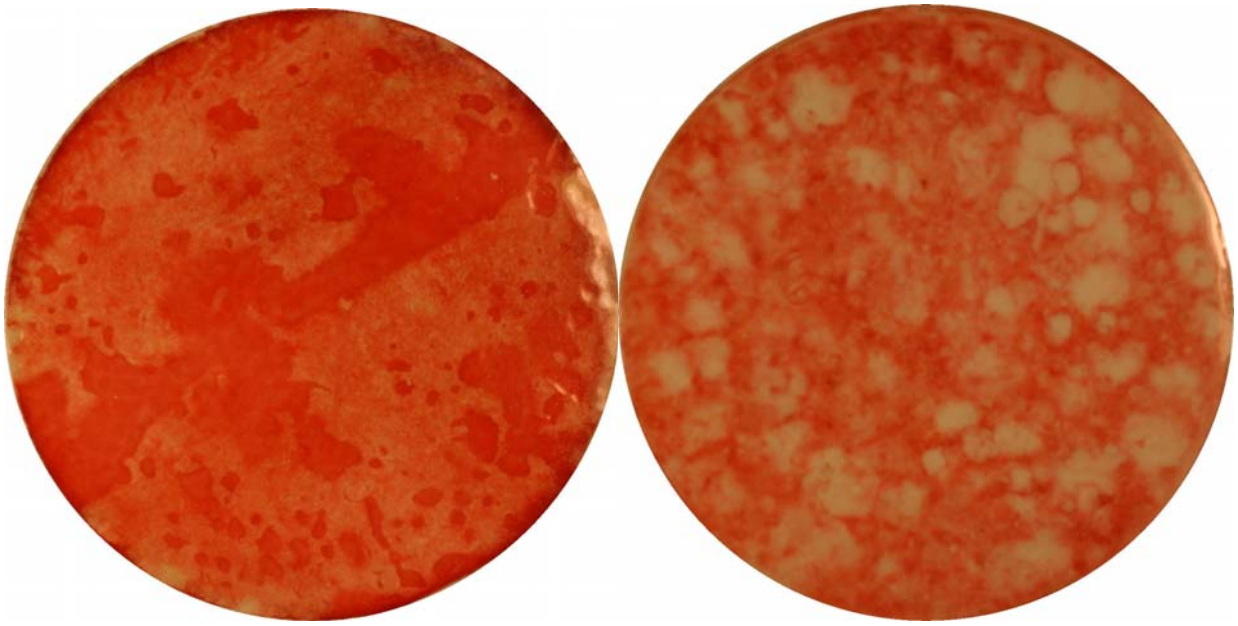

Figure 4.9. Air Dry (left) and High Dry (right) Backside of Bottom Heated Surface (Face 5)

Figure 4.10. Air Dry (left) and High Dry (right) Bottom Heated Surface (Face 2)

Four average intensity values are generated and plotted versus the z-direction fiber mass corresponding to those faces. Since multiple images were taken of each face, these intensity values were averaged for that particular face. Table 4.7 shows the faces used to compute an average intensity for four locations through the thickness of the sheet. The intensity values from the thinnest splits were not used because the thickness of the split began to affect the intensity value for that location.

Table 4.7. Faces Used for Average Intensity Values at Locations in Sheet

Location in sheet	Faces used
0 – Bottom (hot surface)	2, 6
0 – Interior	5
WS – Interior	4
WS – Top (Open air surface)	1, 3

The average intensity values from Table 4.7 versus the z-directional fiber mass corresponding to those faces are shown in Figure 4.11.

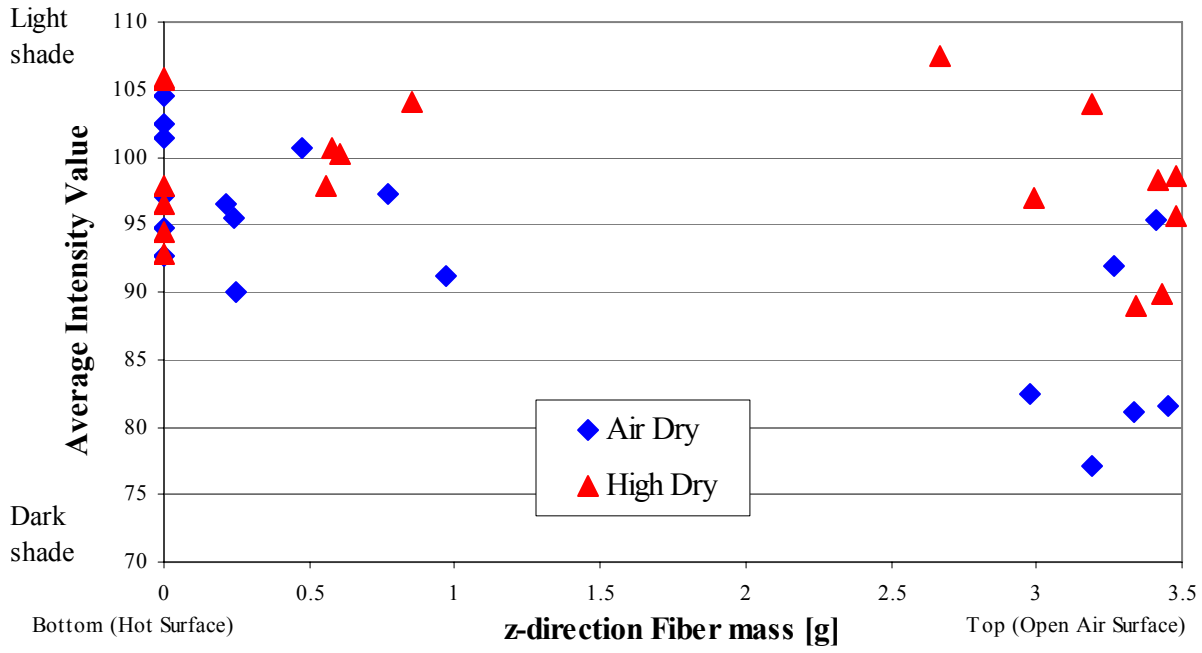

Figure 4.11. Average Intensity versus z-direction Fiber Mass for PCC/Dye Experiment

After the residue from the high dry sheet was washed off the platen, dye still remained on the platen surface. This unknown quantity of dye was unable to be collected and analyzed. The dye on the platen could be "added" to the concentration at the bottom surface of the high dry sheets, which would give a slightly lower intensity (darker) value at this surface.

CHAPTER 5

ANALYSIS AND DISCUSSION

5.1 Introduction

The discussion and analysis is divided into seven sections. The first four sections present a concentration profile of each filler particle across the thickness of the sheet. The concentration profiles are integrated and compared to the average filler mass recovered from the set of samples for each drying level. The integrals of the concentration profiles agree with the average filler mass recovered for all filler types. The concentration profiles for different drying levels are similar for G-800 and G-200 experiments but the concentration profiles separate for the PCC/Dye experiment. Mechanisms for the differences in concentration profiles are discussed in Chapter 6. In section 5, the digital images of the handsheet and the intensity versus z-directional fiber mass figure are discussed. The dye concentration shows where water evaporated during the drying process. Section 6 contains calculations for determining the time scales for which a PCC particle could settle through the thickness of the sheet based on the data from the PCC/Dye experiment. A particle settling simulation was performed to determine if particle settling was a contributing mechanism to the differences in concentration profile for the PCC/Dye experiment. A percent solids versus time plot was generated for each drying case for the PCC/Dye experiment. The percent solids versus time plot shows how long a continuous water phase exists in the sheet during the two drying levels of the PCC/Dye experiment. The final sub-section for the Section 6 discusses the possibility that a PCC particle could settle through the thickness of the sheet in a continous water phase in the sheet based on the time scale calculations. The average velocity of fluid through the sheet during evaporation was computed using a constant evaporation rate in section 7.

5.2 G-800 (2-75 µm diameter)

For G-800 Test 1, a continuous concentration profile was determined for air drying, low drying and high drying. A polynomial was fit to the points in each series. These concentration curves are shown in Figure 5.1.

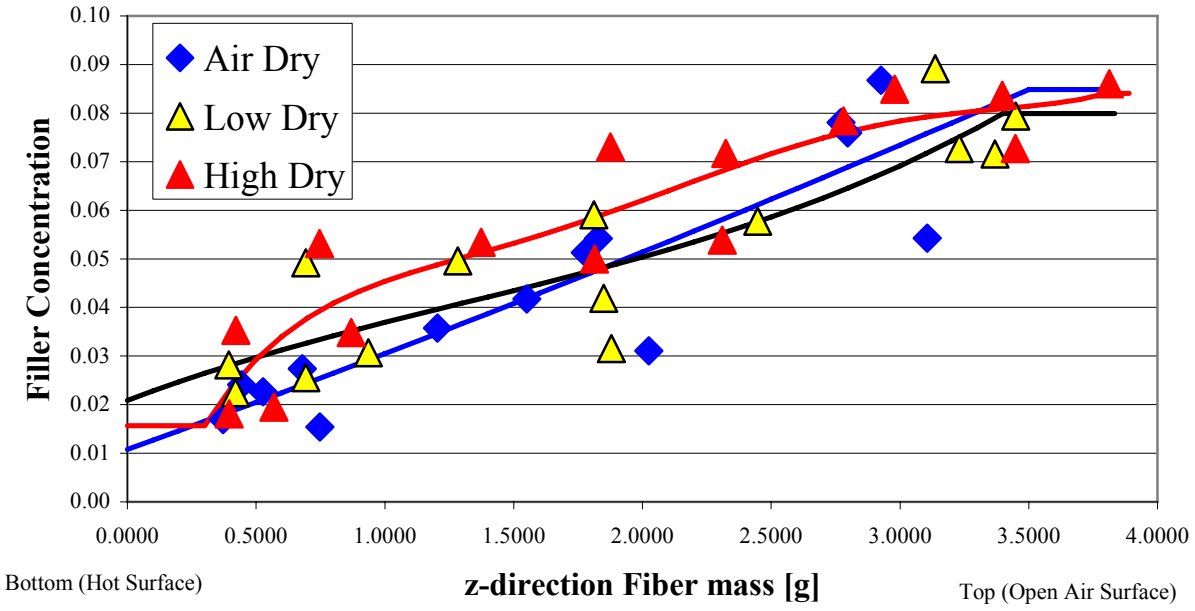

Figure 5.1. Concentration Profiles for G-800 Test 1

This polynomial can be integrated over the z-direction fiber mass to give the average total particle mass in each sheet. The polynomials for each drying case with their respective R^2 values for the z-direction fiber mass for which they apply are shown in Table 5.1. The computed filler mass is compared to the average filler mass to check that the polynomial accurately fits the true concentration distribution for a sheet. The values predicted by the polynomial can only be trusted in the domain of the fiber mass values.

Table 5.1. G-800 Test 1 Polynomial Fit Lines

	Polynomial	R^2	z-direction fiber mass [g]
Air Dry	$C = 0.00057z^2 + 0.01915z + 0.01078$	0.795	0.0-3.5
Low Dry	$C = 0.00131z^3 - 0.00519z^2 + 0.01989z + 0.02090$	0.793	0.0-3.4
High Dry	$C = 0.00160z^5 - 0.01823z^4 + 0.07746z^3 - 0.15291z^2 + 0.15707z - 0.01963$	0.844	0.3-3.8

For polynomials with large derivatives at the end points, the concentration is assumed to be equal to the concentration of the end points. This concentration is assumed to be constant from the smallest z-direction fiber mass value to zero and from the largest z-direction fiber mass value to the average sheet fiber mass for the samples dried at that particular level. Table 5.2 shows where the concentration was assumed to be constant at the minimum and/or maximum z-direction fiber mass.

Table 5.2. G-800 Test 1 z-direction Fiber Mass Constant Concentration Domain

	Minimum		Maximum	
	z-direction fiber mass [g]	Concentration	z-direction fiber mass [g]	Concentration
Air Dry	N/A	N/A	3.5-3.8	0.08485
Low Dry	N/A	N/A	3.4-3.8	0.07990
High Dry	0.0-0.3	0.01568	3.8-3.9	0.08405

Table 5.3 compares the average filler mass from the sample handsheets to the filler mass computed by integrating the curves in Figure 5.1.

Table 5.3. G-800 Test 1 Average Filler Mass and Computed Integral Filler Mass

	Average filler mass [g]	Integral [g]
Air Dry	0.2118	0.1881
Low Dry	0.2304	0.1963
High Dry	0.2237	0.2255

The maximum difference between the average filler mass and the integral of the polynomials is 17%. This agreement shows that the polynomial fit lines give an accurate representation of how the concentration of filler particle varies through the thickness of the sheet. The concentration profiles for the large particles are similar. This indicates that although the sheets were dried at different levels, the driving force created by the drying was not great enough to induce a change in the particle distribution for particles with a 2-75 μm diameter. The higher concentration of particles at the top (wire side) surface is consistent with the particle and fines distribution found in literature [1-3, 10]. In retrospect, this result may have been anticipated. The sheet was uncompressed which would yield pores larger than those in a pressed sheet. In a pressed sheet, one would not normally expect a large number of pores with sizes greater than 20-30 μm.

As with G-800 Test 1, a concentration profile for G-800 Test 2 was plotted using a least squares polynomial approximation of the data set. Figure 5.2 shows these fit lines with the discrete data points for G-800 Test 2. These fit polynomials were smooth at the ends of the fiber mass so the values for the integrals are from zero to the average fiber mass for each sample set. Table 5.4 shows the fit polynomials used in Figure 5.2 along with their respective R^2 values and the domain of z-direction fiber mass values for which they apply. The ends of these polynomials were smooth so no constant concentration had to be assumed at the ends of the domain of z-directional fiber mass.

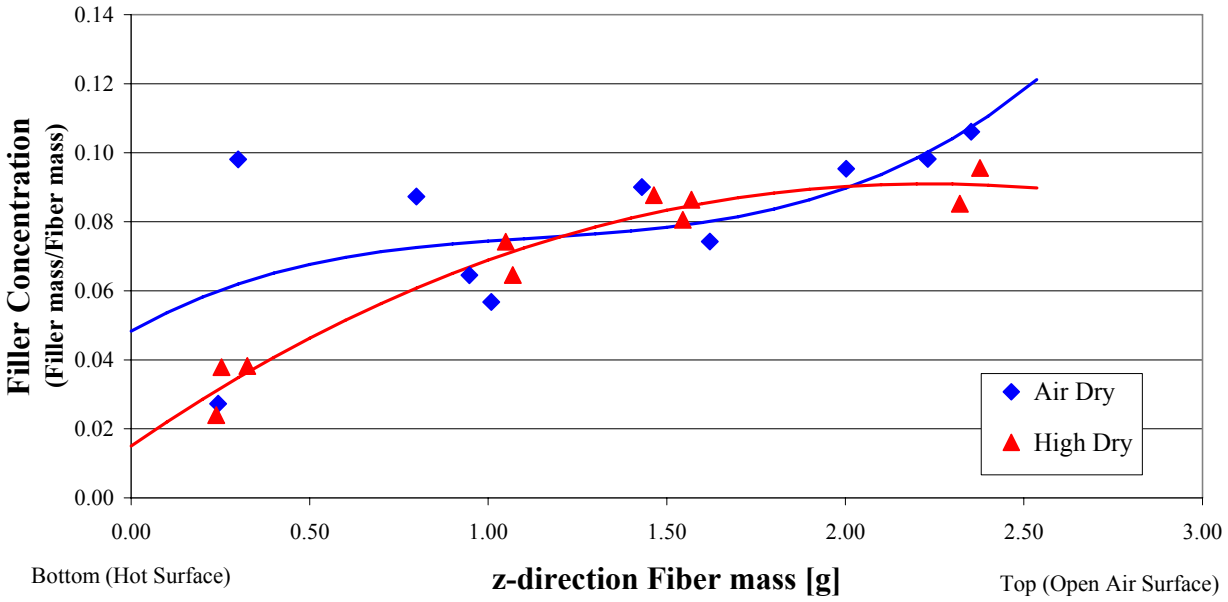

Figure 5.2. Concentration Profiles for G-800 Test 2

Table 5.4. G-800 Test 2 Polynomial Fit Lines

	Polynomial	R^2	z-direction fiber mass [g]
Air Dry	$C = 0.01329z^3 - 0.04528z^2 + 0.05810z + 0.04828$	0.395	0.0-2.5
High Dry	$C = 0.00074z^3 - 0.01847z^2 + 0.07160z + 0.01501$	0.957	0.0-2.5

Table 5.5 compares the average filler mass from the sample handsheets to the filler mass computed by integrating the curves in Figure 5.2.

Table 5.5. G-800 Test 2 Average Filler Mass and Computed Integral Filler Mass

	Average filler mass [g]	Integral [g]
Air Dry	0.1969	0.2005
High Dry	0.1864	0.1755

The maximum difference between the average filler mass and the integral of the polynomials is 6%. This agreement shows that the polynomial fit lines give an accurate representation of how the concentration of filler particle varies through the thickness of the sheet. The concentration profiles for the air drying and high drying cases for G-800 Test 2 are similar. This is again consistent with G-800 Test 1 and that the particles were not subjected to enough force to change their distribution. The higher concentration of particles for both drying levels is at the top (wire side) of the sheet, which is consistent with the literature reviewed [1-3, 10].

The same concentration profile shape exists for both the tests of the G-800 particles even though the procedure to manufacture, dry, split and ash the sheets were slightly different. The conditions of the tests for inducing particle transport were maximized by having a thick sheet with an open sheet structure being dried at a high level. The conditions of the G-800 experiments were designed to give the maximum probability of particle movement during drying. However, the concentration profiles show that particles larger than 20 μm, which would constitute the majority of the mass of a G-800 sample, are not prone to movement through the thickness of a sheet during drying. Therefore, contaminant particles that are 20 μm or larger in diameter inside the sheet would not contribute to contaminant buildup on the dryer cans because the drying forces and capillary flows through the pores created by the heated surface are not large enough to pull particles of this size through the pores to the dryer can surface. Furthermore, despite the sheet being uncompressed, the pores in the paper may be smaller than the particle diameter, which would inhibit transport of particles through the thickness of the sheet.

5.3 G-200 (1-10 µm diameter)

A polynomial was fit to the concentration data points for each drying level of the G-200 experiment so that these polynomials could be integrated to give an average filler mass, which could then be compared to the average filler mass obtained from the samples. The concentration profiles are found in Figure 5.3.

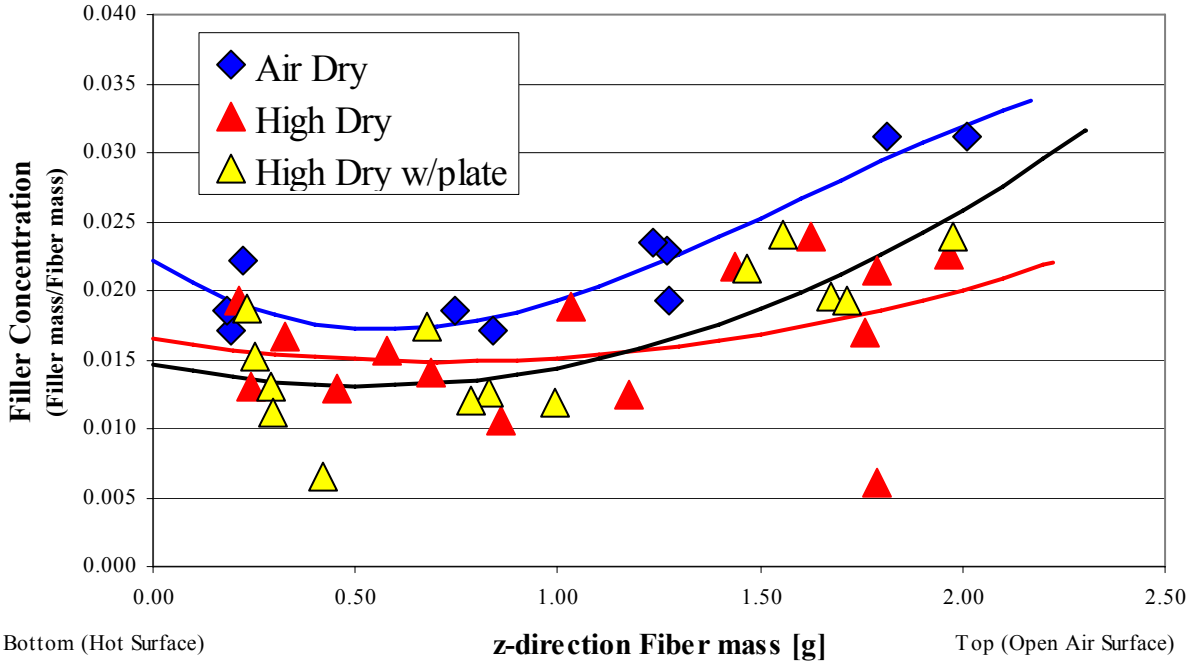

Figure 5.3. Concentration Profiles for G-200 Test

The polynomials for each drying case with their respective R^2 values for the z-direction fiber mass for which they apply are shown in Table 5.6. The computed filler mass is compared to the average filler mass to check that the polynomial accurately fits the true concentration distribution for a sheet. The values predicted by the polynomial can only be trusted in the domain of the fiber mass values. The ends of these polynomials were smooth so no constant

concentration had to be assumed at the ends of the domain of z-directional fiber mass. The integrals of these profiles and the average filler mass recovered for the medium particles are shown in Table 5.7.

Table 5.6. G-200 Test Polynomial Fit Lines

	Polynomial	R^2	z-direction fiber mass [g]
Air Dry	$C = -0.00418z^3 + 0.02031z^2 - 0.01906z + 0.022$	0.869	0.0-2.2
High Dry	$C = 0.00317z^2 - 0.00456z + 0.01649$	0.110	0.0-2.2
High Dry w/ plate	$C = 0.00585z^2 - 0.00615z + 0.01471$	0.589	0.0-2.3

Table 5.7. G-200 Average Filler Mass and Computed Integral Filler Mass

	Average filler mass [g]	Integral [g]
Air Dry	0.0466	0.0494
High Dry	0.0371	0.0397
High Dry w/plate	0.0402	0.0413

The maximum difference between the integral and the average filler mass is 6% so these profiles are a good representation of how the concentration of filler changes through the thickness of the sheet. There is no distinct separation or change in the shape of the profile between the air dry and high dry cases. Blocking vapor from escaping through the top of the sheet by placing a couch plate on top of the sheet during drying did not change the distribution of filler through the sheet. From Figure 3.5, it appears that the water vapor escaping from the sides of the handsheet would produce some kind of radial distribution of particles. However, as with the large particles, particles of a diameter distributed between 1 and 10 μm are still too large for

any movement to occur in the z-direction of the sheet during drying. Therefore, the particles are also too large for any movement to occur in the radial direction.

5.4 PCC (0.1-1 µm diameter)

Since an average of 80% of the filler was recovered in the PCC/dye test, a polynomial was fit to each drying case. The filler concentration curve for the air dry and high dry cases deviate from one another at the bottom of the sheet where the heat was applied. Figure 5.4 shows the two data sets for the two drying cases with their respective polynomial concentration curves.

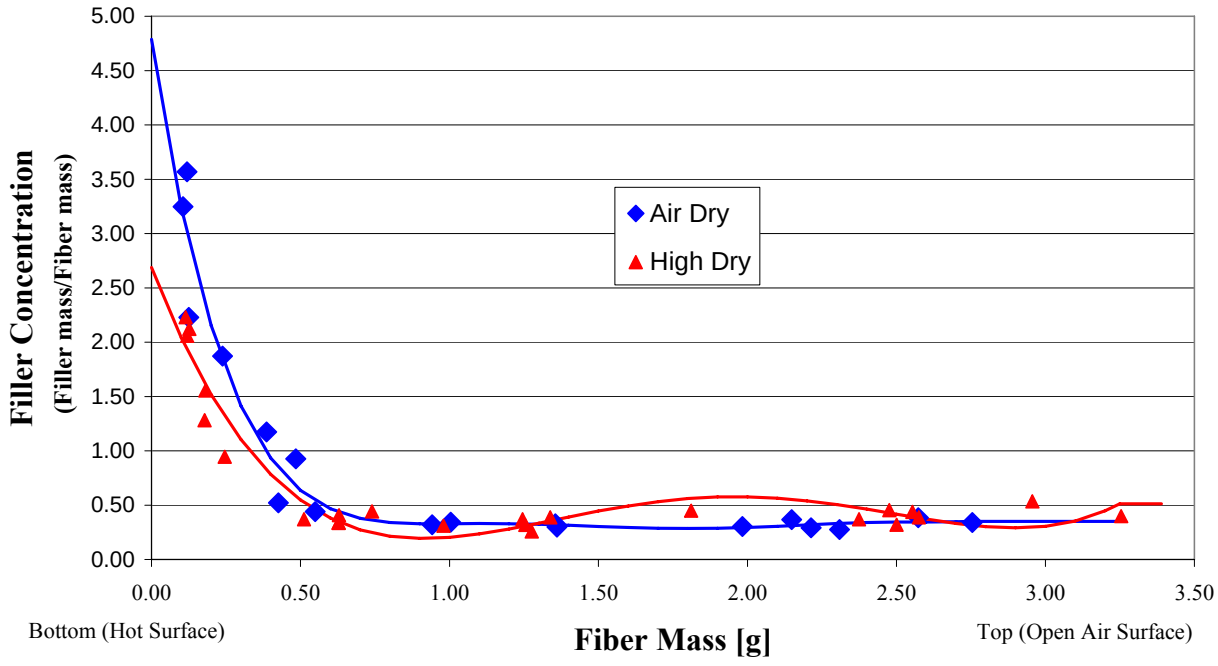

Figure 5.4. Concentration Profiles for PCC/Dye test

The polynomials for each drying case with their respective R^2 values for the z-direction fiber mass for which they apply are shown in Table 5.8. The values predicted by the polynomial can only be trusted in the domain of the fiber mass values.

Table 5.8. PCC/Dye Test Polynomial Fit Lines

	Polynomial	R^2	z-direction fiber mass [g]
Air Dry	$C = 0.23376z^6 - 2.54682z^5 + 11.12783z^4 - 24.83910z^3 + 29.79093z^2 - 18.22527z + 4.78739$	0.945	0.0-2.8
High Dry	$C = 0.34422z^4 - 2.64903z^3 + 6.96675z^2 - 7.14776z + 2.68960$	0.935	0.0-3.3

For polynomials with large derivatives at the end points, the concentration is assumed to be equal to the concentration of the end points. This concentration is assumed to be constant from the smallest z-direction fiber mass value to zero and from the largest z-direction fiber mass value to the average sheet fiber mass for the samples dried at that particular level. Table 5.9 shows where the concentration was assumed to be constant at the minimum and/or maximum z-direction fiber mass.

Table 5.9. PCC/Dye Test z-direction Fiber Mass Constant Concentration Domain

	Minimum		Maximum	
	z-direction fiber mass [g]	Concentration	z-direction fiber mass [g]	Concentration
Air Dry	N/A	N/A	2.8-3.3	0.35056
High Dry	N/A	N/A	3.3-3.4	0.51316

The integrals of these profiles and the average filler mass recovered for the PCC/dye test is shown in Table 5.10.

Table 5.10. PCC/Dye Average Filler Mass and Computed Integral Filler Mass

	Average filler mass [g]	Integral [g]
Air Dry	1.7590	1.9674
High Dry	1.6868	1.8592

The maximum difference between the integral and the average filler mass is 11%. Both integrals are about the same percentage higher than the average filler mass so the comparison between the two profiles is an accurate representation of the concentration differences between each drying case. The concentration profiles for air and high dry are similar through the thickness of the sheet except for the bottom 15% of the sheet at the heated surface. Since there are many possible processes occuring for both drying levels, the parameters governing them need to be explored to see whether the geometry and time parameters of the system would allow such phenomena to occur.

5.5 Digital images of dyed handsheets

From examining the faces of the handsheets in Figures 4.7-4.10, there is a difference in "redness" between the air and high dry cases for the same approximate location in the sheet. There is also a change in "redness" through the thickness of the sheet for each of the drying levels. Figure 4.11 gives a more quantitative representation of how the level of dye changes through the thickness of the sheet assuming the intensity corresponds to the concentration of dye present in that particular section of the sheet. The centroid of the three groups of data points displayed in Figure 4.11 was found. The groups of points are shown circled in Figure 5.5.

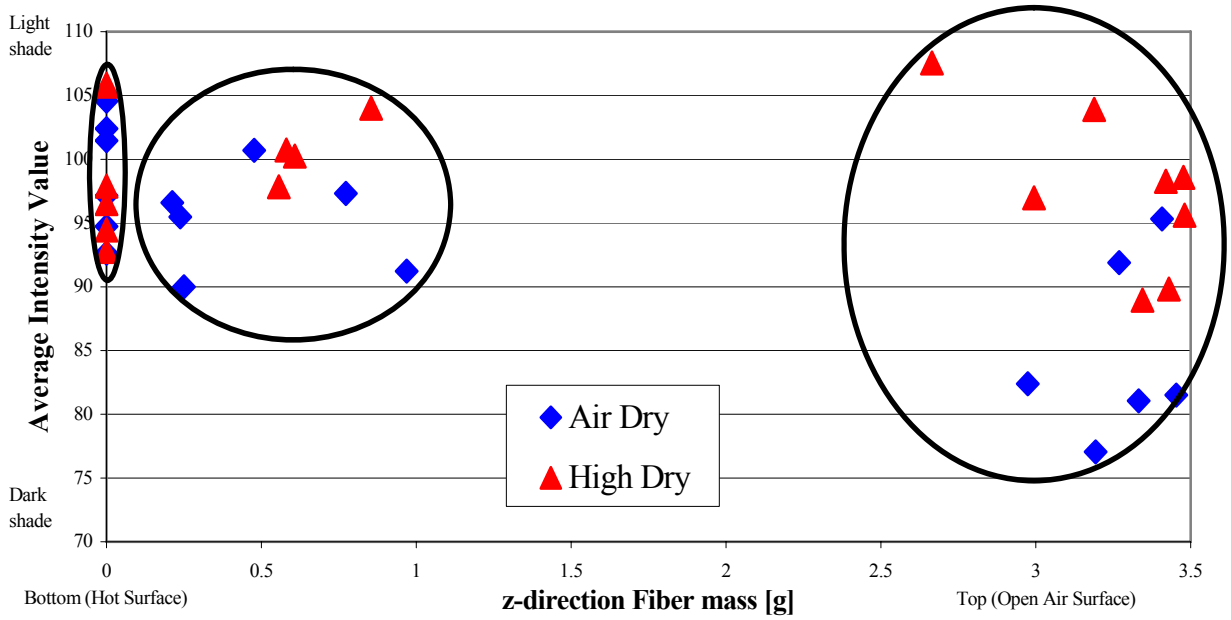

Figure 5.5. Centroid Groups for Intensity versus z-direction Fiber Mass

The centroids of the three groups shown in Figure 5.5 are displayed which smoothed lines connecting the points in Figure 5.6

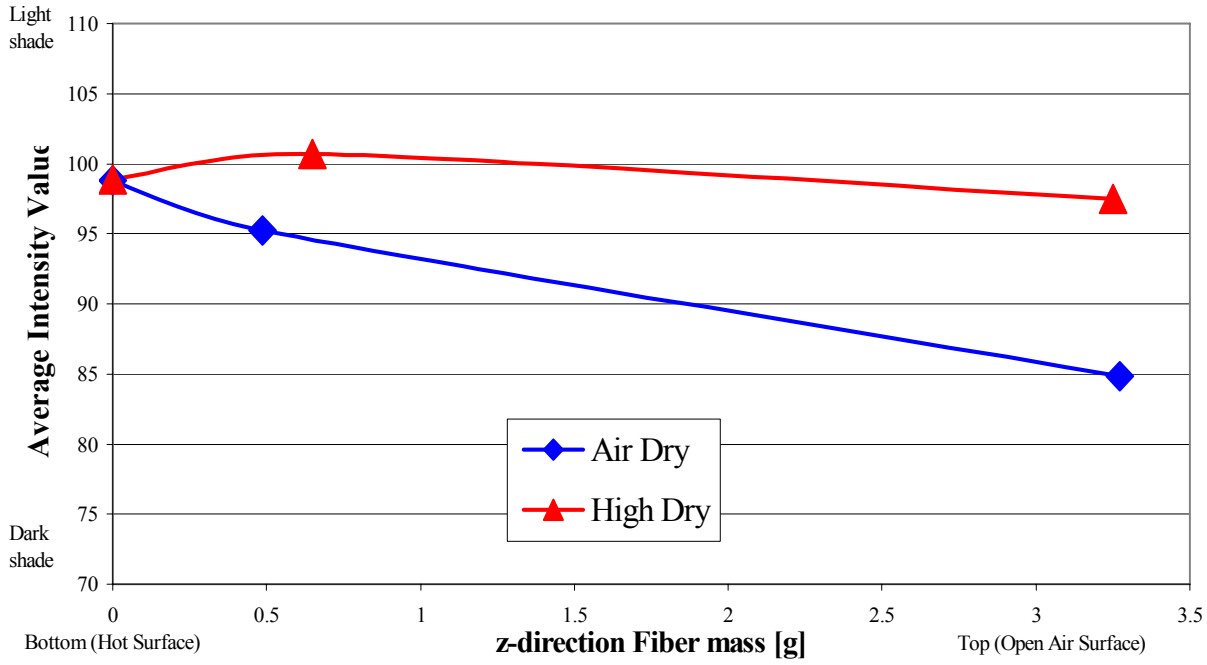

Figure 5.6. Intensity Centroid Versus z-direction Fiber Mass Centroid for PCC/Dye Experiments

Since the dye only moves with the liquid, the concentration of dye is representative of the quantity of water that was evaporated at a particular location in the thickness of the sheet. The intensity across the air dry sheet shows a noticeable decrease across the thickness of the sheet with the lower (darker) intensity being on the top surface where the dye was added as seen in Figure 5.6. The top surface was also open to the air so evaporation could readily occur there. In contrast, the intensity across the thickness of the high dry sheet is essentially constant with a noticeably higher intensity (lighter) at the top surface and a slightly lower intensity (darker) at the bottom surface as shown in Figure 5.6. There is also a slight rise in intensity just above the heated surface for the high dry case. The high dry case had evaporation across the thickness of the sheet. The heated surface would evaporate water at the bottom of the sheet and the drying would cause some liquid movement in the direction of the lower moisture level at that surface thereby pulling dye along with it. The fact that dye ended up on the hot platen shows that the drier bottom part of the sheet caused water containing dye to be wicked towards the heated surface. The rise in intensity near the bottom surface is the point of minimum dye concentration for the sheet at this location. This is in agreement with the results found in the literature [5, 9] for dye concentration profiles across the thickness of sheets. Water flowed from the point of minimum dye concentration just above the bottom surface towards the heated surface and towards the open air surface to be evaporated. The vapor could only leave through the top of the sheet so as it flowed up, it also heated the remaining water via convection. Conduction of heat by the fibers and remaining water in the pores resulted in the final evaporation of the water. A somewhat uniform dye distribution would show that evaporation of water was occurring at multiple “surfaces” as predicted by the different methods above.

5.6 Time Scales for PCC Settling

5.6.1 Particle Kinematics

A simulation of a microparticle falling in water is used to determine the time for a particle to settle through the thickness of a sheet of paper. The time for the particle to travel through the thickness of the sheet will be compared versus the time that a continuous water phase is present in the sheet during drying to determine the significance, if any, of particle settling in the final particle distribution for the PCC/Dye experiment.

A force balance is performed on the particle as shown in the free-body diagram in Figure 5.7.

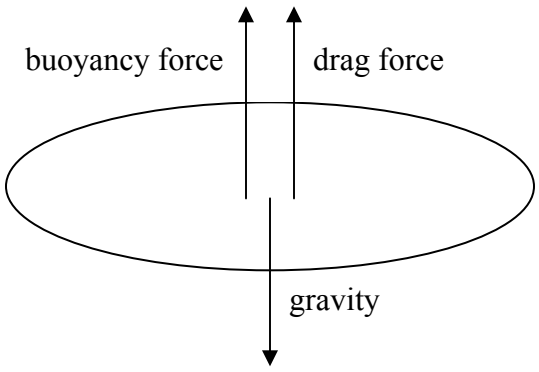

Figure 5.7. Free Body Diagram for Particle in Water

Equation (5.1) shows this force balance on the particle assuming the particle is moving down, where F_g is the force due to gravity, F_d is the drag force, F_b is the buoyancy force, m is the mass of the particle, and a is the particle's acceleration.

$$F_g - F_d - F_b = ma \tag{5.1}$$

To determine the dependence of the drag force on velocity, the terminal velocity is solved for assuming the drag force depends either linearly or quadratically on velocity. The two terminal

velocities can be used to find the Reynolds number in each case. The Reynolds number will determine how the drag force will actually depend on velocity, u. The drag force for the linear and quadratic cases is shown in Equations (5.2) and (5.3).

$$F_d = bu \tag{5.2}$$

$$F_d = qu^2 \tag{5.3}$$

b and q are coefficients that depend on the size of the particle and the viscosity of the fluid. b is the drag coefficient for a linear dependence on velocity and q is the coefficient for a quadratic dependence on velocity. Equations (5.4) and (5.5) show how the coefficients, b and q, for an elliptical particle depend on the viscosity of water, μ_{water}, the equatorial semi-axis of the ellipsoid, a, and the shape factor, K' [32-35].

$$b = 6\pi\mu_{water} aK' \tag{5.4}$$

$$q = 6\pi\mu_{water} a^2 K' \tag{5.5}$$

Substituting the expressions for the drag force into the force balance equation gives the following differential equations after replacing the acceleration as the derivative of the velocity shown as Equations (5.6) and (5.7).

$$m\frac{du}{dt} + bu = F_g - F_b \tag{5.6}$$

$$m\frac{du}{dt} + qu^2 = F_g - F_b \tag{5.7}$$

An analytical expression for the velocity can be found for each differential equation as shown in Equations (5.8) and (5.9) with an initial velocity of zero.

$$u(t) = \left(\frac{F_g - F_b}{b}\right)\left[1 - \exp\left(-\frac{b}{m}t\right)\right] \tag{5.8}$$

$$u(t)=\frac{\sqrt{qF_g - qF_b}}{q}\tanh\left(\frac{\sqrt{qF_g - qF_b}}{m}t\right) \tag{5.9}$$

The terminal velocity can be found by finding the limit of the velocity functions as $t\to\infty$. The terminal velocity is shown in Equations (5.9) and (5.10).

$$u(t\to\infty)=\left(\frac{F_g - F_b}{b}\right) \tag{5.9}$$

$$u(t\to\infty)=\frac{\sqrt{qF_g - qF_b}}{q} \tag{5.10}$$

The velocity can now be plugged into the formula for the Reynolds number shown in Equations (5.11) and (5.12), where ρ_{water} is the density of water, u_t is the terminal velocity of the particle, r_{eff} is the effective radius of the particle, and μ_{water} is the viscosity of water.

$$\mathrm{Re}_{linear}=\frac{\rho_{water}u_t r_{eff}}{\mu_{water}}=\frac{\rho_{water}r_{eff}\left(F_g - F_b\right)}{\mu_{water}b} \tag{5.11}$$

$$\mathrm{Re}_{quad}=\frac{\rho_{water}u_t r_{eff}}{\mu_{water}}=\frac{\rho_{water}r_{eff}\sqrt{qF_g - qF_b}}{\mu_{water}q} \tag{5.12}$$

Since the geometry of the system is on the micron scale, the factors depending on the radius of the particle will simply be a function of that radius, 10^{-6} m. The equations for the force of gravity and the buoyancy force are given in Equations (5.13) and (5.14), where ρ_{PCC} is the density of PCC, V_{part} is the approximate volume of the particle, g is the gravitational acceleration, and γ_{water} is the specific weight of water.

$$F_g=\rho_{PCC}V_{part}g=(2170)\left(1\times10^{-6}\right)^3(9.81)=2.129\times10^{-14} \tag{5.13}$$

$$F_{\mathrm{b}} = \gamma_{\mathrm{water}} V_{\mathrm{part}} = (9789)\left(1\times10^{-6}\right)^3 = 9.789\times10^{-15} \tag{5.14}$$

Approximate expressions for b and q are given in Equations (5.15) and (5.16) by simplifying Equations (5.4) and (5.5) by eliminating the terms that only scale the coefficients and do not effect the order of magnitude of the coefficients. The equatorial radius, a, becomes the effective radius, r_{eff}.

$$b \approx r_{\mathrm{eff}}\,\mu_{\mathrm{water}} \tag{5.15}$$

$$q \approx r_{\mathrm{eff}}^2\,\mu_{\mathrm{water}} \tag{5.16}$$

Substituting the numerical values into the Reynolds equations gives Equations (5.17) and (5.18).

$$\mathrm{Re}_{\mathrm{linear}} = \frac{(1000)\left(1\times10^{-6}\right)\left(2.129\times10^{-14} - 9.789\times10^{-15}\right)}{\left(1.002\times10^{-3}\right)^2\left(1\times10^{-6}\right)} \tag{5.17}$$

$$\mathrm{Re}_{\mathrm{linear}} = 1.145\times10^{-5}$$

$$\mathrm{Re}_{\mathrm{quad}} = \frac{(1000)\left(1\times10^{-6}\right)\sqrt{\left(1\times10^{-6}\right)^2\left(1.002\times10^{-3}\right)\left(2.129\times10^{-14} - 9.789\times10^{-15}\right)}}{\left(1.002\times10^{-3}\right)^2\left(1\times10^{-6}\right)^2} \tag{5.18}$$

$$\mathrm{Re}_{\mathrm{quad}} = 3.388\times10^{-3}$$

The Reynolds numbers for both linear and quadratic dependences are less than $10^3<\mathrm{Re}<10^5$ where the quadratic model is appropriate. For Re << 1, the hydrodynamic drag force on a moving object is simply linearly proportional to the object's velocity through the fluid, and being a frictional (or energy-dissipating) force, it acts to oppose the motion [32-35]. Stoke's Law applies for Reynolds numbers less than 1.0. The drag force according to Stoke's law for an

ellipsoid particle is given by Equation (5.19), by combining substituting Equation (5.4) into Equation (5.2), where u is the particle velocity, a is the equatorial semi-axis of the ellipsoid, K' is a shape factor.

$$F_d = 6\pi\mu_{\text{water}} aK'u \tag{5.19}$$

The shape factor depends on the direction of movement of the ellipsoid. An ellipsoid could move in the two general directions shown in Figure 5.8 [35].

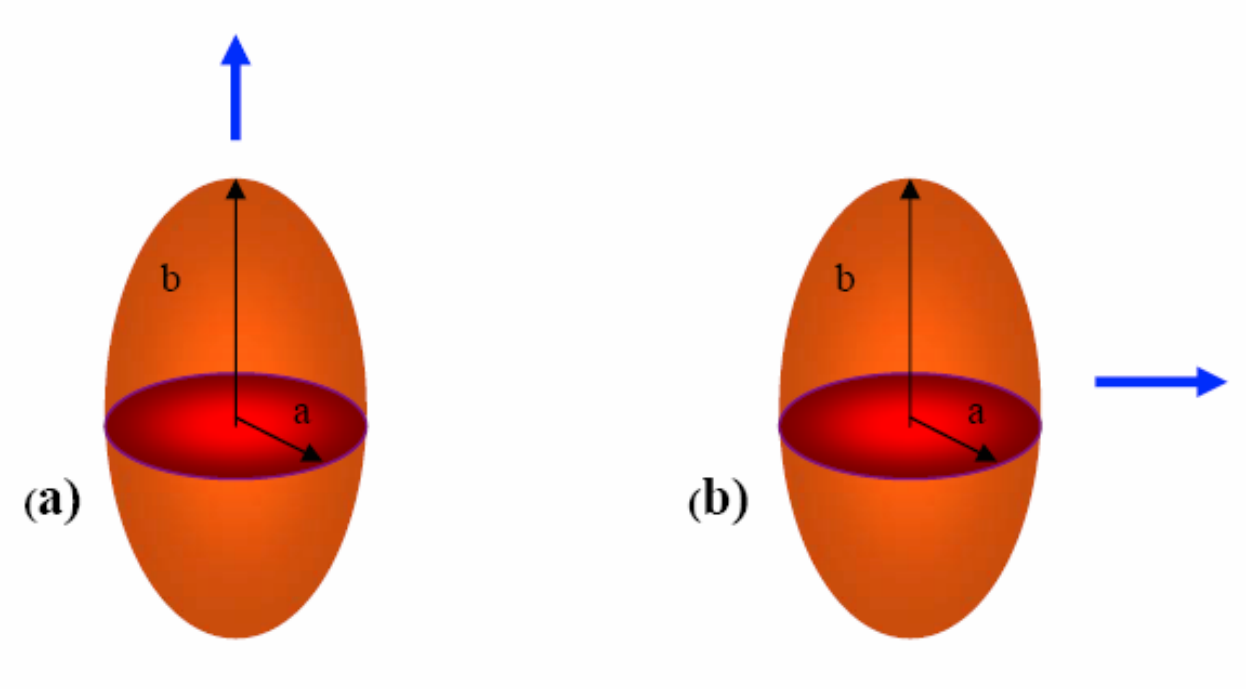

Figure 5.8. Principal Directions of Motion for an Ellipsoid

The shape factor for an ellipsoid moving as shown in Figure 5.8(a) is found using Equation (5.20) [34].

$$K' = \frac{\frac{4}{3}\left(\beta^2 - 1\right)}{\frac{\left(2\beta^2 - 1\right)}{\left(\beta^2 - 1\right)^{1/2}} \ln\left[\beta + \left(\beta^2 - 1\right)^{1/2}\right] - \beta} \qquad \left(\beta = \frac{b}{a}\right) \tag{5.20}$$

Since the aspect ratio is 1.5-2.0 for the PCC particles, the shape factor for PCC oriented as in Figure 5.8(a) is 1.10-1.20, respectively. The shape factor for an ellipsoid moving as shown in Figure 5.8(b) is found using Equation (5.21) [34].

$$K' = \frac{\frac{8}{3}\left(\beta^2 - 1\right)}{\frac{\left(2\beta^2 - 3\right)}{\left(\beta^2 - 1\right)^{1/2}} \ln\left[\beta + \left(\beta^2 - 1\right)^{1/2}\right] + \beta} \qquad \left(\beta = \frac{b}{a}\right) \tag{5.21}$$

Since the aspect ratio is 1.5-2.0 for the PCC particles, the shape factor for PCC oriented as in Figure 5.6(b) is 1.19-1.38, respectively. The appropriate equation of motion (5.6) has its analytical solution (5.8) which is repeated here in Equation (5.22).

$$u(t) = \left(\frac{F_g - F_b}{b}\right)\left[1 - \exp\left(-\frac{b}{m}t\right)\right] \tag{5.22}$$

Equation (5.23) shows the value of the time constant, τ, for Equation (5.22).

$$\tau = \frac{m}{b} \approx 1 \times 10^{-9}\ \text{s} \tag{5.23}$$

The small value of the time constant means that the particle reaches a constant velocity almost instantly. Integrating Equation (5.22) will give the dependence of the position of the particle with time, which is shown in Equation (5.24), where y_0 is the position at the top of the handsheet.

$$y(t) = y_0 - \frac{F_\text{g} - F_\text{b}}{b} t\left[1 - \exp\left(-\frac{b}{m}t\right)\right] \tag{5.24}$$

The handsheets for the experiments were on average 2 mm thick. The range of time for a particle to settle is found by finding where Equation (5.24) crosses the x-axis. Equation (5.24) is plotted in Figure 5.9 to show how the position varies with time and at what time the particle reaches the bottom of the sheet.

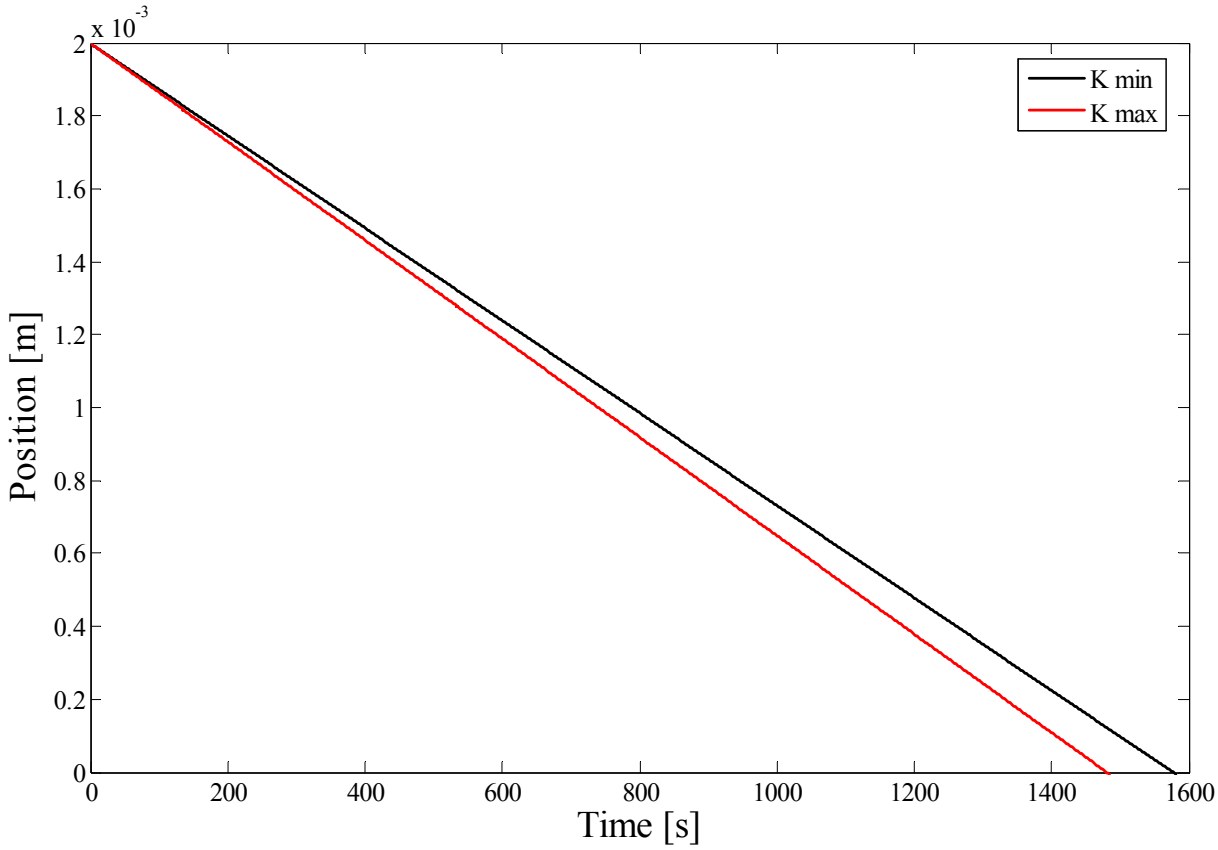

Figure 5.9. Position versus Time for PCC Particle Settling in Water for Max and Min K'

Since the time constant is small, Figure 5.9 shows a linear dependence of position on time because the transient acceleration dies out quickly. By realizing that Equation (5.24) is essentially linear in time, the derivative of the linear terms will give the constant velocity

experienced by the particle during settling. The derivative of Equation (5.24) is approximated in Equation (5.25).

$$u(t)=\frac{dy(t)}{dt}\approx\frac{d}{dt}\left[y_0-\frac{F_g-F_b}{b}t\right]=\frac{F_g-F_b}{b}=0.5\times10^{-7}\,\frac{\mathrm{m}}{\mathrm{s}} \tag{5.25}$$

The settling time was found to the nearest second. Table 5.11 gives the settling times based on the orientation of the particle falling and the aspect ratio of the particle. The duration of the PCC/Dye drying tests were 16 min and 18 min or 960 s and 1080 s.

Table 5.11. Settling Time of PCC

Orientation	Aspect ratio	Settling Time [s]	Settling Time [min]
Figure 5.6(b)	2	1481	24.5
Figure 5.6(a)	1.5	1578	26.3

5.6.2 Percent solids versus time for the drying sheet

To determine when there is no longer a continuous phase of water in the PCC/Dye handsheet during drying, percent solids is plotted versus time using a constant evaporation rate. The constant evaporation rate was computed by dividing the average drying time to reach 95% solids for the air dry and high dry cases by the average mass of water contained in a sheet that was removed from the wire after forming. Figure 5.10 is the percent solids versus time for the high dry case.

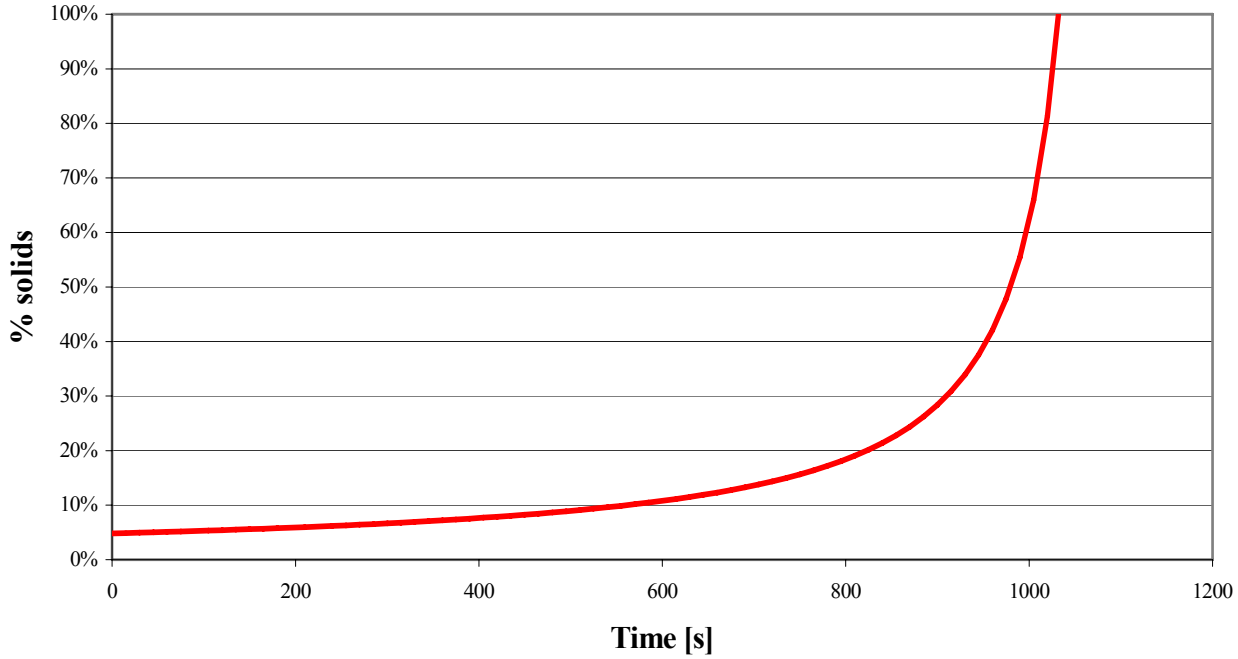

Figure 5.10. Percent Solids Versus Time for PCC/Dye Test (high dry)

Figure 5.11 is the comparison of percent solids versus time for the high dry and air dry cases for the PCC/Dye test.

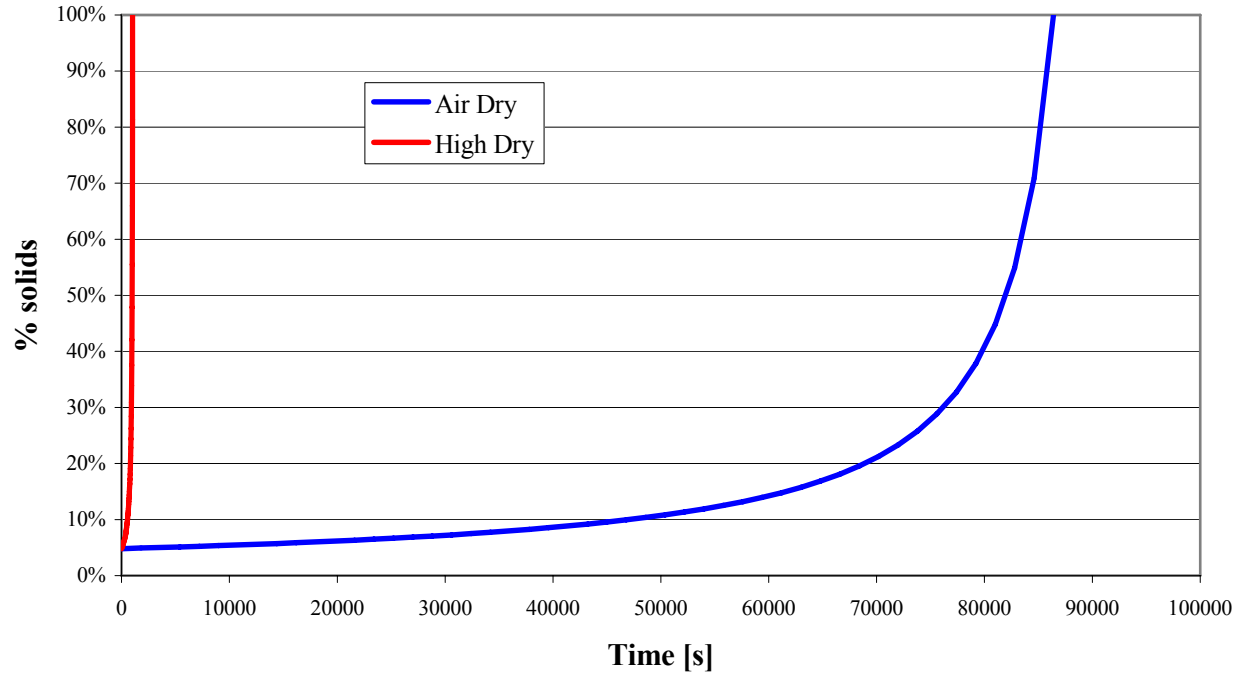

Figure 5.11. Percent Solids Versus Time Comparison for PCC/Dye Test

The evaporation rate, surface temperature and moisture contents from the PCC/Dye experiment are compared versus a simulation of a dryer section performed by Ascensio and Seyed-Yagoobi [36]. The drying parameter values in Table 5.12 show how the conditions in the PCC/Dye experiment compare to conditions on the dryer section of a paper machine.

Table 5.12. Parameter Comparison between PCC/Dye Test and Ascensio Simulation

	Evaporation rate [kg/m^2-hr]	Surface temperature [°C]	Initial moisture content	Final moisture content
PCC/Dye	13.8	200	900%	5%
Simulation	10-20	84.2-113.4	127%	4%

The surface temperature and initial moisture contents for the PCC/Dye experiment were higher than the conditions seen on a typical dryer section from the Ascensio simulation. The evaporation rate produced by the PCC/Dye experiment was in the range as for the simulation based on an actual dryer section. The fluid flow velocity depends on the evaporation rate so the driving force created by the PCC/Dye experiments is comparable to the conditions on an actual paper machine.

5.6.3 Comparison of time scales

The air dried PCC/Dye sheets had a continuous water phase in the sheets, assuming a continuous water phase is around 30% solids, for approximately 20 hours. Robertson [37] predicted that inter-fiber free water would be removed at 30% solids. The longest time for a PCC particle to settle took on the order of minutes to settle through the thickness of the sheet. In the air dry case, the settling phenomena seems to be reason for the particle distribution in the thickness of the sheet assuming a pathway that the particle is capable of following. Air drying of

the sheets is simply too slow, by a factor of 60, compared to settling to be the main driving force. A sheet at a low solids content (<30%) would have a very open structure to allow micron sized particles to fall to the bottom with limited interaction with the fibers. The sheet would also contain a continuous water phase in which the particle could move.

The high dried PCC/Dye sheets only had a continuous water phase on a time scale of minutes. The settling phenomenon is also on a time scale of minutes. For the high dry case, the scales of time are very similar with the settling time being slightly larger in a range of 24-25 minutes compared to the drying time to reach 30% solids in a time of 14-15 minutes. Settling is less of a factor for the movement of particles completely through the thickness. Local settling of the particles could occur assuming water evaporation only occurred at the surface from which the particle began its initial motion. The evaporation front would have to "follow" the particle through the sheet for the particle to traverse the thickness of the sheet.

5.7 Velocity calculation

A simple calculation can be performed to determine an average velocity of fluid through the paper assuming a constant evaporation rate. The constant evaporation rate was computed by dividing the average drying time to reach 95% solids for the air dry and high dry cases by the average mass of water contained in a sheet that was removed from the wire after forming. Equation (5.25) is the mass flow rate, $\dot{m}$, in terms of the density of water, ρ_{water}, velocity of the water, V_{water}, and the cross sectional area of the sheet, A_{cross}.

$$\dot{m} = \rho_{\text{water}} V_{\text{water}} A_{\text{cross}} \tag{5.25}$$

Solving for the velocity gives Equation (5.26).

$$V_{\text{water}} = \frac{\dot{m}}{\rho_{\text{water}} A_{\text{cross}}} \tag{5.26}$$

The velocity of water due to evaporation for the air and high dry cases for the PCC/Dye experiment is shown in Table 5.13. The settling velocity calculated from the slope of the line in Figure 5.7 is also shown in Table 5.13.

Table 5.13. Velocity of Water for Air and High Dry PCC/Dye Experiment Compared to Particle Settling Velocity

Air Dry [m/s]	4.567×10^{-8}
High Dry [m/s]	3.824×10^{-6}
Settling Velocity [m/s]	0.500×10^{-7}

The settling velocity is between the velocity calculated for the air dry and high dry tests for the PCC/Dye experiment. The high dry velocity is one order of magnitude greater than the settling velocity so the movement contribution by settling would be minimal in the high dry case. The settling velocity is an order of magnitude greater than the velocity for the air dry case. Here, the settling velocity would provide the contribution to the movement of the particle assuming the particle had a pathway in which to move through the thickness of the sheet. Figure 5.12 shows the distance the particle would be transported given the velocities shown in Table 5.13 and the time for the sheet to reach 30% solids for each drying case since the particle needs to have a continuous water phase through the sheet to traverse the sheet.

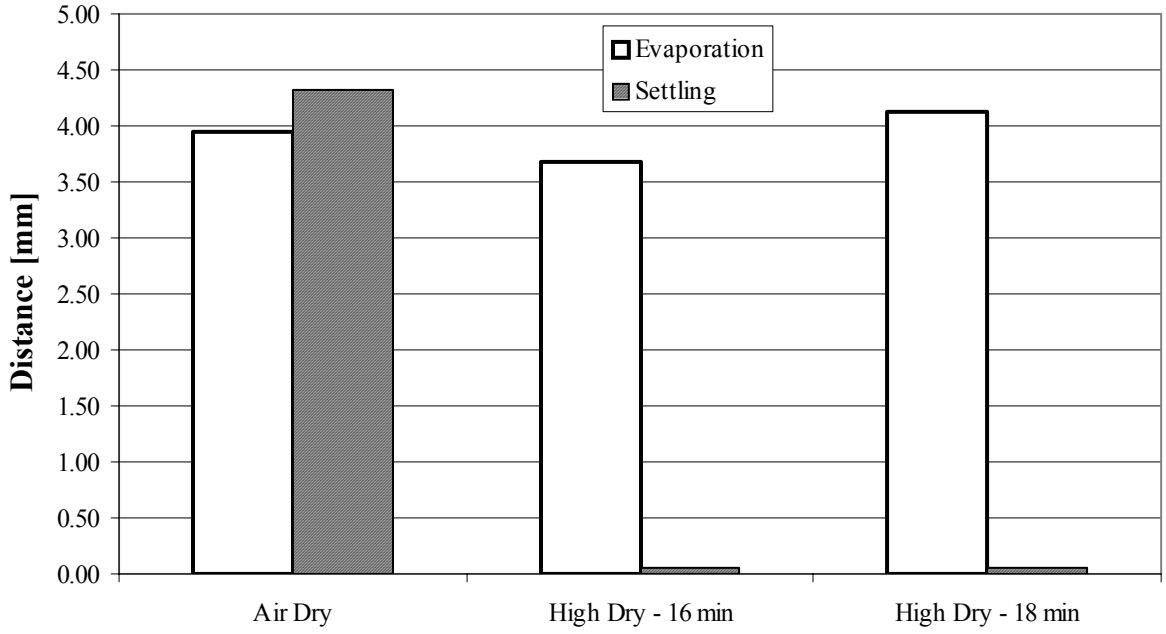

Figure 5.12. Transport Distance for PCC Particle

For the air dry case, the particle would travel the same distance compared to the velocity contribution from settling compared to evaporation. The particles would reach the bottom of the sheet for settling and evaporation because the sheet thickness is 2 mm. The high concentration of PCC particles at the bottom of the sheet was most likely a combination of settling and evaporation induced transport for the air dry case. The evaporation velocity in the high dry case would move the particle through the thickness of the sheet. The concentration of PCC at the bottom of the sheet for the high dry case was not as large as the concentration of PCC for the air dry case because the air dry case had settling and evaporation induced transport to move the particles towards the bottom surface while the high dry case only had the evaporation velocity to transport the particles. The distances above were computed using the time for a continuous water phase in the sheet at 30% solids.

5.8 Summary of Discussion and Analysis

5.8.1 G-800 and G-200 Tests

The concentration profiles for the G-800 Test 1 and 2 and the G-200 Test showed little separation between the air dry and high dry case. The conditions for these tests were set to maximize the possibility of movement of the particles, which ranged in diameter from 1-75 μm. Particles in this size range are not likely to move through the z-direction of a sheet during the drying process. Also, the number of pores with a diameter greater than the particle diameter is small, which inhibits particle transport through the thickness of the sheet.

5.8.2 PCC in the PCC/Dye Test

The PCC particles from the PCC/Dye Test did move through the thickness of the sheet during the drying process. The filler concentration at the bottom of the sheet for the air dry case was larger than the filler concentration for the high dry case. The difference was explored by performing settling velocity calculations and evaporation velocity calculations. It was found that settling and evaporation could be the contributors to the large concentration at the bottom of the air dry sheets because particles traveling at the settling and evaporation velocities for the duration of the air dry experiment would travel over 2 mm, which is the thickness of the sheet. The transport in the high dry case could be due to the velocity of fluid induced by evaporation. This velocity over the time duration for the high dry experiments would carry the particle through the thickness of the sheet. The transport distance by just evaporation for the high dry case could explain the lower concentration of filler at the bottom surface for the high dry case as compared to the air dry case.

5.8.3 Dye in the PCC/Dye Test

The average intensity profile across the thickness of the PCC/Dye sheets had a different shape for the air dry case compared to the high dry case. A high intensity corresponds to a low dye concentration and a low intensity corresponds to a high dye concentration. From the average intensity profile for the air dry case, the dye concentration was shown to decrease from the top surface to the bottom surface of the sheet. Since the dye concentration is a measure of the quantity of water evaporated at a particular location, the top surface of the air dry sheets was where the majority of the evaporation occurred. The majority of the water and dye mixture remained at the top surface of the sheet where the water could be evaporated. Dye was present across the thickness of the sheet so the dye did settle and diffuse into the sheet for the air dry case. From the average intensity profile for the high dry case, a near constant dye concentration was observed. The dye concentration at the bottom and top surfaces was slightly greater than the concentration in the interior of the sheet. Water moved from a location near the bottom of the sheet where there was a minimum dye concentration, or a smaller quantity of water evaporated, towards the top and bottom surfaces where a larger quantity of water was evaporated.

CHAPTER 6

PROPOSED MECHANISMS

6.1 Differences in Filler Particle Distributions

From the experimental conditions recorded and the calculations performed, the differences in the filler particle distributions for the PCC/Dye experiment can be explained with the following proposed mechanisms.

6.1.1 Air Dry

1. Sedimentation – Sedimentation of PCC particles was estimated to take 25 minutes assuming there was a continuous water phase available in which the particles could settle. For the air dry case, there was a continuous water phase for hours which would be adequate time for the particles to settle and collect forming a growing filler cake at the bottom surface. The filler cake at the bottom would yield the high concentration of filler at the bottom surface of the sheet as shown in Figures 4.6 and 5.4 for the air dry case.

2. Evaporation – Mechanisms for inducing flow such as the capillary flow action due to evaporation velocity values as shown in Table 5.7 is very small. However, the time scale for which they occur is long enough that the particles would travel a distance greater than the thickness of the sheet even at such a slow velocity.

6.1.2 High Dry

1. Sedimentation – Sedimentation could occur on a local scale because water for a continuous fluid phase in the sheet was evaporated before a PCC particle could travel from the top of the sheet to the bottom of the sheet.
2. Wicking – The hot surface would evaporate water in the vicinity of the bottom of the sheet which would draw water from the level above towards the heated surface. The moisture flow and hence particle movement would only occur for 10-12 minutes and then the particles would remain in place in the sheet. The lower concentration of filler particles for the high dry case as shown in Figures 4.6 and 5.4 shows that the fluid flow due to wicking of moisture towards the heated surface actually draws less of the mass of particles than if the particles were simply allowed to settle through the sheet. The wicking action only acts for a short time while the time for which sedimentation is allowed to occur in the air dry case is much larger. The shorter time scale for wicking does not lend itself to moving a significant mass of particles as compared to sedimentation.
3. Heat pipe – The vapor forming by the evaporating water at the hot surface travels up towards the top of the sheet. The vapor is convectively cooled by the water moving towards the hot surface. The vapor would then recondense and flow towards the heated surface to vaporize again creating a heat pipe effect. The particle distribution for the high dry case as shown in Figures 4.6 and 5.4 shows less concentration than the air dry case which could be attributed to the heat pipe and vapor flow effects. The water flowing towards the hot surface could pull particles towards the hot surface but the high

temperature of the heated surface could evaporate water at an interface just above the heated surface. Therefore, the particles being transported down with the flow of liquid would be stopped when this water evaporated just about the heated surface.

6.2 Differences in Intensity/Dye Concentration

From the experimental conditions recorded and the calculations performed, the differences in the dye distributions for the PCC/Dye experiment can be explained with the following proposed mechanisms.

6.2.1 Air Dry

1. Atmospheric convection – The moisture at the top surface of the air dry sheet would evaporate by atmospheric convection. Taking the dye concentration to be a measure of the quantity of water evaporated at a given surface, the high concentration of dye at the top surface of the air dry sheet shows that the dye solution remained at the top of the sheet and evaporated first before the moisture from the bottom of the sheet was drawn up to evaporate.
2. Diffusion/sedimentation and wicking – The steep drop in concentration across the air dry sheet can be attributed to the small effect of dye diffusion and sedimentation while the sheet was evaporating moisture off the top surface. Dye that started off at the top of the sheet did move towards the bottom of the sheet due to diffusion created by the initial dye concentration gradient across the sheet and settling of the dye particles. This process was slow enough that evaporation of the solution at the top of the sheet trapped a larger concentration of dye at the top of the sheet. Dye that diffused or settled into the sheet

could be moved slightly towards the surface when moisture was wicked up towards the top surface where evaporation was taking place.

6.2.2 High Dry

1. Wicking – Evaporation caused by the heated surface would draw moisture from the top of the sheet towards the heated surface because of a moisture gradient across the thickness of the sheet. Dye in this moisture would be carried along with the flow and be deposited at the heated surface where the water was evaporated. A higher concentration of dye at the bottom of the sheet for the high dry case compared to the air dry case can be explained by this flow of moisture and evaporation at the bottom surface.
2. Heat Pipe – The heat pipe effect described in the particle flow mechanisms would apply to the high dry case with dye. However, dye would only be drawn towards the heated surface after the vapor recondensed and started flowing towards the heated surface again. This action would carry more dye to the bottom of the sheet, creating a higher dye concentration at the bottom surface.
3. Evaporation at multiple surfaces – The relatively uniform dye concentration through the thickness of the high dry sheet can be explained by having evaporation occur at multiple "surfaces" within the sheet thickness. Heat conducted by the fibers and interpore water would help to vaporize water above the heated surface. Vapor flowing up through the sheet would convectively heat water in the middle of the sheet causing it to vaporize and deposit dye on the fibers. Also, the top surface, which is open to the air, would have moisture evaporating from its surface. While the driest part of the sheet would be the heated surface, other surfaces would have evaporation taking place whereby wicking would occur at those surfaces bringing the dye along with it creating a slightly larger concentration of dye at the

heated surface but a more uniform concentration across the thickness as compared to the air dry case.

4. Diffusion/Sedimentation – The effects of diffusion and sedimentation of the dye are too slow to create a noticeable impact on the dye concentration throughout the high dry sheet. The flows of moisture due to the heated surface happen much faster before the dye could begin to diffuse or settle.

6.3 Hypotheses for Differences in Filler and Dye Distribution

6.3.1 Filler Distribution

The most likely hypothesis for the differences in the PCC filler distribution at the bottom surface of the sheet shown in Figure 4.6 and 5.4 is due to sedimentation and evaporation in the air dry case and wicking in the high dry case. For the air dry case, the particles would move a distance of 2 mm, or the thickness of the handsheet, in ~11 hours by using the computed settling velocity of 0.5×10^{-7} m/s. The particles would also move the distance of the thickness of the sheet in ~12 hours by using the computed evaporation velocity of 4.567×10^{-8} m/s. The continuous water phase in the air dry case existed for ~18 hours so there was ample time for a particle, assuming it had a path through the sheet, to settle and be transported by evaporating fluid velocities to the bottom of the sheet. The particles in the high dry case were most likely pulled towards the bottom of the sheet by wicking action from the flow of water toward the heated surface. The water would evaporate at a slightly higher level above the heated surface the longer the handsheet was allowed to dry as the temperature of the bottom of the sheet increased. The particles in the high dry case would move a distance of over 3.5 mm at the average water velocity of 3.824×10^{-6} m/s computed in Section 5.8 for the 13 minutes of drying time when a

continuous water phase existed. Since evaporation was the only contributor to particle transport for the high dry case, the filler concentration at the bottom surface was lower for the high dry case compared to air dry case.

6.3.2 Dye Distribution

The most likely hypothesis for the differences in the dye distribution is the dominance of atmospheric convection in the air dry case versus the wicking of fluid towards the top and bottom surfaces of the sheet in the high dry case. The larger dye concentration at the top surface of the air dry sheet shows that a larger quantity of water was evaporated at that surface than any other location in the sheet. The majority of the dye poured onto the top surface of the air dry sheets remained at the surface and was evaporated by atmospheric convection. Dye did reach the bottom surface of the sheet but this was due to a small contribution of settling and diffusion. For the high dry case, fluid flow occurred in two directions by wicking. Evaporation at the bottom, heated surface pulled water from just above this surface towards the hot platen to be evaporated. Water was also pulled by wicking towards the top, open air surface. The hot vapor from the bottom of the sheet could flow up through the sheet and evaporate water as it is transported through the sheet with the majority of that evaporation happening at the top, open air surface. The higher evaporation rates at the top and bottom surfaces would draw fluid by wicking towards these surfaces to be evaporated as shown by the higher dye concentration present at these surfaces.

CHAPTER 7

CONCLUSION

The particle and dye movement studies performed showed an array of processes at work simultaneously. However, some bounds of when flow of particles or dye occur have been determined that can be applied to the deposition of contaminant on dryer can surfaces. For contaminant to be extracted from the sheet to deposit on the dryer can, the following criteria were found to cause particle transport.

1. The particle diameter must be ~1.0 μm or less.
2. A very open sheet structure is required
3. Solids content less than 30% in the sheet for an extended period of time (~17 minutes) is required for flows to develop.
4. A high surface temperature to dry the paper was required (200°C surface temperature).

The particles for the G-800 Tests and the G-200 Test, which were from 1-75 μm in diameter, were not transported across the thickness of the sheet during drying. The particle diameter was not small enough so that the particles could move through the pores of the sheet. The number of pores that were the same size as the particle diameter was too few for any significant particle transport to occur.

The PCC particles with a diameter of 0.1-1.0 μm in the PCC/Dye Test could be transported through the thickness of a handsheet. The most probable mechanism for PCC transport in the air dry case is sedimentation and evaporation induced transport of the particles. The time that the sheet contains a continuous water phase and the particle settling velocity would allow a particle with a path through the sheet to travel ~3.5 mm which is greater than the

thickness of the sheet (2 mm). The most probable mechanism for PCC transport in the high dry case is wicking action from the flow of water toward the heated surface. The fluid velocity due to evaporation combined with the time that the sheet contained a continuous water phase would transport the particle ~4.0 mm which is less than the thickness of the sheet. The primary contribution to transport distance due to the fluid velocity from evaporation for the high dry case explains the lower concentration of filler at the bottom surface for the high dry case as compared to the air dry case, which had evaporation and settling velocities contributing to particle transport.

The red dye was also transported through the thickness of the sheet during drying. The majority of the dye poured onto the top surface of the air dry sheets remained at the surface and was evaporated by atmospheric convection. Dye did reach the bottom surface of the sheet for the air dry case. The most probable mechanism for the small quantity of dye transport in the air dry case is diffusion and settling of the dye. For the high dry case, the most probable mechanism for dye transport is the wicking of fluid towards the bottom, heated surface and the top, open air surface. The hot vapor from water evaporated at the bottom of the sheet could flow up through the sheet and evaporate water as it is transported through the sheet with slightly larger quantities of water being evaporated at the top and bottom surfaces compared to the interior of the sheet. The higher evaporation rates at the top and bottom surfaces would draw fluid to be evaporated from these surfaces by wicking.

CHAPTER 8

FUTURE WORK

Since the hypothesis of particle flow from the interior of the sheet was proven to exist in a very specialized case, this may not be the main process by which contaminant deposits on dryer cylinders. Further investigation of the particle flow hypothesis will be needed to completely eliminate this possibility especially in the area of solute transport similar to the dye experiments performed here. Some contaminants are in solution and could "plate out" or precipitate as the liquid evaporates at the hot surface. The dye results from this study begin to explore the behavior of dissolved contaminants but further investigation is needed to understand the processes that would yield deposition on dryer cylinders from dissolved contaminants. Besides bulk sheet phenomena, the deposition of contaminant on the dryer cylinders could be simply surface phenomena. Investigating the factors and parameters of a surface phenomena system would yield more insight into how to prevent the contaminant build up on dryer cylinders. A computational fluid dynamics model would give information to guide the design of future experiments.

APPENDIX A

MATLAB PROGRAM FOR DIGITAL IMAGE ANALYSIS

```
% Andrew Clarke
% Master's Thesis Research
% Converts jpg image into histogram of color values
% Computes various data values for the color/intensity peaks generated

clear all

% Input the number of pictures to compare or compute intensity or color
% values for.
num_pic = input('How many pictures do you want to compare? ');

% Variables initialized to save color and intensity values
% A is 0-254 for each bit of intensity or color minus 255 which is
% the color for white
% White was around the edges of the picture so it was filtered out
% grayscale pictures have one color matrix of intensity values 0-255
A = [0:254]';
pic_colorvector = 0;
average_color_filename = 0;
pic_info = 0;
for n = 1:num_pic

    % Picture file must be in current directory
    % imread reads the color/intensity values into a matrix
    pic_filename = input('Enter picture filename: ','s');
    pic_colormatrix = imread(pic_filename, 'jpg');

    % The size of the picture in pixels is found
    pic_size = size(pic_colormatrix);
    num_row = pic_size(1,1);
    num_col = pic_size(1,2);

    % The color/intensity values are put in a column vector
    Z = 0;
    for i = 2:num_col
        Z((i-1)*num_row+1:i*num_row,1) = pic_colormatrix(:,i);
    end
    pic_colorvector(1:length(Z),n) = Z;
    % The values in the column vector are counted for frequency
    % by the histogram function, histc
    A(:,n+1) = histc(Z, 1:254);

    % Data like the number of pixels, the average color/intensity
    % and the value of the maximum frequency
    num_pixels = sum(A(:,n+1));
    average_color = sum(A(:,1).*A(:,n+1))/num_pixels;
    max_pixel = max(A(:,n+1));

    % The color associated with the maximum frequency is found in
```

```
% this loop and placed in max_color
max_color = 0;
counter = 1;
while counter < length(A)
    if max_pixel == A(counter, n+1)
        max_color = counter;
        counter = length(A);
    else
        counter = counter + 1;
    end
end

% The bounds of the peak of color intensity is found
% using the following 2 loops.
% The amount of pixels in these peaks are counted
pixel_ratio = 1;
counter_plus = 1;
while pixel_ratio > 0.01
    max_color_plus = max_color + counter_plus;
    if max_color_plus < length(A)
    plus_n_pixels = A(max_color_plus,n+1);
    pixel_ratio = plus_n_pixels/max_pixel;
    counter_plus = counter_plus + 1;
    else
        pixel_ratio = 0;
    end
end

pixel_ratio = 1;
counter_minus = 1;
while pixel_ratio > 0.01
    max_color_minus = max_color - counter_minus;
    if max_color_minus > 0
    minus_n_pixels = A(max_color_minus, n+1);
    pixel_ratio = minus_n_pixels/max_pixel;
    counter_minus = counter_minus + 1;
    else
        pixel_ratio = 0;
    end
end

% The centroid of the color peak is found
pixel_sum = sum(A(max_color_minus:max_color_plus,n+1));
xA = 0;
yA = 0;
for k = max_color_minus:max_color_plus
    xA = k*A(k,n+1) + xA;
    yA = 0.5*A(k,n+1)^2 + yA;
end
x_centroid = xA/pixel_sum;
y_centroid = yA/pixel_sum;


% The data is saved to a matrix so it can be exported to excel
pic_info(n,1) = max_color_minus;
pic_info(n,2) = max_color;
pic_info(n,3) = max_color_plus;
```

```
    pic_info(n,4) = pixel_sum;
    pic_info(n,5) = average_color;
    pic_info(n,6) = x_centroid;
    pic_info(n,7) = y_centroid;
    pic_info(n,8) = pixel_sum/(max_color_plus - max_color_minus);

end

% This commented section allows the user to plot the histograms
%pic_info
%A;
% max_vec = max(A);
% YMAX = max(max_vec);
% hist(pic_colorvector, 254)
% axis([0 254 0 YMAX]);
% xlabel('Colors');
% ylabel('Number of Pixels');

% Data is exported to excel for further analysis
heading = {'Low Color','Max Color','High Color','Area','Average Color','X
Centroid','Y Centroid'};
xlswrite('sheet.xls', heading, 'Sheet2', 'B1')
xlswrite('sheet.xls', pic_info,'Sheet2', 'B2')
```

REFERENCES

[1] Wei, H., P. Kumar, B. V. Ramarao, and C. Tien, "Drainage and Fine Particle Retention in a Forming Incompressible Fibrous Mat," *Journal of Pulp and Paper Science*, Vol. 22, No. 11, November 1996, pp. J446-J450.

[2] Estridge, R., "Initial Retention of fibers by wire grids," *TAPPI Journal*, Vol. 45, No. 4, April 1962, pg. 285.

[3] Tanaka, H., P. Luner and W. Cote, "How Retention Aids Change the Distribution of filler in Paper", *TAPPI Journal*, Vol. 65, No. 4, April 1982, pg. 95.

[4] Kilpelainen, Riitta, and Jochen Schlegel, "Forming fabric wear and filler distribution of the paper," *Wochenblatt für Papierfabrikation*, Vol. 123, No. 11, November 1995, pp. 486-496.

[5] Devlin, Christopher P., "An investigation of the mechanism of high-intensity paper drying," *IPST Thesis*, June 1986.

[6] Preston, J. M., and J. C. Chen, "The migration of liquids in textile fabrics," *Journal Society of Dyers and Colourists*, Vol. 64, No. 2, February 1948, pp 60-64.

[7] Preston, J. M., and A. Bennett, "The migration of liquids in yarns," *Journal Society of Dyers and Colourists*, Vol. 67, No. 3, March 1951, pp. 101-103.

[8] Dreshfield, Arthur Charles Jr., "A study of transverse moisture distribution and movement during hot-surface drying of paper," *IPST Thesis*, June 1956.

[9] Szikla, Zoltan and Hannu Paulapuro, "Z-directional distribution of fines and filler material in the paper web under wet pressing conditions," *Paperi ja Puu-Papper och Tra*, September 1986, pp. 654-664.

[10] MacGregor, M.A., "Some effects of wet pressing on sheet structure", *TAPPI 1981 Engineering Conference*, San Franscisco, CA, September 13-16, 1982 Proceedings, Book I9-24.

[11] Busker, L.H., "The effects of wet pressing on paper quality", *TAPPI 1985 Engineering Conference*, Atlanta, GA, Sept. 16-19, 1985 Proceedings, Book 1, pp. 117-129.

[12] Rajala, Pasi, Heikki Hakkanen, Carl-Gustav Berg, and Richard Solin, "The Effect of Intense Air Drying on Material Distribution and Quality in Coated Papers", *Drying Technology*, Vol. 21, No. 10, October 2003, pp. 1941-1956.

[13] Li, Xiqing, Timothy D. Scheibe and William P. Johnson, "Apparent decreases in colloid deposition rate coefficients with distance of transport under unfavorable deposition conditions: a general phenomenon," *Environmental Science and Technology*, August 19, 2004.

[14] Camesano, Terri A., Kenneth M. Unice and Bruce E. Logan, "Blocking and ripening of colloids in porous mediam and their implications for bacterial transport," *Colloids and Surfaces A: Physicochemical and Engineering Aspects*, Vol. 160, 1999, pp. 291-308.

[15] Yao, K. M., M. T. Habibian and C. R. O'Melia, "A model for colloid filtration," *Environmental Science and Technology*, November 1971, pp. 1105-1112.

[16] Rajagopalan, R. and C. Tien, "Trajectory analysis of deep-bed filtration with the sphere-in-cell porous media mode," *AIChE Journal*, Vol. 22, 1976, pp. 523-533.

[17] Harvey, R. W., and S. P. Garabedian, "Use of colloid filtration theory in modeling movement of bacteria through a contaminated sandy aquifer," *Environmental Science and Technology*, Vol. 25, No.1, January 1991, pp 178-185.

[18] Song, L. and M. Elimelech, "Transient deposition of colloidal particles in heterogeneous porous media," *Journal of Colloid Interface Science*, Vol. 167, 1994, pp. 301-313.

[19] Gross, M. J., O. Albinger, D. J. Jewett, B. E. Logan, R. C. Bales and R. G. Arnold, "Measurement of baterial collision efficiencies in porous media," *Water Research*, Vol. 29, 1995, pp. 1151-1158.

[20] Rajagopalan, R., and R.Q. Chu, "Dynamics of adsorption of colloidal particles in packed beds," *Journal of Colloid Interface Science*, Vol. 86, 1981, pp. 299-317.

[21] Dabros, T. and T. G. M. van de Ven, "Kinetics of coating by colloidal particles," Journal *of Colloid Interface Science*, Vol. 89, 1982, pg. 232.

[22] Ryde, N., N. Kallay, and E. Matijevic, "Particle adhesion in model systems, 14, Experimental evaluation of multilayer deposition," *J. Chem. Soc. Faraday Trans.*, Vol. 87, 1991, pp. 1377-1381.

[23] Liu, D., P.R. Johnson, and M. Elimelech, "Colloid deposition dynamics in flow through porous media: role of electrolyte concentration," *Environmental Science and Technology*, Vol. 29, 1995, pp. 2963-2973.

[24] Camesano, T.A., and B.E. Logan, "Influence of fluid velocity and cell concentration on the transport of motile and nonmotile bacteria in porous media," *Environmental Science and Technology*, Vol. 32, No. 11, November 1998, pp. 1699-1708.

[25] Gannon, J., Y. Tan, P. Baveye, and M. Alexander, "Effect of sodium chloride on transport of bacteria in a saturated aquifer material," *Applied Environmental Microbiology*, Vol. 57, No. 9, September 1991, pp. 2497-2501.

[26] Bai, G., M.L. Brusseau, and R.M. Miller, "Influence of a rhamnolipid biosurfactant on the transport of bacteria through a sandy soil," Applied Environmental Microbiology, Vol. 63, No. 5, May 1997, pp 1866-1873.

[27] Sugihara-Seki, Masako, "Motion of a sphere in a cylindrical tube filled with a Brinkman medium," *Fluid Dynamics Research*, Vol. 34, No. 8, August 2004, pp. 59-76.

[28] Brinkman, H.C., "A calculation of the viscous force exerted by a flowing fluid in a dense swarm of particles," *Appl. Sci. Res.*, Vol. A, No. 1, January 1947, pp. 27–34.

[29] Sugihara-Seki, M., and Skalak, R., "Asymmetric flows of spherical particles in a cylindrical tube," *Biorheology*, Vol. 34, 1997, pp. 155–169.

[30] Brown, Richard, "The effect of filler particle size on retention," *Paper Technology*, April 1990, pg. 22-23.

[31] Shapiro, Ascher H., *Shape and Flow: The fluid dynamics of drag*, Doubleday & Company, Inc. New York, 1961.

[32] Berg, Howard C., *Random Walks in Biology*, Princeton University Press, 1983.

[33] Donley, H. Edward, "Drag force on a sphere", *UMAP Journal*, Vol. 12, No. 1, Spring 1991, pp. 47-80.

[34] Ahmadi, G., "Hydrodynamic Forces: Drag Force and Drag Coefficient", Clarkson University, ME 437/537, pp. 1-11.

[35] Ascensio, Maria C., and Seyed-Yagoobi, Jamal, "Theoretical drying studying of single tier versus conventional two-tiered dryer configurations", *TAPPI Journal*, Vol. 75, No. 10, October 1992, pp. 203-211.

[36] Robertson, A. A., "Measurement and significance of the water retention of papermaking fibers," l.c. [1], pg. 90.